PhD Dissertation

博士論文

Studies on lake ice thickness evolution with emphasis on roles of snow at Lake Abashiri, Hokkaido, Japan

（北海道網走湖における湖氷の氷厚発達過程

および雪の役割に関する研究）

Graduate School of Environmental Science,

Hokkaido University

北海道大学大学院環境科学院

Yu Ohata

大畑　有

February, 2017

Abstract

To clarify the properties of lake ice at mid-latitudes subject to moderate air temperature, heavy snow, and abundant solar radiation even in winter, field observations were conducted at Lake Abashiri, Hokkaido, Japan for three winters and a 1-D thermo-dynamical ice growth model was developed. Using this model with meteorological datasets, the roles of snow in the ice thickening process, as well as the Lake Abashiri ice phenology (including the interannual trend) for the past 55-years were examined to compare with high latitude lakes. The ice was composed of two distinct layers: a snow ice (SI) layer and a congelation ice layer. The SI layer occupied a much greater fraction of total ice thickness than that at high latitude lakes. *In-situ* observations served to demonstrate the validity of the model. Freeze-up and break-up dates supplied by satellite imagery enabled further model validation prior to the availability of field data (2000/01-2015/16). Based on both observations and numerical experiments, it was found that one important role of snow is to mitigate the variability of ice thickness caused by changes in meteorological conditions. Furthermore, ice thickness is more sensitive to snow depth than air temperature. When applied to an extended 55-year period (1961/62-2015/16) for which local meteorological observations are available, the mean dates of freeze-up and break-up, ice-cover duration, and ice thickness in February were estimated to be 12 December (no significant trend), 17 April (-1.7 d/decade), 127 d (-2.4 d/decade), and 43 cm (-1.4 cm/decade). For this long-term period, while snow still played an important role in ice growth, the surface air temperature warming trend was found to be a strong factor influencing ice growth, as reported for the high latitude lakes.

Contents

1. Introduction

This study aims to clarify the properties of lake ice at mid-latitudes, subject to relatively moderate air temperature, much snow, and abundant solar radiation even in winter, as contrasted with lakes at high latitudes. So far, seasonally ice-covered lakes have been studied mainly for the North American and northern European lakes, and little attention has been paid to the lakes at mid-latitudes in other regions. Lake Abashiri is covered with ice from December to April every year. The lake water is composed of two layers with significantly different salinities (0.1 psu to 20 psu) during the winter, and ice is formed in the upper fresh water layer. In this study, the properties of lake ice at Lake Abashiri, Japan were investigated as a case study for the lakes at mid-latitudes.

For this purpose, field observations at Lake Abashiri were conducted for three winters, and a 1-D thermo-dynamical model for predicting ice growth at Lake Abashiri was developed. Using this model forced by meteorological datasets from Abashiri Meteorological Observatory (AMO), the roles of snow in the ice thickening process were examined and also ice phenology parameters were estimated. Interannual trends at this lake for the past 55-year period were compared with lakes at high latitudes.

This section introduces the relationships of seasonally covered lakes with climate and social activities, previous researches on lake ice structures and thermodynamic models of ice thickness evolution, the definition of lake-ice phenology parameters and reported trends of the parameters, the climate conditions for lake ice growth at mid-latitudes and an overview of this study.

1.1. Seasonally ice-covered lakes

Seasonal ice cover is characteristic of lakes located in boreal and temperate regions. Bates and Biello (1966) estimated the southern boundary of seasonal ice cover in the North Hemisphere to follow approximately the latitude 45^{o}N, higher in the Western Europe and lower in Asia and North America. In this latitude band, there are also permanently ice-covered lakes in very high latitudes. Basically, where the mean air temperature in the coldest month is below the freezing point, shallow fresh water lakes are potential to freeze over (Fig. 1.1) (Kirillin et al., 2012; Leppäranta, 2015).

Lakes affect the local climate and weather by modulating the temperature, wind, humidity and precipitation (Bonan, 1995; Ellis and Johnson, 2004; Rouse and others, 2008). Essentially lake ice prevents heat and momentum transfer between the atmosphere and the lake water through its insulating effect from winter to spring. If the lake is covered by snow, this influence is further strengthened due to the lower thermal conductivity of snow. Therefore the duration and growth processes of lake ice are important for understanding the local/regional winter climate. The seasonality of lake ice also influences the lake ecosystem and its biogeochemical properties (Vanderploeg and others, 1992; Salonen and others, 2009; Shuter and others, 2012). Furthermore, freezing lake-ice winter cover has an effect on social activities (Leppäranta, 2009). Various fishing techniques with drills on ice-covered lakes have been developed, and lake-ice functions as infrastructure for transportation in winter. Frozen lakes are also used as venues for recreation (e.g. ice fishing, skiing, long-distance skating and ice sailing). Thus, the properties and the growth processes of lake ice are very important for not only for understanding the local/regional winter climate, but also for social activities.

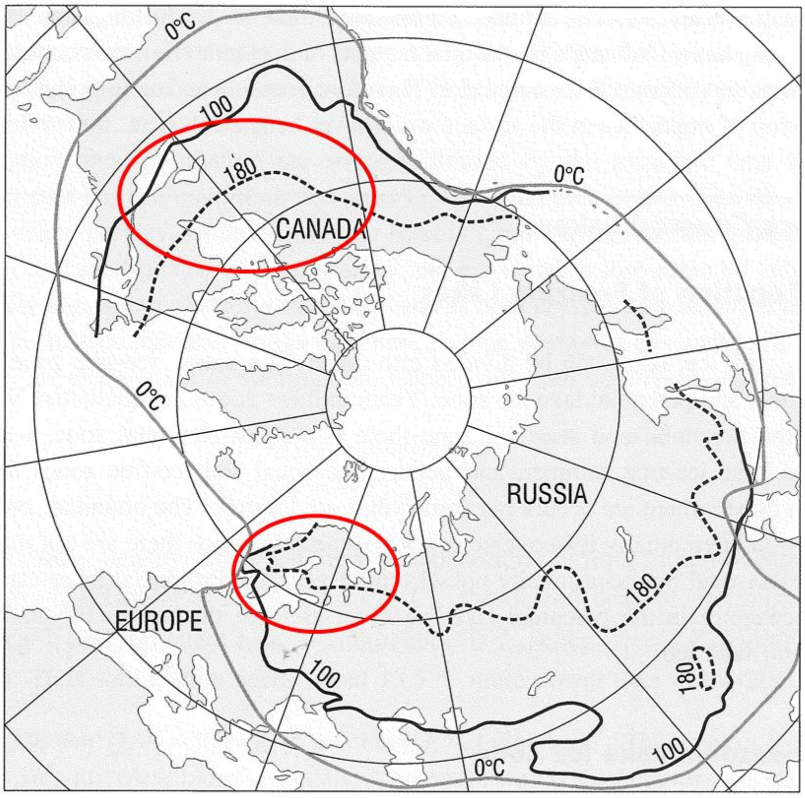

Fig. 1.1. The zone of seasonally freezing lakes in the northern hemisphere (Bates and Bilello, 1966) and the 0^{o}C climatological isotherm in January. The contours 100 and 180 refer to the mean length of ice season (days). Red circles show the lake areas having been mainly studied so far; the North America and the northern Europe. Modified from Leppäranta, (2015)

1.2. Lake ice structure

So far the ice structure and formation processes for seasonally ice-covered lakes have been studied mainly for the North American and northern European lakes. Michel and Ramseier (1971) classified freshwater ice (river and lake ice) based on crystal structure and growth processes into primary ice (the first type of ice of uniform structure and texture which forms on a water body), secondary ice (which forms parallel to the heat flow which in most cases is perpendicular to the primary ice) and superimposed ice (which always forms on top of the primary ice and is caused by water flooding the ice cover from any water source (e.g. lake water, rainfall and snowmelt) and its freezing; if there is snow on the ice surface, snow ice may form). According to the Michel and Ramseier (1971) classification, secondary ice can be divided into two main classes: S1 type, which has macro-crystals with a vertical *c*-axis orientation, and S2 type, where the crystallographic orientation of the *c*-axis changes continuously with depth to a preferred horizontal orientation, and forms vertically elongated columnar crystals.

From observations of the northern North American lakes, Gow and Langston (1977), Barns and Laudise (1985) and Gow (1986) reported that the S1 type was dominant. Gow (1986) concluded from his laboratory experiment that the two different types of secondary ice can be attributed to the presence of atmospheric seeding, and that there was no evidence that frazil ice contributes to the formation of S2 type unlike in the case of sea ice. From observations of southern Finnish lakes for 7 years (1993-99), Leppäranta and Kosloff (2000) also reported that the S1 type prevailed, and there was no evidence for the occurrence of frazil ice. The occurrence of frazil ice as secondary ice has not been reported in the history of the lake-ice studies (Leppäranta, 2009; Kirillin et al., 2012). This may be because lake water is usually in a still condition with a vertically strong stability after water is cooled to 4^{o}C (maximum density). Even so, Leppäranta (2009) pointed out the possibility of frazil ice formation induced by wind over the open water of large lakes (longer than about 50 km; e.g. northern European lakes Peipsi, Ladoga and Vänern).

These results were obtained mainly at relatively high latitudes. At mid-latitude, however, observations have been very limited (e. g. Muguruma and Kikuchi, 1963;

Kawamura and Ono, 1978), and therefore, this growth condition here might be quite different.

1.3. Thermodynamic ice growth model

Up till the 1980s, analytical or semi-empirical models were widely used to predict the thickness evolution of lake ice. At that time, the major input parameters were freezing degree-days. Differences in ice type and various other factors were not taken into account. A numerical thermodynamic growth-model for sea ice was first developed for Arctic sea ice with a snow layer by Maykut and Untersteiner (1971). In their model, vertical ice thickness evolution was calculated by solving the heat conduction equation. Later this model was extended to include the process of SI formation (Leppäranta, 1983; Liston and Hall, 1995; Flato and Brown, 1996; Launiainen and Cheng, 1998; Saloranta, 2000; Menard et al., 2002; Duguay et al., 2003; Cheng et al., 2003; Shirasawa et al., 2005). Duguay et al. (2003) presented the Canadian Lake Ice Model, including SI formation from flooded snow and freeze-up date simulation from heat storage during ice-free summer months by mixed-water layer depth parameterization. Saloranta (2000) introduced the process of SI formation by snow compaction and slush formation due to flooding and percolation of rain- and snow meltwater for Baltic Sea ice. This model was further applied to fast ice in the Sea of Okhotsk (Shirasawa et al., 2005). Recently, a 1-D high-resolution thermodynamic model was developed for lake ice, which shows good agreement with observations in Finnish lakes (Yang et al., 2012). However, even with the newest model, a significant discrepancy between calculated and observed ice thickness still exists with the inclusion of SI thickness. This is mainly because the growth processes of lake ice have not yet been fully understood. It is highlighted that, in order to improve accuracy, observations are important, especially for the realistic snow-related processes (Leppäranta, 1983, 2009; Saloranta 2000; Menard et al., 2002; Jeffries et al., 2005). In this study, to understand the thickening processes of the lake ice, a thermodynamic model was developed, based on the observations at Lake Abashiri, Hokkaido, Japan located at mid-latitudes (44^{o}N), where SI formation is enhanced under snow. In addition to the good access to the lake for field observation, meteorological datasets for the model are available from two meteorological stations of Japan Meteorological Agency (JMA) located at the distance of ~10 km from the lake. Since the climate at Lake Abashiri is similar to that around the five Great Lakes of North America, it is anticipated that this study will also contribute to understanding of the formation process of lake ice there.

1.4. Lake-ice phenology

Lake-ice phenology studies the dates of freeze-up and ice break-up, and the ice-cover duration. Conventionally, the freeze-up date is defined as the first date when a lake is completely ice-covered, whereas the break-up date is the first date when it is completely ice-free. Sometimes, the freezing date, which means the date of the first occurrence of ice in a winter, has been used as the basis for the ice season and consequently the length of ice season is then defined as the period between the freezing date and the break-up date. Therefore, care should be taken in conducting a comparative analysis whether the freeze-up date or freezing date has been consistently used (Kirillin et al., 2012; Leppäranta, 2015). Here in this paper, the duration of ice season is defined as the time between the freeze-up and break-up dates.

Several recent studies of global warming (IPCC, 2001, 2007, 2013) have reported that lake-ice phenology (dates of freeze-up and break-up, ice-cover duration) has changed significantly worldwide. Magnuson et al. (2000) showed that on average the freeze-up date of 26 lakes and rivers in the Northern Hemisphere became later at a rate of 0.58 d/decade, and the break-up date earlier at a rate of 0.65 d/decade, over the period 1846-1995. According to more recent studies, ice-cover duration reduction appears to be accelerating. For example, Benson et al. (2012) showed that the freeze-up date of 75 lakes in the Northern Hemisphere became later at a rate of 1.1 d/decade, and the break-up date earlier at a rate of 0.9 d/decade over the period 1855/56 - 2004/2005, while the freeze-up date became later at a rate of 1.6 d/decade and the break-up date earlier at a rate of 1.9 d/decade over the period 1975/76 - 2005/06.

As for timing of ice formation and decay, the regression analysis for the 90 lakes in Northwest Russia by Efremova and Palshin (2011) yielded the most influential predictors for the average freeze-up dates: (1) mean depth; (2) geographic latitude; and (3) elevation above sea level. The break-up dates correlated best with factors such as: (1) geographic latitude, (2) elevation above sea level and (3) lake area. Thus freeze-up dates depends first on heat storage of the water body expressed by the mean depth, whereas break-up depends on the solar radiation input expressed by the latitude (Fig. 1.2, Kirillin et al., 2012). For mid-latitude lake ice, in other regions than the North America, there have been few phenology studies except the freeze-up date at Lake Suwa, Japan (36^{o} N, 138^{o} E), where the freeze-up date was shown to have become later at a rate of 0.2 d/decade over the 550-year record (Magnuson et al., 2000). Due to lack of ice thickness data and analysis of ice structure, however, factors involved in such trends remain unknown. In this study, using the model based on observations, interannual trends at this lake for the past 55-year period are estimated to compare with those of the

North American lakes and the European lakes at high latitudes.

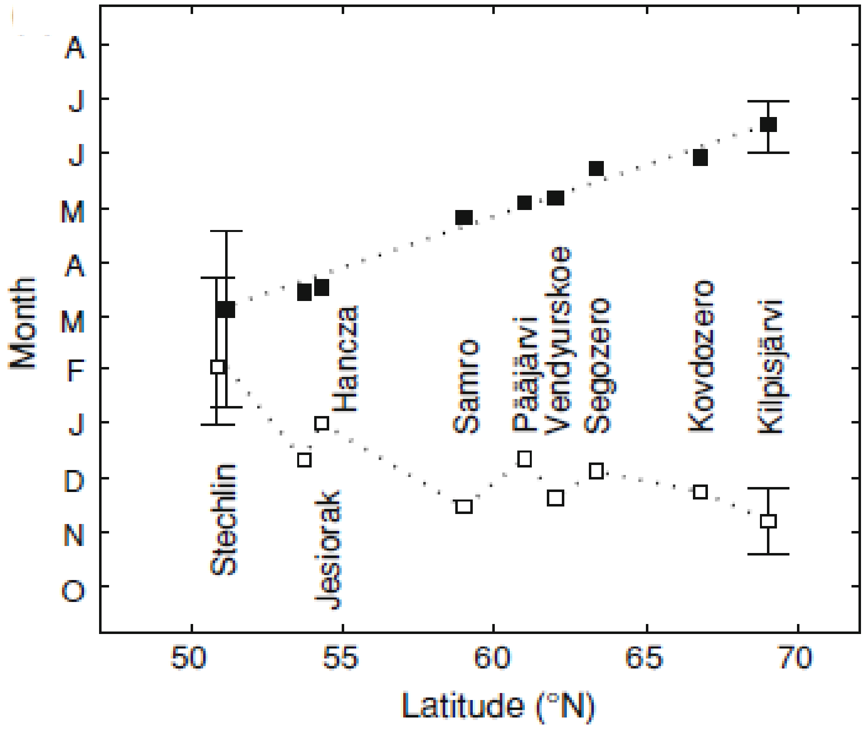

Fig. 1.2. Long-term average of the dates of freeze-up (white squares) and break-up black squares) in several European lakes (Kirillin et al., 2012). Data are from: Lake Stechlin, Germany, 1961–2002 (Bernhardt et al. 2011); Lakes Jesiorak and Hancza, Poland, 1961–2000 (Marszelewski and Skowron2006); Lakes Samro, Segozero, and Kovdozero, Russia, 1936–1989 (Efremova and Palshin 2011); Lake Vendyurskoe, Russian Karelia,1994–2000 and 2007–2011 (Terzhevik, unpublished); Lake Pääjärvi, Finland, 1910–1988 (Kärkäs 2000); and Lake Kilpisjärvi, Finland, 1964–2008 (Lei et al. 2012). The error bars for Lakes Stechlin and Kilpisjävi show the earliest and the latest observed values.

1.5. Meteorological conditions at mid-latitudes

To understand the growth processes of mid-latitude lake ice and discuss the influence of climate on a global scale, it is necessary to clarify the properties of lake ice at lower latitudes with different growth conditions. Meteorological conditions (air temperature, precipitation, incoming solar radiation and specific humidity, 1981-2010) of high-latitude and mid-latitude lake regions in the Northern Hemisphere are listed in Table 1.1, and monthly air temperature and total precipitation in winter are shown in Figure 1.3. As shown in Figure 1.3, air temperature and precipitation are relatively moderate and heavy at Lake Abashiri respectively, whereas a few sites at high-latitude regions, e.g. Jokioinen, Finland, have the similar air temperature and precipitation to Abashiri. However, as shown in Table 1.1, the incoming solar radiation at Abashiri is much higher than at Jokioinen, although the specific humidity is similar at both sites. The abundant incoming solar radiation even in winter works to suppress the congelation ice at Lake Abashiri. This gives a different ice-growth condition at mid-latitudes from high latitudes. As seen in the Table 1.1 and Figure 1.3, the climate at mid-latitudes is characterized by relatively (1) moderate air temperature, (2) high atmospheric water content and a considerable amount of snow, which activates the snow-ice (SI) growth compared with that at high latitudes, and (3) abundant solar radiation even in winter, which works to suppress the congelation ice (CI) growth. This figure also shows that the climate at Lake Abashiri is similar to that around the five Great Lakes of North America (e.g. Holroyd, 1971; Ellis and Johnson, 2004). So far, lake ice growth related to snow has been studied mainly for high latitudes, and little attention has been paid to lakes at mid-latitudes. This study on lake ice at Lake Abashiri is expected to contribute to the understanding of lake ice formation processes at mid-latitudes.

Table 1.1. Monthly mean air temperature, total precipitation, incoming solar radiation and specific humidity in lake regions (1981-2010) (Pirinen and others, 2012; Japan Meteorological Agency, 2015; Leppäranta, 2015). Cited from Ohata et al. (2016a)

Meteorological Station	Latitude	Longitude	Altitude	Mean air temperature			Total precipitation			Incoming solar radiation			Specific humidity		
				Dec.	Jan.	Feb.	Dec.	Jan.	Feb.	Dec.	Jan.	Feb.	Dec.	Jan.	Feb.
			m	°C	°C	°C	mm	mm	mm	$W\ m^{-2}$	$W\ m^{-2}$	$W\ m^{-2}$	$g\ kg^{-1}$	$g\ kg^{-1}$	$g\ kg^{-1}$
Abashiri	44.02°N	144.28°E	38	-2.4	-5.5	-6.0	59	55	36	60	71	115	2.2	1.8	1.8
Concord	43.20°N	71.5°W	103	-2.9	-5.8	-4.6	83	70	60						
Wiarton	44.73°N	81.1°W	222	-2.6	-6.6	-5.8	118	87	70						
Marquette	46.53°N	87.55°W	434	-7.6	-9.9	-9.3	61	67	48						
Irkutsuk	52.27°N	104.32°E	469	-15.3	-17.7	-14.4	16	14	8						
Karlstad	59.43°N	13.33°E	107	-1.7	-2.3	-2.8	55	51	38						
Saint Petersburg	59.97°N	30.3°E	6	-3.9	-5.5	-5.8	49	44	33						
Jokioinen	60.80°N	23.50°E	104	-3.9	-5.6	-6.3	47	46	32	6	11	38	2.6	2.2	2.0
Yellowknife	62.45°N	114.43°W	205	-23.0	-25.8	-23.7	16	14	15						
Fairbanks	64.80°N	147.87°W	134	-19.8	-21.9	-18.2	17	15	10						
Kilpisjarvi	69.05°N	20.78°E	478	-10.8	-11.7	-12.1	51	50	36						
Utsjoki	69.75°N	27.00°E	107	-12.3	-14.0	-12.8	25	27	24	0	1	15	1.3	1.1	1.2

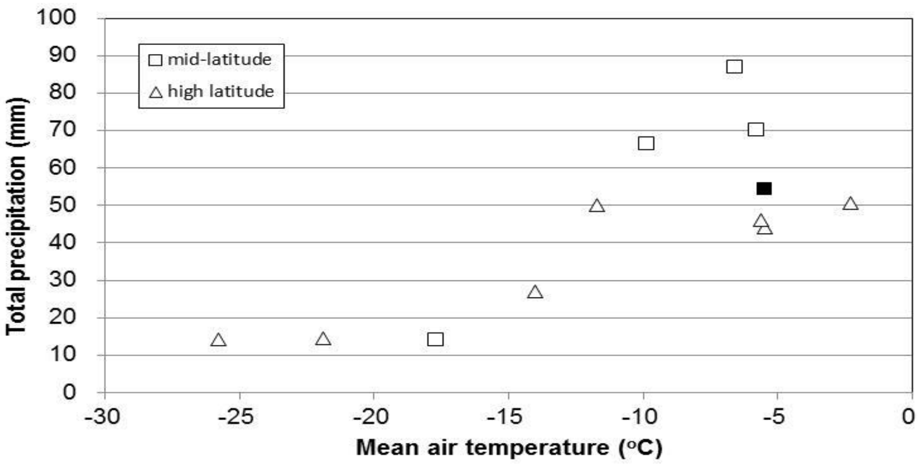

Fig. 1.3. Mean air temperature and total precipitation in January 1981-2010 in lake regions. Regions at higher and lower latitudes than ~60° N are shown by triangles (high latitude) and squares (mid-latitude) respectively. Abashiri is shown by a filled black square. (Table 1.1 shows location details, air temperature and precipitation in other winter months.) Sources: Japan Meteorological Agency (2015); Pirinen et al. (2012). Cited from Ohata et al. (2016a)

1.6. Overview of this study

This study aims to clarify the properties of lake ice at mid-latitudes, subject to moderate air temperature, relatively heavy snow, and abundant solar radiation even in winter, as contrasted with lakes at high latitudes. For this purpose, firstly, the lake ice properties at Lake Abashiri, Hokkaido, Japan, located at mid-latitudes (44.0N 144.2E) were investigated and a 1-D thermo-dynamical model for predicting ice growth at Lake Abashiri was developed, based on observations throughout the 2012/13 winter.

Next, to confirm the observational results and verify the model, obtained from observations in 2012/13, the lake ice properties were investigated and the model was verified for various meteorological conditions, using the additional data obtained from the follow-up campaigns in two winters (2014/15, 2015/16) and meteorological datasets. Then, using this model forced by meteorological datasets from Abashiri, the roles of snow in the ice thickening process were examined and also ice phenology parameters were estimated at this lake for the past 55-year period and interannual trends were compared with lakes at high latitudes.

As for the validation of the model, special attention to the validity of the snow compression rate (β) and the time scale of the conversion of flooded snow (slush) layer to snow ice was paid because these are critical assumptions in the model. For this purpose, during the observations in two winters (2014/15 and 2015/16) the freeze-up conditions were directly observed from a small boat in December, and the thickness measurements of snow, CI, and SI were conducted at fixed sites once per month from January to March. The process of SI formation was monitored with a set of thermistors installed in the ice and snow.

To further examine the roles of snow in the lake ice growth under various meteorological conditions, numerical model experiments were carried out for the three winters (2012/13, 2014/15 and 2015/16), and then the analysis period was extended with meteorological data records at Abashiri for the past 16 years (2000/01-2015/16) during which the freeze-up dates can be determined with minimal uncertainty from NASA Moderate Resolution Imaging Spectroradiometer (MODIS) satellite images. Finally, to examine the ice phenology for Lake Abashiri, the interannual variability of ice thickness and dates of break-up and freeze-up were calculated for the past 55 years (1961/62-2015/16) using the model, using nearby staffed weather station air temperature records as proxy data. The results will be compared with the phenology data from elsewhere in the Northern hemisphere reported by Benson et al. (2012), and meteorological factors responsible for the interannual trends will be discussed.

Although this study is limited to the properties of lake ice at mid-latitudes in Japan, the results are expected to apply to other lakes, such as the Great Lakes of North America, where meteorological conditions are relatively similar. In addition, since SI formation is regarded as an important sea ice growth processes, especially in the Antarctic regions, the results are also expected to be applicable to this domain.

2. Observation

2.1. Observation and analysis methods

2.1.1. Observation

Lake Abashiri is located in the northeastern part of Hokkaido, Japan (43.97° N, 144.17° E), at a distance of 4 km from the Sea of Okhotsk, to which it is connected by the Abashiri River (Fig. 2.1). The water depth is ~16 m at its maximum and 7 m on average, and the lake covers 32.3 km^2, with dimensions of ~10 km x 3 km.

Six observation sites were set along the line running from upstream (southwest) to downstream (northeast) on Lake Abashiri (Fig. 2.1b). In the 2012/13 winter season, on-site observations were carried out four times between November 2012 and March 2013: on 15-16 November (before freezing), 17-18 January, 18-19 February and 17-18 March. In the 2014/15 and 2015/16 winter seasons, follow-up on-site observations were carried out at sites 1, 3 and 6 once per month from December to March in the 2014/15 and 2015/16 ice seasons (11 December, 30 January, 24 February and 12 March in the 2014/15 ice season, and 11 December, 29 January, 19 February and 11 March in the 2015/16 ice season). At each site, vertical profiles in the lake water of salinity, temperature and density, from 15 cm below the surface to the bottom of the lake, were measured with a conductivity/temperature/depth (CTD) profiler (CastAway-CTD from Son Tek/YSI Inc.), and lake ice, lake water and snow on ice were sampled. The positions of the sites were determined by GPS (GPSMAP62SCJ, GARMIN Ltd). To collect samples of lake water and ice, a water sampler of 1300 mL capacity (Rigo, type 5023-A) or ~100mL plastic bottles, and a chainsaw or hand auger, respectively, were utilized.

In addition, to estimate the conductive heat flux within ice, the vertical profile of ice temperature was monitored at site 3 from 17 January to 18 March 2013, using thermorecorders RT-32S from ESPEC MIC Corporation, with a measurement accuracy of 0.1°C. Four thermistor probes were installed at depths of 44, 34, 24 and 14 cm from the ice surface (Fig. 2.2). The sensor at the greatest depth (44 cm) was set in water while the other sensors were embedded in ice. These data are used to estimate sensible heat flux from the underlying water.

In addition, to understand the SI formation processes, the temperatures of air, snow, ice and water were monitored at site 3 from 29 January to 11 March in 2016, using the 12 thermo-recorders (RT-32S) with a measurement accuracy of 0.1°C. The evolution of the temperature profile is expected to detect the conversion process of snow or slush layer to SI because of their significant difference in thermal conductivity among them. Before the measurement, the sensors were calibrated in an ice-water-filled bath in which temperature was set to 0^oC in equilibrium. Among the 12 thermistor sensors, two were installed in the air, five in snow, one at the snow/ice interface, two in ice and two in water beneath the ice, as shown in Figure 2.3. On the set-up day (29 January 2016), snow depth was 31 cm, containing a 22-cm thick slush layer composed of flooded snow layer (15 cm) and the resultant wet snow layer (7 cm) just above it. The sensors were set at an interval of 5 cm in the snow layer (4 in slush and 1 in dry snow).

Besides, to verify the values of the incoming solar radiation (Q_s) at Abashiri Meteorological Observatory (AMO) as input data for the surface heat budget calculation in the model (see Section 3), the short wave radiation on the lake was measured from 09am 29 to 08am 30 February.

(a)

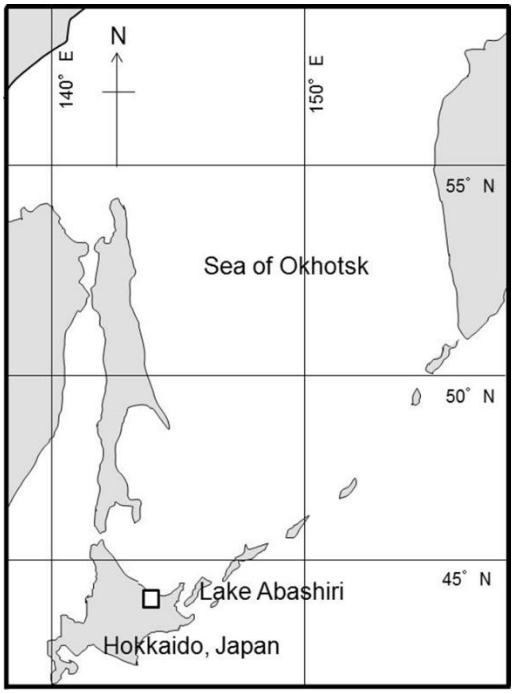

(b)

Fig. 2.1. Locations of observation sites: (a) a location map of Lake Abashiri in the southern Sea of Okhotsk; (b) a local-scale map for the six observation sites on the lake; two Japan Meteorological Agency sites, Abashiri Meteorological Observatory and Memanbetsu Airport; the photograph site at the top of Tento-san mountain, and the near shore site for the past ice thickness record (Yobito). Cited from Ohata et al. (2016a)

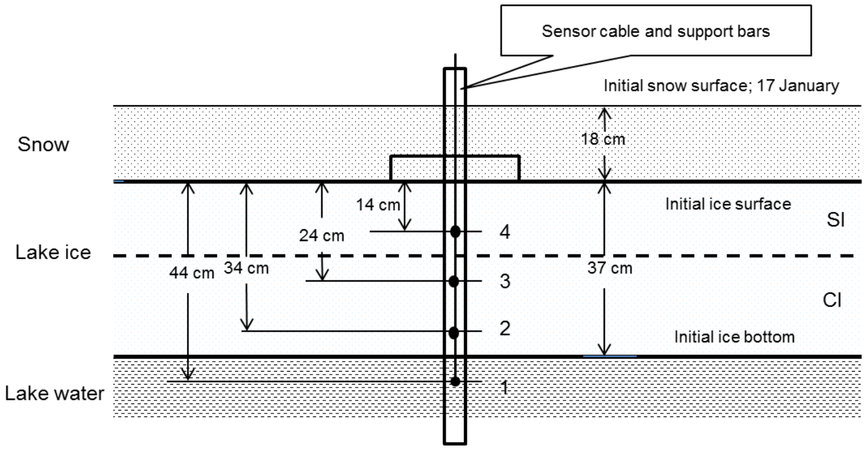

Fig. 2.2. A schematic picture of the installation of four thermistor sensors for measuring ice and water temperatures at site 3 in 2013. The horizontal dashed line shows the boundary of SI and CI. Modified from Ohata et al. (2016a)

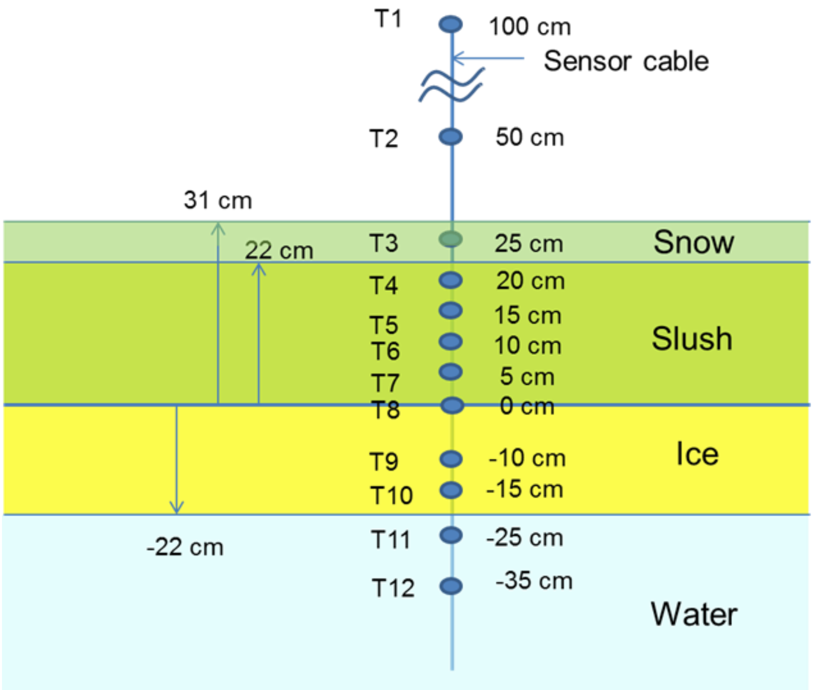

Fig. 2.3. A schematic picture of the installation of 12 thermistor sensors for measuring air, dry snow, slush, ice and water temperatures at site 3. The vertical line represents the sensor cable with thermistor sensor depths referenced to the slush/ice interface on 29 January 2016.

2.1.2. Sample analysis

To clarify the ice structures with the thickness of each layer and its origin, thick/thin-sections of ice samples were analyzed, and the stable oxygen isotopic compositions ($\delta^{18}O$) were measured for samples of ice, snow and water to distinguish meteoric ice from ice of lake water origin. In addition, the salinity of samples for lake water and ice was measured, as this may affect the ice structure and the freezing temperature, the value of which is used in the model calculation.

All samples obtained were processed and analyzed at the Institute of Low Temperature Science, Hokkaido University. In the cold room (-15°C), the ice samples were split lengthwise into two pieces. One piece was used for thick/thin-section analysis; the other was used partly for measuring salinity and stable oxygen isotopic compositions ($\delta^{18}O$), and the rest was archived.

For thick/thin-section analysis, an ice sample was sectioned at 10 cm intervals, then each section was sliced into 5 mm thick sections to observe inclusions within the ice under scattered light. Each section was further sliced to 1 mm thickness with a microtome, to examine crystallographic alignments through crossed polarizers.

The other ice sample was sectioned at 10 cm intervals. Each ice section and snow sample was melted at room temperature for the measurement of $\delta^{18}O$ and salinity. $\delta^{18}O$ was measured for lake water and the melted samples of snow and ice with a Wavelength-Scanned Cavity Ring-Down Spectroscopy (WS-CRDS, Kerstel and others, 1999; Gupta and others, 2009) instrument (Picarro, Inc.). The analytical precision of $\delta^{18}O$ was estimated to be 0.05‰ from the standard deviation of triple measurements. Salinity was measured for each sample with a salinometer (Guildline Instruments Ltd, Model 8400B AUTOSAL) and for lake water with CTD. The samples were measured against standard water and calibrated using International Association for Physical Sciences of the Ocean (IAPSO) standard sea water. The measurement accuracy of salinity was <0.001 psu.

From these analyses, the ice structure and its origin were clarified, and the relative SI portion of the total ice thickness was revealed at this lake along with the freezing temperature of lake water for the model.

2.2. Meteorological conditions

Meteorological conditions were quite different between these three ice seasons. The time series of air temperature and snow depth from December to March are shown in Figure 2.4. When we look at the mean air temperature and snow depth (given by the increased amount of snow depth) from freeze-up date to 20 February to characterize the meteorological conditions during the ice growth period, it is found that the temperature was higher and the snow deeper in the 2014/15 winter than in the two other winters (Table 2.1). In Figure 2.4, also note that air temperature was relatively high and the freeze-up was relatively late in December 2015/16. On the other hand, snow depth on land around the lake was relatively deep on the freeze-up date in the 2012/13 winter, while quite small in the 2014/15 and 2015/16 winters. Moreover, the snow depth in 2015/16 is characterized by relatively small accumulation rate for about three weeks after freeze-up date, while several heavy snowfall events took place after the freeze-up in 2014/15.

The weather condition at the time of observation in 2012/13 were cloudy sometimes fair on 16 November, fair sometimes snow on 17-18 January, fair sometimes snow on 18-19 February and cloudy with 4-10^{o}C on 18 March. The weather conditions at the times of observation in 2014/15 and 2015/16 were as follows: For 2014/15, the freeze-up conditions observed on the boat were calm and cloudy with an air temperature of 0 – 1^{o}C on 11 December 2014 and calm and cloudy with 1 – 2^{o}C on 11 December 2015. The weather conditions on ice in early 2015 were cloudy with -5 – 0^{o}C on 30 January, cloudy sometimes fair with 0 – 4^{o}C on 24 February and fair with 0 – 5^{o}C on 12 March. For 2016, conditions were fair sometimes cloudy with -5 - -4^{o}C on 29 January, fair with -8 - -4^{o}C on 19 February and fair with -4 – 3^{o}C on 11 March. On all days, winds were relatively weak and the observations were conducted from 0800 to 1500 local time.

Table 2.1. Meteorological conditions from the freeze-up date to 20 February. The mean air temperature and mean snow depth (given by the snow thickness increment from freeze-up date) are the averages at the two meteorological stations; Abashiri Meteorological Observatory and Memanbetsu Airport. Increase of snow depth just after freeze-up is the mean increase of snow depth for 2 days after freeze-up.

Year	Freeze-up date	Mean air temperature	Mean snow depth	Increase of snow depth just after freeze-up
		^{o}C	cm	cm d^{-1}
2012/13	11 December	-7.5	23.5	4.9
2014/15	10 December	-4.6	41.0	0.0
2015/16	23 December	-6.3	24.1	0.7

(a)

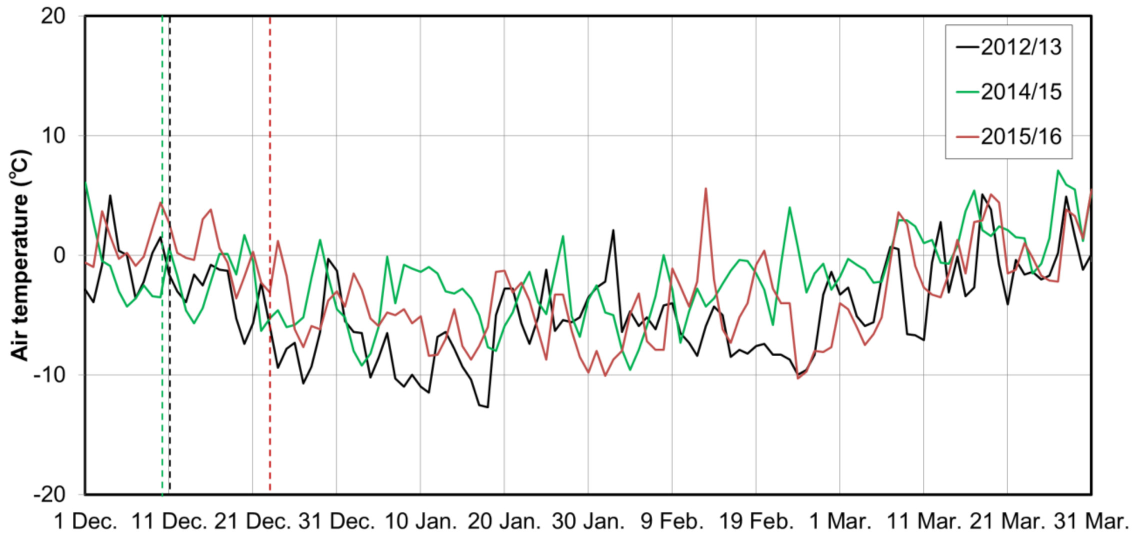

(b)

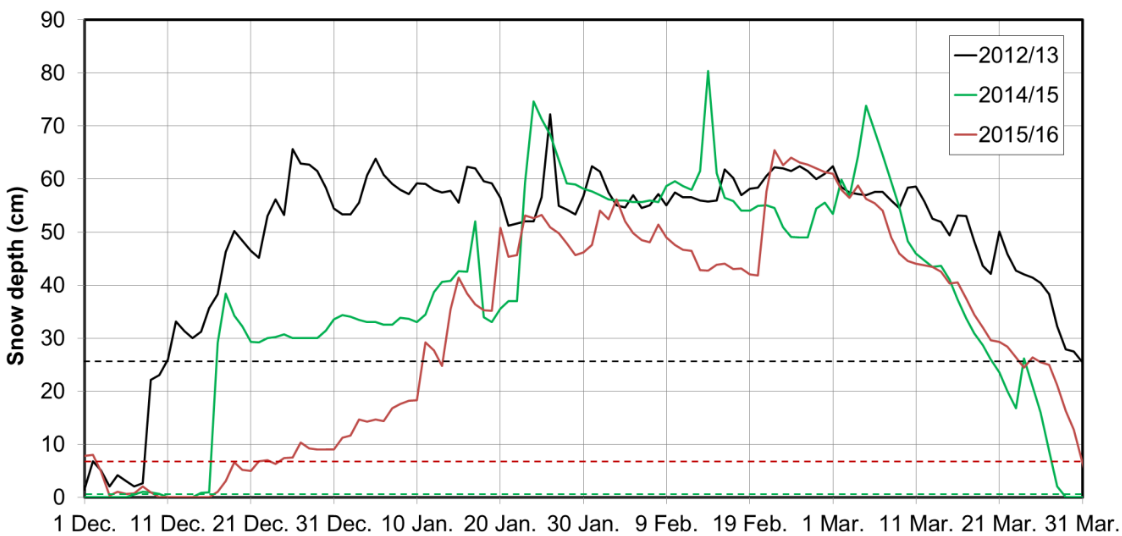

Fig. 2.4. Time series of (a) daily air temperature and (b) snow depth at AMO in 2012/13, 2014/15 and 2015/16. The mean air temperatures and the mean snow depths from 1 December to 31 March were -4.5 ^{o}C, -1.9 ^{o}C, -2.9 ^{o}C and 49.2 cm, 37.2 cm, 31.0 cm in 2012/13, 2014/15, 2015/16, respectively. The vertical dashed lines in (a) indicate the freeze-up dates and the horizontal dashed lines in (b) indicate the snow depths on the freeze-up dates.

2.3. Observational results and discussion

2.3.1. The lake-ice properties

1) 2012/13

Ice thickness and snow depth at each observation site are shown in Table 2.2. Ice structure at each site was commonly composed of whitish (upper) and translucent (lower) layers, as shown in Figure 2.5. The thicknesses of both layers are also shown in Table 2.2. The origin of each ice layer was examined by the crystal alignments and $\delta^{18}O$ analyses. Firstly, thick/thin-section analysis was carried out to investigate the crystal alignments. The vertical structures of crystal alignments obtained from thin-section analysis are shown in Figure 2.6. These structures can be categorized into three types. The first type consists of a macro-grain layer overlain by a granular ice layer with a clear boundary (S1 type, according to the classification of Michel and Ramseier, 1971), as seen at sites 1–3. The second type consists of a columnar ice layer overlain by a granular ice layer, with a clear boundary between them, as seen at site 4. This type is omitted from the Michel and Ramseier (1971) classification, which does not include columnar ice that extends beneath a granular ice layer without a transition layer. The third type consists of a granular ice layer developing into a columnar ice layer through a transition layer of a few cm (S2 type), as seen at sites 5 and 6. In the transition layer, the orientation of the crystal *c*-axis changes from random to horizontal with increasing depth. Here, note that macro-grained, columnar ice and transition layers, corresponding to transparent layers, are all classified to CI.

Next, to investigate the origin of each ice layer, the $\delta^{18}O$ values of samples for water, ice and snow were measured. Surface lake water had a $\delta^{18}O$ value of -11.9 ± 0.1‰ with little spatial or temporal variability during the ice cover season. This is probably because river inflow is continuously supplied, and distributed widely near the surface of the lake, even in winter. On the other hand, the $\delta^{18}O$ value of snow had large variability, from -11 to -17‰, generally much lower than that of lake water, and with little spatial variability. As for ice, the mean $\delta^{18}O$ values for whitish layers and macro-grained transparent layers of the first type (sites 1-3) were -12.0 ± 0.5‰ and -9.5 ± 0.1‰ respectively. The mean $\delta^{18}O$ values for whitish layers and columnar-grained translucent layers of the second type (site 4) were -11.4 ± 0.5‰ and -9.6 ± 0.0‰ respectively. Table 2.3 summarizes the $\delta^{18}O$ of whitish and translucent ice layers, snow and lake water for three types categorized by vertical textural profiles in February. Whereas $\delta^{18}O$ values for whitish layers had a relatively large variability, those of translucent layers were almost the same, irrespective of ice texture. For example, considering the vertical profile of $\delta^{18}O$ including all the layers of snow, lake ice and water body at the central site 3 (Fig. 2.7), it is found that translucent ice layers (-9.4‰) have higher $\delta^{18}O$ values than lake water, by 2.4‰. Considering that equilibrium oxygen-isotope fractionation between ice and water is 2.91‰ and this value decreases with the increase in ice growth rates (Lehmann and Siegenthaler, 1991), the increase in $\delta^{18}O$ for translucent ice is attributed to fractionation during lake-water freezing. Therefore, it is concluded that the translucent layer is congelation ice that originated from lake water. On the other hand, the $\delta^{18}O$ value of the whitish ice layer is between those for translucent ice and snow, indicating that the whitish layer corresponds to snow ice. A relatively large variation in the $\delta^{18}O$ of the whitish layer (Table 2.3) is probably caused by large variations in snow $\delta^{18}O$.

While the $\delta^{18}O$ profiles showed an abrupt change between whitish and transparent ice for the first and second type textures (sites 1-4), they had intermediate values within the transition layer between white and transparent ice for the third type (sites 5-6). This may suggest the occurrence of frazil ice. Details are discussed further below in Subsection 2.3.4.

In addition, to check that the upper water layer is fresh, the salinity of lake water and ice was measured. Salinity profiles of lake water showed a clear two-layered structure. Whereas the salinity of lake water at depths >~10 m was ~20 psu, that of the surface water was 0.10 ± 0.03 psu at all sites from January to March. As for CI, the salinity was significantly low (0.02 ± 0.01 psu) (Fig. 2.8). Thus, it was found that the salinity of upper lake water and ice are considered to be fresh water and pure ice respectively. The corresponding freezing temperature of the surface water is considered to be essentially 0^{o}C (-0.006°C; Maykut, 1985).

Thus, based on sample analysis, ice structure at each site was found to be commonly composed of whitish and translucent layers, corresponding to snow ice and congelation ice respectively. As shown in Table 2.2, it is found that although the total ice thickness was almost the same in January (33-40 cm) as in February (42-44 cm) except for site 6 which is close to the Abashiri River outlet, the ratio of the two layers is quite different, depending on the site. Whereas the contribution of snow ice to total ice thickness is about 30% at site 1, it is > 50% at sites 4 and 5 and as high as 73% at site 6. This difference will be discussed in Section 3, using a thermodynamic model as an experimental study on the role of snow and snow ice in lake-ice thickening.

Overall thicker SI relative to the total ice thickness was observed at Lake Abashiri (29-73%), significantly higher than the 10-40% generally observed on Finnish lakes (Leppäranta, 2009). Thus SI makes a stronger contribution to lake-ice formation at Lake Abashiri, located at mid-latitudes, than on Finnish lakes at high latitudes.

Table 2.2. Ice thickness and snow depth at each observation site, and snow depths at meteorological observatories. Observations were carried out at sites 1-3 on 17 January and at sites 4-6 on 18 January in 2013, and were also carried out at site 3 on 18 February and at sites 1, 2, 4, 5 and 6 on 19 February in 2013. Meteorological data were recorded on 18 January and 18 February. Cited from Ohata et al. (2016a)

Date	Thickness	Site						Meteorological observatories	
		No.1	N.o.2	No.3	N.o.4	No.5	N.o.6	Abashiri	Memanbetsu
January	Total ice thickness (cm)	38	33	37	40	35.5	26.5		
	Whitish ice layer thickness (cm)	12	15.5	19.5	21	19.5	18		
	Translucent ice layer thickness (cm)	26	17.5	17.5	19	16	8.5		
	Snow depth (cm)	10	18	18	13	13	20	61	51
February	Total ice thickness (cm)	43	41.5	42	44	42	33		
	Whitish ice layer thickness (cm)	12.5	18.5	19	22	20.5	24		
	Translucent ice layer thickness (cm)	30.5	23	23	22	21.5	9		
	Snow depth (cm)	28	33	26	33	28	23	57	57

Table 2.3. $\delta^{18}O$ (‰) of ice, snow and surface water for three ice structure types (February 2013). Cited from Ohata et al. (2016a)

	Ice				Snow		Surface water
	Whitish layer		Translucent layer				
	mean	stdev	mean	stdev	mean	stdev	mean
First type(sites 1-3)	-12.0	0.5	-9.5	0.14	-14.2	1.1	-11.8
Second type(site 4)	-11.4	0.5	-9.6	0	-12.8	1.0	-11.8
Third type (sites 5 and 6)	-12.7	1.0	-9.6	0.3	-12.7	1.0	-11.9

(a)

(b)

Fig. 2.5. The appearance of the ice blocks collected at site 3 on (a) 17 January 2013 (37 cm thick) and (b) 18 February 2013 (42 cm thick). Cited from Ohata et al. (2016a)

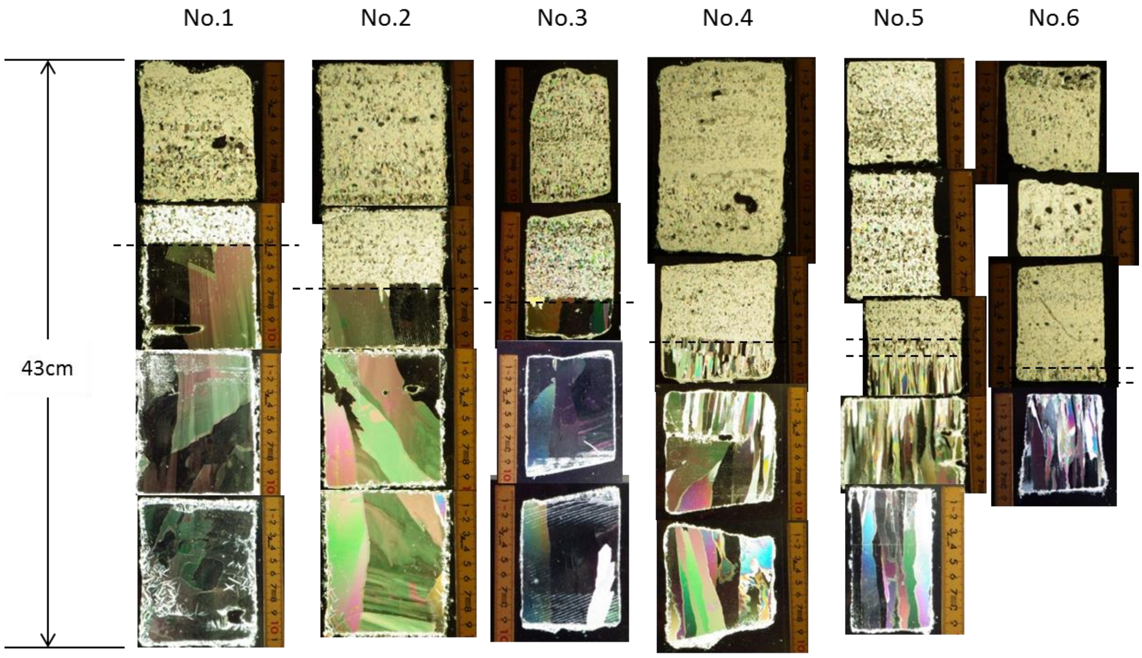

Fig. 2.6. Vertical cross sections of crystal alignments at sites 1-6 on 18-19 February 2013. Horizontal dashed lines show the boundaries between SI and CI. Cited from Ohata et al. (2016a)

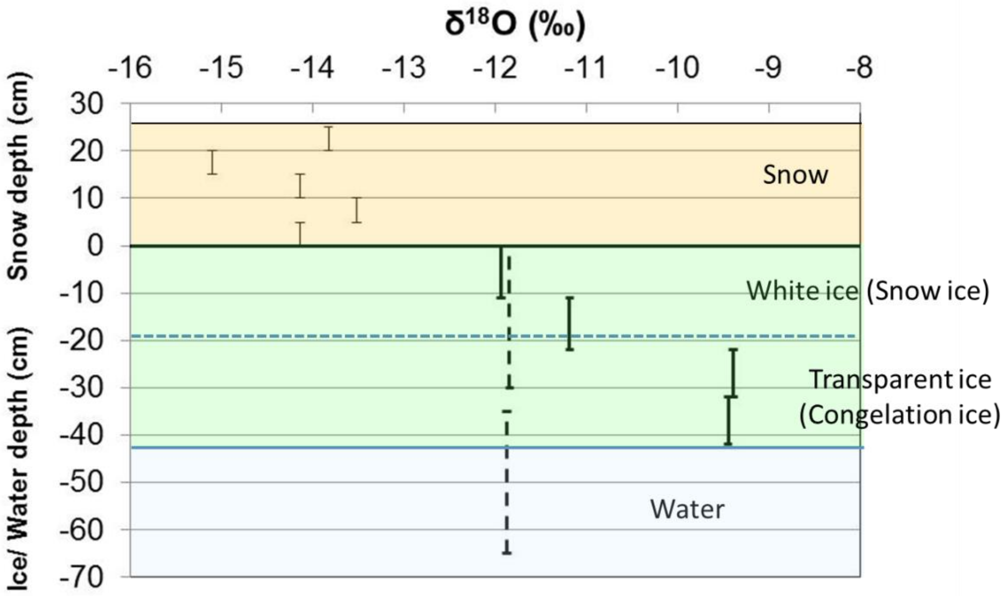

Fig. 2.7. Vertical profile of $\delta^{18}O$ for snow, ice and lake water at site 3 on 18 February 2013. The vertical axis is the depth referenced to the snow/ice interface. The vertical thin solid line, thick solid line and thick dashed line are the $\delta^{18}O$ values of snow, ice and water, respectively. The blue horizontal dashed and solid lines are the boundaries between CI and SI or water, respectively. Modified from Ohata et al. (2016a)

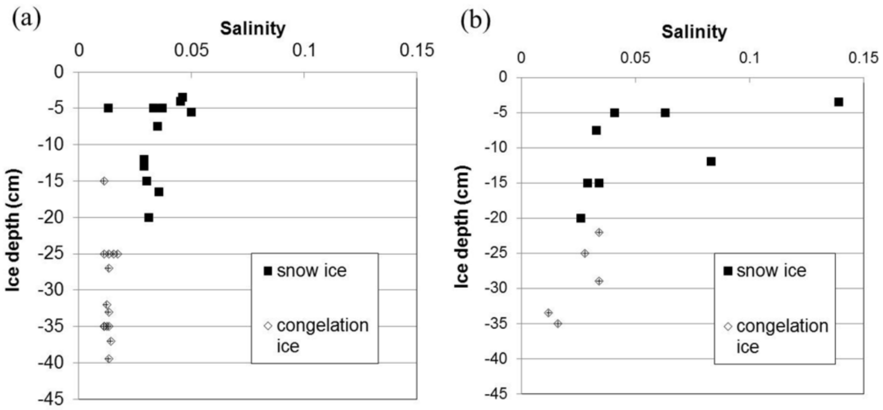

Fig. 2.8. Vertical profiles of salinity within the lake ice at (a) sites 1-4 and (b) sites 5-6 in January and February 2013.

2) 2014/15 and 2015/16

Firstly, we describe how we determined the freeze-up dates from the observations. On 11 December 2014, the lake had already frozen at the central part, the upstream part and along the shore region except for a few of ice-free regions near site 6 and some offshore regions from shore (Fig. 2.1). The ice thickness along the shore and near the site 6 was 1 to 1.5 cm with translucent color and the water temperature just beneath the ice was +0.1^{o}C. Based on this result, MODIS images, and the negative surface heat budget estimated from meteorological data (-47 Wm^{-2}), 10 December was regarded as the freeze–up date in the 2014/15 ice season. For the 2015/16 ice season, most of the lake surface was ice-free except for translucent thin ice plates (0.1-1.2 cm thick) floating near the shore and site 6 on 11 December 2015. The surface water temperature was still somewhat high (+0.4 to 1.3^{o}C). Based on this result and MODIS images, taking the meteorological conditions into account, 23 December was regarded as the freeze-up date.

Next, ice thicknesses and snow depths on ice in February at each site for three winters are listed in Table 2.4. To check the spatial representativeness of the obtained ice thickness, the spatial variability was examined by measuring thicknesses at 9 points with a 10 m x 10 m grid on 19 February 2016. The average ice thickness was 40.2±2.1 (std.) cm at site 1, 41.9±3.2 cm at site 3, and 47.9±1.5 cm at site 6, showing that the obtained ice thickness is considered to be representative of the surrounding area.

Ice structures were commonly composed of whitish (upper) and translucent (lower) layers, and it was confirmed from the δ^{18}O measurements that they correspond to SI and CI, respectively. The contribution of SI to total ice thickness was significant: 29-73% for 2012/13, 40-60% for 2014/15 and 28-65% for 2015/16 in contrast to 10-40% for lakes in Finland (Leppäranta, 2009). This result indicates that SI makes a stronger contribution to lake-ice formation at Lake Abashiri, located at mid-latitudes, than at high latitudes. The densities of CI (ρ_{ci}) , SI (ρ_{si}) and snow (ρ_s) at site 3 were 898±14 kg m^{-3} , 821±81 kg m^{-3} and 380±31 kg m^{-3} from the observation on 24 February 2015, and 872±16 kg m^{-3}, 838±13 kg m^{-3} and 243±37 kg m^{-3} on 19 February 2016, respectively, suggesting that SI has a somewhat lower density than CI.

From the CTD measurements, it was shown that lake water was composed of two layers with significantly different salinities during the winter: an almost fresh water layer (0.19 ± 0.05 psu) for the surface water and a saline water layer (~20 psu) for depth ≳10 m. Thus the lake ice here can be assumed to be formed from fresh water.

Table 2.4 Ice thickness and snow depth at sites 1, 3, 6. The numbers in parentheses denote relative portion of whitish ice layer to total ice thickness in %.

Year	Date	Thickness	Site		
			No.1	No.3	No.6
2013	18 - 19 February	Total ice thickness (cm)	43	42	33
		Whitish ice layer thickness (cm)	12.5 (29)	19 (45)	24 (73)
		Translucent ice layer thickness (cm)	30.5	23	9
		Snow depth (cm)	28	26	23
2015	24 February	Total ice thickness (cm)	48	55	53
		Whitish ice layer thickness (cm)	19 (40)	31 (56)	32 (60)
		Translucent ice layer thickness (cm)	29	24	21
		Snow depth (cm)	26	17	29
2016	19 February	Total ice thickness (cm)	40	42	48
		Whitish ice layer thickness (cm)	11 (28)	19 (45)	31 (65)
		Translucent ice layer thickness (cm)	29	23	17
		Snow depth (cm)	14	20	11

2.3.2. Estimation of the heat flux from lake water

The thickness growth of CI within lake ice is affected by the heat flux from lake water to ice. Therefore, the heat flux value needs to be estimated to establish a thermo-dynamical model. Here, heat flux is estimated by comparing the growth of CI with the vertical temperature gradient measured within ice. The time series of ice temperature monitored at four depths at site 3 is shown in Figure 2.9. The internal temperature varied almost proportionally to the distance from the surface. The heat flux transferred from lake water to ice (Q_w) is given by the heat balance equation at the bottom of the ice:

$$Q_w = k_i \, \mathrm{d}T/\mathrm{d}z - \rho_i L \, \mathrm{d}h/\mathrm{d}t \tag{1}$$

where k_i is the thermal conductivity of ice, ρ_i is the ice density, L is the latent heat of fusion of ice, h is the ice thickness and T is the ice temperature. In this equation, the increase in ice thickness is estimated from the observed value of 5.5 cm (23.0 – 17.5) for congelation ice thickness at site 3 from 17 January (17.5 cm) to 18 February (23.0 cm) 2013. Substituting k_i = 2.07 W m^{-2} (Yen, 1981) and ρ_i = 910 kg m^{-3} (Palosuo, 1965) gives the evolution of ice thickness for Q_w = 0, 1, 2, 3, 5, 10 W m^{-2} shown in Figure 2.10. By examining the optimal value in this figure, Q_w is estimated at 2 W m^{-2}.

The validity of this value was checked using a different method. According to the bulk method, Q_w is described as

$$Q_w = \rho_w c_w C_H (T-T_0) U_w \tag{2}$$

where ρ_w is the density of lake water, c_w is the water specific heat, C_H is the heat transfer coefficient, T is the water temperature beneath the ice, T_0 is the temperature at the ice bottom and Uw is the water current velocity (Shirasawa et al., 2006). At the center of Lake Abashiri, T = 0.4°C (observational result, ~5 cm beneath the ice), T_0 = 0°C, U_w = 0.2-1.7 cm s^{-1} (Ikenaga et al., 1999), ρ_w = 1000 kg m^{-3}, c_w = 4.186 × 10^3 J (kg K)$^{-1}$ and C_H = 4 × 10^{-4} is taken from the value for nearby Lake Saroma (Shirasawa et al., 2006). Equation (2) then gives Q_w = 1-11 W m^{-2}, showing that our estimation is not unrealistic. In addition, the Q_w value of 2 W m^{-2} is almost the same as the value of 2-5 W m^{-2}

obtained for freshwater lakes under calm conditions in Finland (Shirasawa et al., 2006; Leppäranta, 2009).

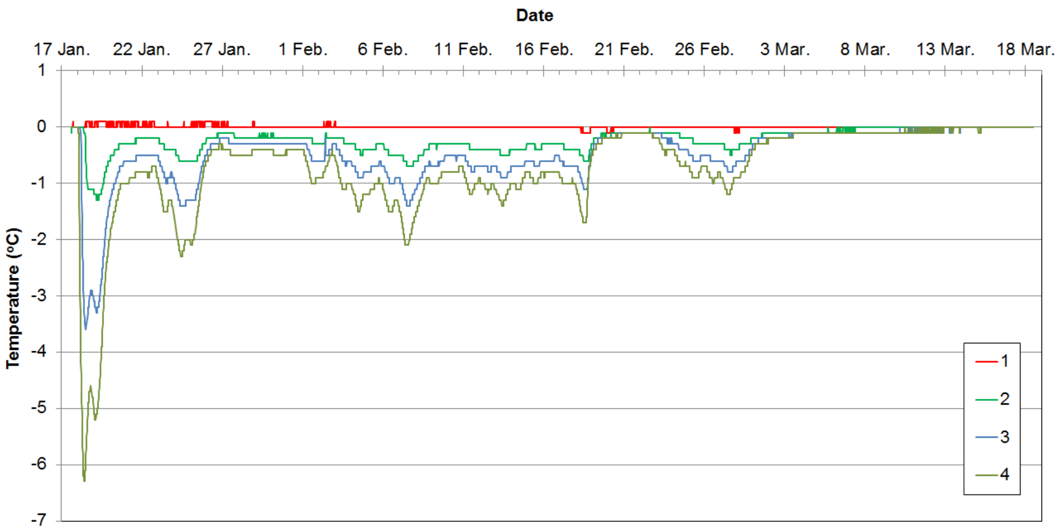

Fig. 2.9. Time series of lake water and internal ice temperatures at site 3 from 17 January to 18 March 2013. Line 1 denotes water temperature at 44 cm depth, while Line 2, 3 and 4 denote internal ice temperatures at depths of 34, 24 and 14 cm from the ice surface, respectively (refer to Fig. 2.2). Cited from Ohata et al. (2016a)

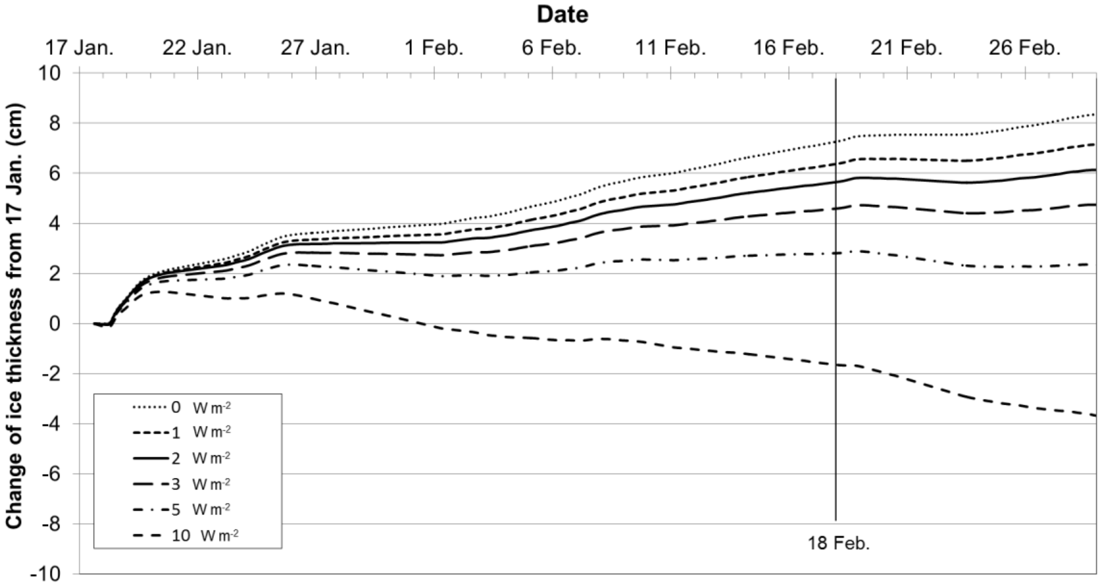

Fig. 2.10. The temporal evolution of the change in CI thickness from 17 January 2013 at site 3 for Q_w = 0, 1, 2, 3, 5 and 10 W m^{-2}. From observation, the thickness of CI increased from 17.5 to 23 cm by 18 February 2013. Note that Q_w = 2 W m^{-2} gives the best fit with the observations. Cited from Ohata et al. (2016a)

2.3.3. Snow ice formation process

1) Time scale for snow ice formation

To reproduce h_{si} and h_i well in a thermo-dynamical model, it is necessary to clarify the freezing process of slush layer. However, to the authors' knowledge, no direct measurement has been done so far on the freezing process of slush layer for lake ice. Therefore, in this section, the freezing process of slush layer is examined from the observation conducted in the 2015/16 ice season, focusing on the time scale of SI formation, which is essential for the model.

According to in-situ observations, a 22 cm-thick slush layer just above the ice on the day of instrument deployment (29 January 2016) had been completely transformed to SI at the observation on 19 February 2016. Fortunately, the evolution of vertical temperature profile within the snow, slush, and ice layers could be monitored, using the string of 12 thermistors during this period (Fig. 2.3). Due to the low thermal conductivity and large specific heat of slush, the amplitude of the diurnal variation, forced by the surface temperature, would be significantly reduced in the slush layer. Since SI usually grows from the top of slush layer due to the cooling by cold air (Leppäranta, 2015), it is expected that the thickness growth of SI can be detected by the decrease in temperature and the enhancement of temperature variation in slush layer. In this way, the growth rate of SI was analyzed as a case study.

Time series of temperatures monitored at 12 depths at site 3 are shown in Figure 2.11. It is seen that the air temperatures showed a large diurnal variation, ranging from -25^{o}C to +10^{o}C or more. Except the temperature variation at T2 (Fig. 2.11a) was significantly reduced due to snow drift from 21 February to 7 March, the air temperatures at T2 and T1 varied almost in-phase during the period. Corresponding to this variation, the temperatures within dry snow at T3 (25 cm above the slush/ice boundary) shows a relatively large variation, ranging from -5^{o}C to 0^{o}C (Fig. 2.11b). Note that the temperature at T4 (20 cm) in slush layer, kept at nearly 0^{o}C at the beginning, started to decrease and vary with an amplitude of about 1^{o}C about one day after set-up. This indicates that SI formed down to the depth of T4. As for T5 (15 cm), the temperature was kept at nearly 0^{o}C until 1 February and then started to decrease and vary with an amplitude less than 1^{o}C, indicating that SI formed down to the depth of T5 on 1 February. On the other hand, the temperatures at T6 (10 cm) and T7 (5 cm) were kept at 0^{o}C during the period except for several very small variations at T6 between

19-21 February. This is probably because the temperature variation attenuated significantly at such depths due to the insulating effects of snow and snow ice, and suggests the limitation of this method to detect SI formation. The temperatures at T8 (0 cm) at the interface between ice and slush, at T9 (-10 cm), T10 (-15 cm) in the ice and at T11 (-25cm), T12 (-35 cm) in the water were kept at 0^{o}C during the observation, as expected.

To see it more clearly, the temperature gradients between the sensors in snow, slush, and ice layers are shown in Figure 2.12. It is found that about one day after set-up the temperature gradient (T3-T4) started to decrease and instead the gradient (T4-T5) started to increase, indicating the formation of SI at T4 about one day after set-up. On the other hand, the gradient (T5-T6) was kept at 0^{o}C until 12:00 pm on 1 February, indicating that slush layer was maintained between T5 and T6 until this time. These results coincide with the above speculation based on Figure 2.11. Besides, note that the temperature gradients between T4-T5 and T5-T6 varied in phase with equivalent amplitude from 12:00 pm on 7 February onward. This indicates that transformation from slush to SI between T6 and T5 was completed by this time, since the value of heat flux between T5 and T6 was the same as that between T4 and T5, and the slush between T5 and T6 were considered to have homogeneous thermal properties with SI between T4 and T5 from this time onward.

As for the remaining 10 cm thick slush layer between T6 and T8, in light of the fact that the entire slush layer was transformed to SI by 19 February and SI formed up to the depth of T6 until 12:00 pm on 7 February, it was considered to be totally frozen for the preceding 12 days (8 to 19 February). On the other hand, the upward growth of SI should be negligible during the period, judging from the fact that h_{si} formed during this period (22 cm) almost coincided with the value (21 cm) estimated from the ice block collected in the vicinity on 19 February.

All these results are summarized in Figure 2.13, which shows how slush layer was transformed to SI during the observation period. It is found from this figure that the growth rate of SI in the slush layer is estimated to almost constantly 1.0 cm/d. Since the mean air temperature (-6.5^{o}C) and snow depth on ice (10-27 cm) during the observation period (29 Jan – 19 Feb) were typical at the time of this season here, the estimated SI growth rate might be assumed as representative at Abashiri. This value of 1.0 cm/d is also comparable with a value of 0.6 cm/d estimated similarly from the measurement of the vertical temperature profile in snow for the saturated basal snow layer on Antarctic sea ice with a surface air temperature of -11.6^{o}C and a snow depth of 14 cm (Toyota et al., 2011).

Finally, based on these results, the validity of the assumption used in the model, that slush is transformed to SI on a few days' time scale (see Section 3), is checked. According to datasets from AMO, the maximum accumulation rate of snow during 2015/16 is 20 cm/5d (4 cm/d). Taking the compression rate of β = 2 during the formation of SI in the model, the SI growth rate is estimated to be mostly less than 10 cm/5d. This means that in most cases the slush layer becomes frozen within 2 days. Therefore, the assumption used in the model is considered to basically hold true. The exact reason why such thick slush layer existed on 29 February in 2016 is not clear, but some ice crack might be supposed to have occurred to induce a big flooding event before the observation.

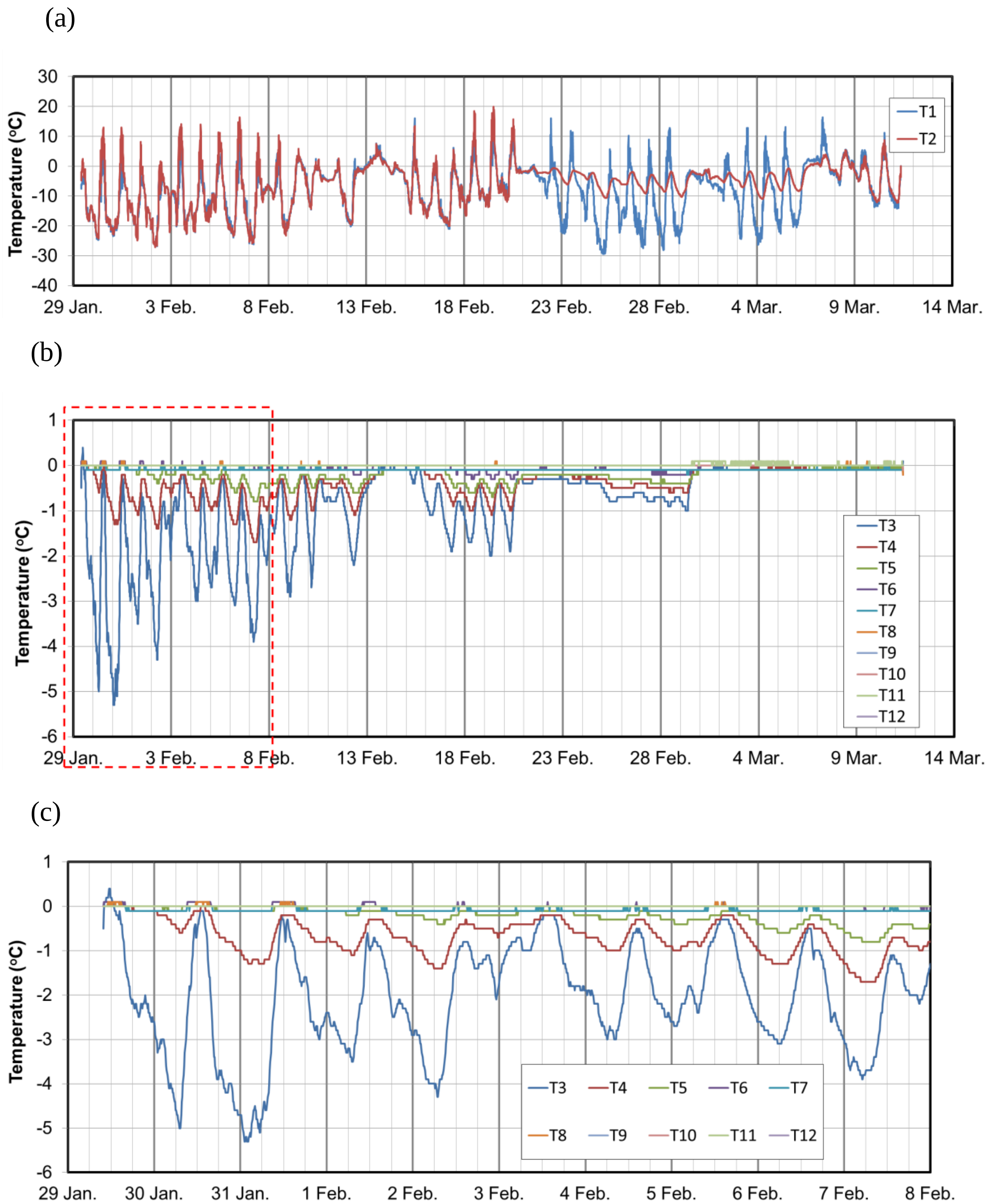

Fig. 2.11. Time series of temperatures of (a) air, (b) snow, ice and water at site 3 from 29 January to 11 March 2016, and (c) a magnified figure of the area enclosed with red dashed lines in (b) from 29 January to 7 February 2016. (See Fig. 2.3 for the depth of sensors T1-T12)

(a)

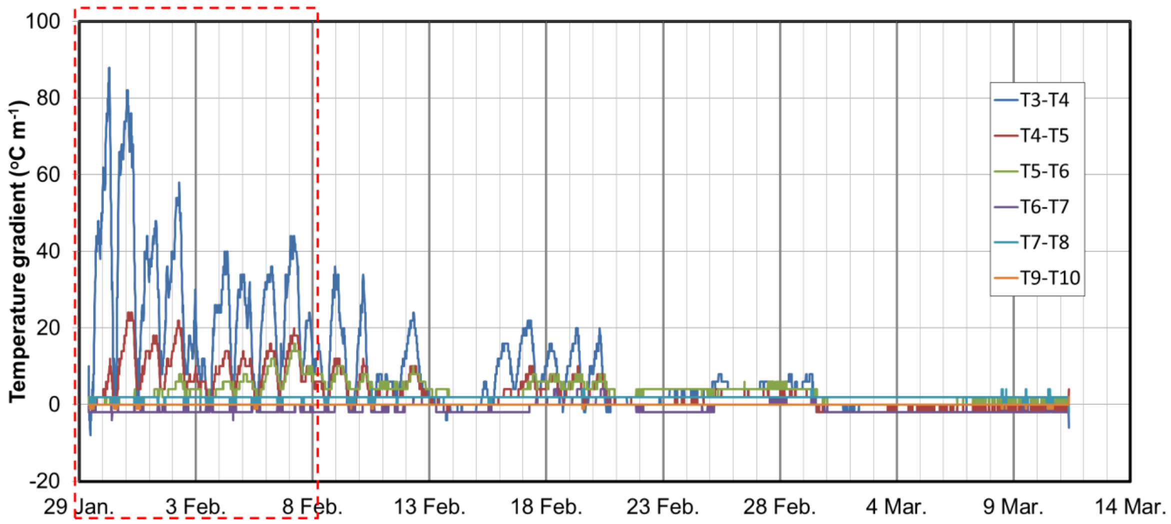

(b)

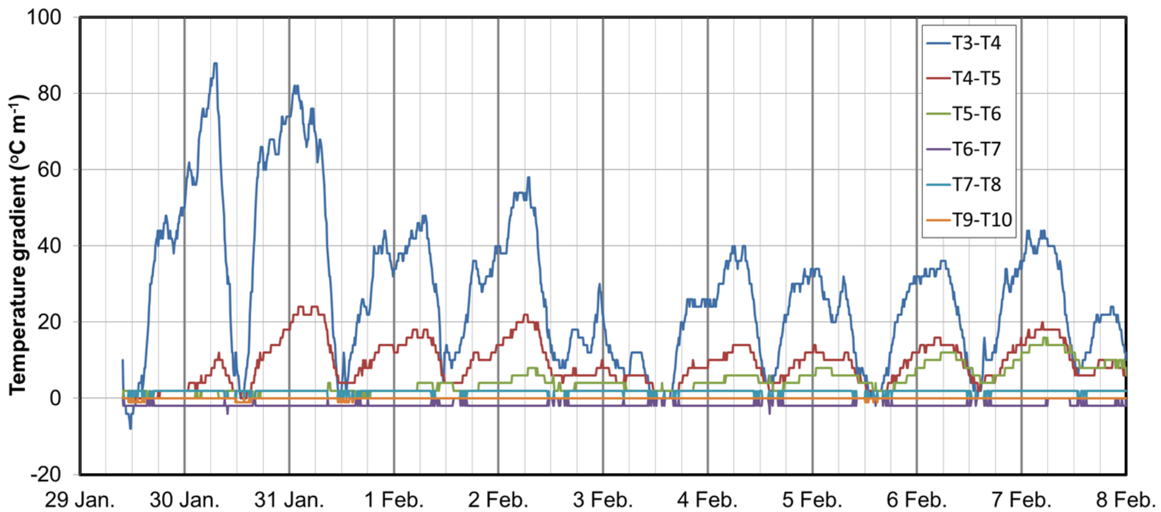

Fig. 2.12. (a) Time series of temperature gradients within snow and ice at site 3 from 29 January to 11 March 2016, (b) a magnified figure of the area enclosed with red dashed lines in (a) from 29 January to 7 February 2016. (See Fig. 2.3 for the depth of sensors T3-T10)

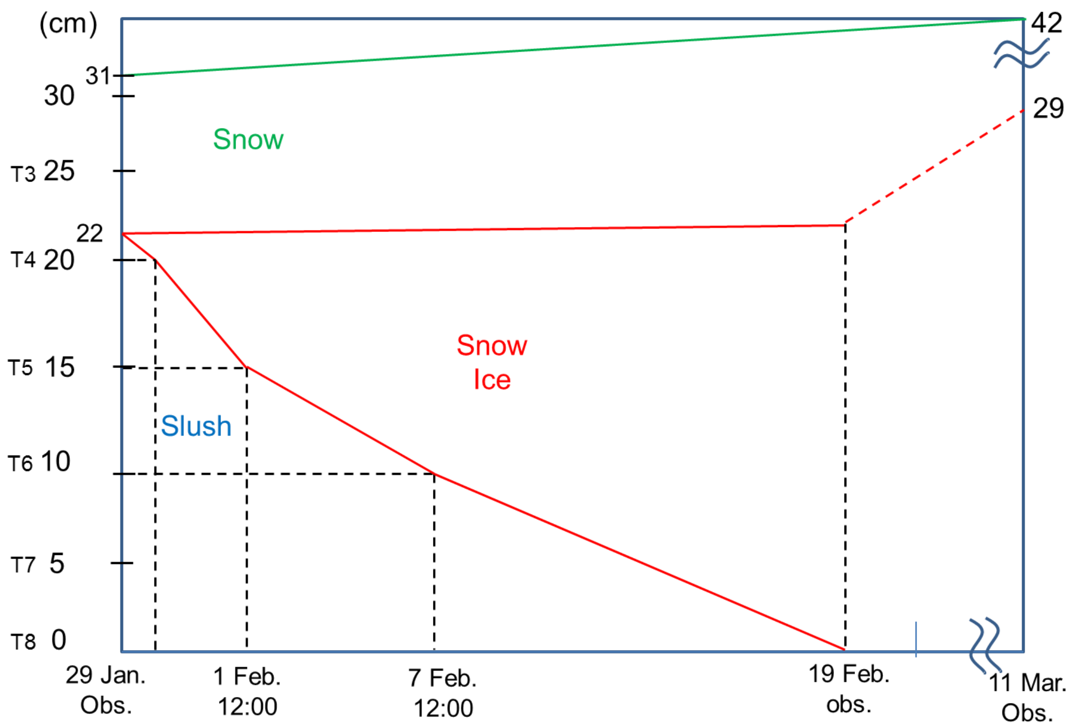

Fig. 2.13. A schematic picture of snow ice growth at site 3. The vertical axis represents the heights with sensor names referenced to the ice/slush interface on 29 January 2016. The horizontal axis represents time. The red line represents the boundaries between SI and slush or dry snow. The green line represents the snow surface. The red dashed line represents the supposed boundary between SI and dry snow which was not observed. The black dashed vertical and horizontal lines represent the dates and the corresponding heights of slush, respectively.

2) Physical parameters in snow ice formation process

SI grows from the top of the slush, forced by the cold air. The contained water in slush freezes downward beneath the new SI layer, which have been already formed until the time. Since the temperature and temperature gradient in slush are kept at freezing point (0^{o}C) and 0^{o}C m^{-1} respectively, using the latent heat of ice production and the conduction heat flux, the SI growth is expressed by Eqn (3),

$$\rho_{si} L v dh_{si}/dt = k_{si}\, \partial T/\partial z \qquad (3)$$

where L is the latent heat of fusion of ice (3.34×10^5 J kg^{-1}), v is the water fraction of the slush layer, k_{si} is the thermal conductivity of snow ice above the slush, t is time, z is vertical depth, and T is the ice temperature. Important physical parameters in SI formation processes are v and k_{si} in Eqn(3), since the values of the parameters are assumed in previous ice growth models despite of uncertainty. In the model developed this time, instead of v, the compression rate β is used (see Section 3). Firstly, in this sub-subsection 2), assuming all water in slush freeze during the conversion of slush to SI, the relationship between β and v is derived here.

The compression rate β is defined as the flooded snow layer thickness divided by the produced SI layer thickness

$$\beta = \Delta h_s / \Delta h_{si} \qquad (4)$$

where Δh_s is the flooded snow depth and Δh_{si} is the thickness of formed snow ice. β is a parameter originally introduced by Leppäranta and Kosloff (2000). Slush is a mixture comprised of snow and water, and the water infiltrated between snow particles freezes during the conversion process to SI. Snow layer is composed of ice and air, and snow is compressed and the porosity in snow layer is reduced during the slush formation and the freezing of slush. The volume (height) of ice from original snow after compression ($\Delta h_s'$) is described as

$$\Delta h_s' = (\rho_s / \rho_{si})\, \Delta h_s \qquad (5)$$

where ρ_s and ρ_{si} is density of snow and snow ice.

From the Eqns (4) and (5), the following equation should hold for the volume of SI,

$$\Delta h_s / \beta = \Delta h_s (\rho_s / \rho_{si}) + V_w \qquad (6)$$

where V_w is the frozen water volume from the original water in slush and includes the increment of volume by expansion at freezing and bubbles in SI.

From Eqn (6), the ice volume frozen from original water in SI is given by

$$V_w = \Delta h_s/\beta - \Delta h_s(\rho_s/\rho_{si}) \tag{7}$$

From Eqn (7), the mass of ice frozen from water in SI (M_w) is given by

$$M_w=V_w\rho_{si} = \Delta h_s\rho_{si}\ (1/\beta - \rho_s/\rho_{si}) \tag{8}$$

The mass of ice from original snow Ms is given by

$$M_s = \rho_s\Delta h_s \tag{9}$$

Based on the assumption that all water in slush freeze during the conversion of slush to SI without outflow, the water content in slush ν is given by

$$\begin{aligned}\nu &=1- M_s/(M_w+M_s)\\ &=1- \rho_s\Delta h_s/(\rho_s\Delta h_s+\Delta h_s\rho_{si}\ (1/\beta - \rho_s/\rho_{si}))\\ &=1- \rho_s/(\rho_s+\rho_{si}(1/\beta - \rho_s/\rho_{si}))\end{aligned} \tag{10}$$

Eqn (10) gives the relationship between β and ν.

Using ρ_{si} = 840 kg m^{-3}, ρ_s = 243 kg m^{-3} in Eqn (10) from observations in 2015/16, ν = 0.57 when β =1.5 and ν = 0.42 when β = 2. Here two ν-values were calculated for one β-value (1.5) in Finland (Lapparanta and Kosloff, 2000) and the other β-value (2.0) used in a thermodynamic ice model shown in Section 3, since β-value may include the snow condition peculiar to the lake (e. g. different snow drift amount by wind at each lake). It was found that the ν-values derived from β of 1.5 or 2.0 with Eqn (10) are almost consistent with that of 0.5 used in the previous studies to some extent (e.g. Leppäranta, 2015).

Next, k_{si} is estimated, using the values of ν calculated above. To calculate the SI growth between T5 and T6 from 12:00 on 1 February to 12:00 on 7 February, the heat flux of T4-T5 was used for the right side of Eqn (3). From the calculation results, to fit the calculated SI growth with 5 cm (the interval between T 5 and T6) from Eqn (3), k_{si} should have a value of 1.64 W m^{-1} K^{-1} for ν = 0.57 (β = 1.5), and k_{si} should have a value of 1.22 W m^{-1} K^{-1} for ν = 0.42 (β = 2.0). The SI growth (the slush decrease) between T5-T6 is shown in Figure 2.14a. The values of k_{si} are lower than that of the pure ice (2.07) and similar to those values (~1.0 W m^{-1} K^{-1}) in the previous models (e.g. Lepparanta, 1983; Saloranta, 2000).

In the same way, the SI growth (slush decrease) between T6-T8 was calculated by using the heat flux of T5-T6 in the right side of Eqn (3) with the thermal conductivity calculated above. To fit the calculated SI growth with 10 cm (the interval between T 6 and T8) from 12:00 on 7 February to 08:00 on 19 February, ν is 0.29 for the k_{si} value of 1.64 W m^{-1} K^{-1} and ν is 0.21 for k_{si} of 1.22 W m^{-1} K^{-1}. The SI growth (slush decrease) between T6-T8 is shown in Figure 2.14b.

From these results, the possibility that the water content in slush may be changed along with the progress of slush freezing was shown through SI growth from T5-T6 to T6-T8, since ν changed from 0.57 to 0.29 for β of 1.5 (k_{si} =1.64 W m^{-1} K^{-1}), and ν from 0.42 to 0.21 for β of 2.0 (k_{si} =1.22 W m^{-1} K^{-1}). Although averaged values of the important physical parameters in a certain period were estimated from these calculations, the parameters have various values along with the progress of SI formation. At the observation in 2012/13, the ice temperature was measured, as shown in Figure 2.9. The sensor Nos.2 and 3 were set in CI layer and sensor No.4 in SI layer (Fig. 2.2). The temperature gradient between Nos.2 and 3 coincided with that between Nos.3 and 4. This means that k_{si} had the same value with k_i (2.07 W m^{-1} K^{-1}), since the continuous conductive heat flux should exist between Nos 2-3 and Nos. 3-4 during the CI growth. To clarify the values of the parameters in a better accuracy, more observations or experiments are needed. In the practical model developed in this study, k_{si} is set at the same value of pure ice (2.07 W m^{-1} K^{-1}), and β is used as a tuning parameter for SI thickness, based on the observations in 2012/13 (see Section 3).

(a)

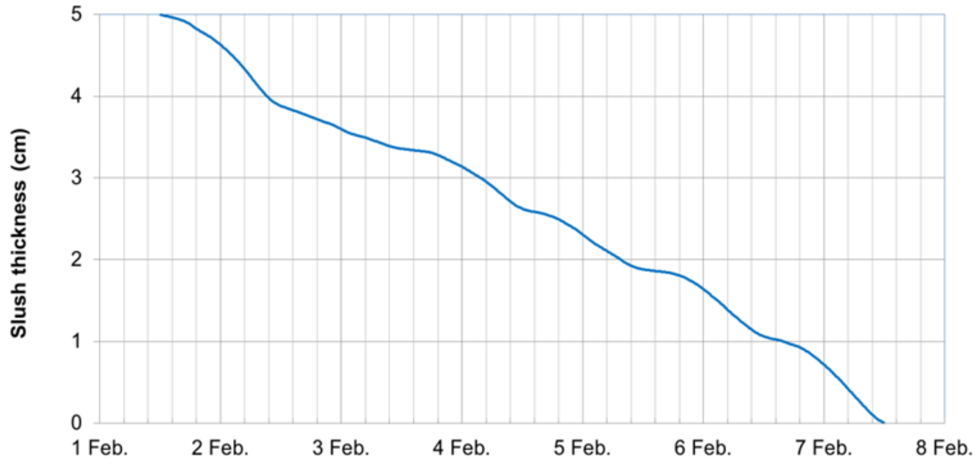

(b)

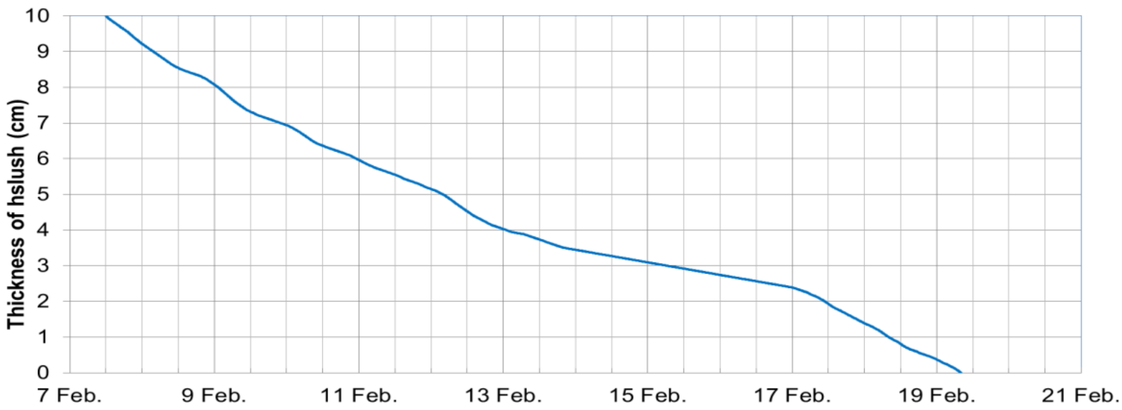

Fig. 2.14. Snow ice growth (slush decrease) (a) between T5 and T6 from 1 to 7 February 2016 and (b) between T6 and T8 from 7 to 19 February 2016 at site 3.

3) Heterogeneity in snow ice formation process

A homogeneous progress of SI formation from the top of slush is assumed in sub-subsections 1) and 2). Here, focusing on the daily periodical variance with the delay of phase and amplitudes of internal temperatures in the ice layers, the assumption of homogeneous progress was examined, using the heat conduction equations.

Assuming much larger temperature gradient and heat flux flow in the vertical direction than in the horizontal direction, a 1-D thermal conduction equation is given by

$$\partial/\partial t(\rho_i c_i T) = \partial/\partial z(k_i \partial T/\partial z) + q \qquad (11)$$

where t is the time, ρ_i is the ice density, c_i is the specific heat of ice, T is the ice temperature, k_i is the heat conductivity of ice and q is an internal heat source term.

If SI are formed homogeneously from the upper as discussed before, since SI had already been formed between T4-T5 by 12:00 on 1 February, no internal latent heat are supposed to exist there during the time of 12:00 pm on 1 to 12:00 pm on 7 February. Thus, q in Eqn (11) can be neglected, and the following equation is given:

$$\partial/\partial t(\rho_i c_i T) = \partial/\partial z(k_i \partial T/\partial z) \qquad (12)$$

Here, assuming that the internal initial temperature in ice T_0 is given by

$$T_0 = T_0(z, 0) = a_0 + b_0 z$$

where a_0 and b_0 are constants, and z is vertical depth,

Eqn (12) gives the solution by

$$T(z, t) = T_0 + T_0(T4)\exp(-z/(2a/\omega)^{1/2})\sin((\omega(t - z/(2a\omega)^{1/2})) \qquad (13)$$

where $T_0(T4)$ is the amplitude of temperature at sensor T4, z is the depth from T4 , a is $k_{si}/(\rho_{si} c_i)$ and ω is $2\pi/(24*3600)$. Using ρ_{si} = 840 kg m^{-3} (observation), $c_i = 2.11\times10^3$ J kg^{-1} K^{-1} and k_{si} = 2.07, 1.64 or 1.22 W m^{-1} K^{-1} (sub-subsection 2)), a is given respectively for k_{si}=2.07, 1.64 or 1.22 W m^{-1} K^{-1}, by

$$a = 1.17\times10^{-6},\ 9.25\times10^{-7} \text{ or } 6.88\times10^{-7} \quad (\mathrm{m^2\ s^{-1}})$$

The delay of phase at T5 (z = 0.05 m) from T4 (z = 0 m) Δt is given by

$$\Delta t = z/(2a\omega)^{1/2} = 64,\ 72 \text{ or } 83 \quad (\mathrm{min})$$

These values are almost consistent with observations, as shown in Figure 2.15.

For the decay of temperature amplitude $\exp(-z/(2a/\omega)^{1/2})$ at T5 , it was given by

$$\exp(-z/(2a/\omega)^{1/2}) = 0.76,\ 0.73 \text{ or } 0.70$$

However, the observed decay of temperature amplitude showed that of 0.3-0.5, much greater than calculations (Fig. 2.15). This shows that Eqn (13) does not hold. The latent heat between T4-T5 was shown to still occur during this period and it shows the conversion of slush to SI does not be carried out from the upper side homogeneously.

To solve Eqn (11), the physical parameters k_i , ρ_i , c_i and q should be given along with space and time variations. These parameterizations are, however, beyond the scope of this paper, and future studies are needed to determine the parameters. To understand the SI growth process in a better accuracy, more observations or experiments to determine parameters in various conditions are required.

As stated here in sub-subsection 1), it was shown that slush is usually transformed to SI on a time scale of a few days. This time scale will be used as an assumption for the new thermodynamic model of lake ice growth in Section 3.

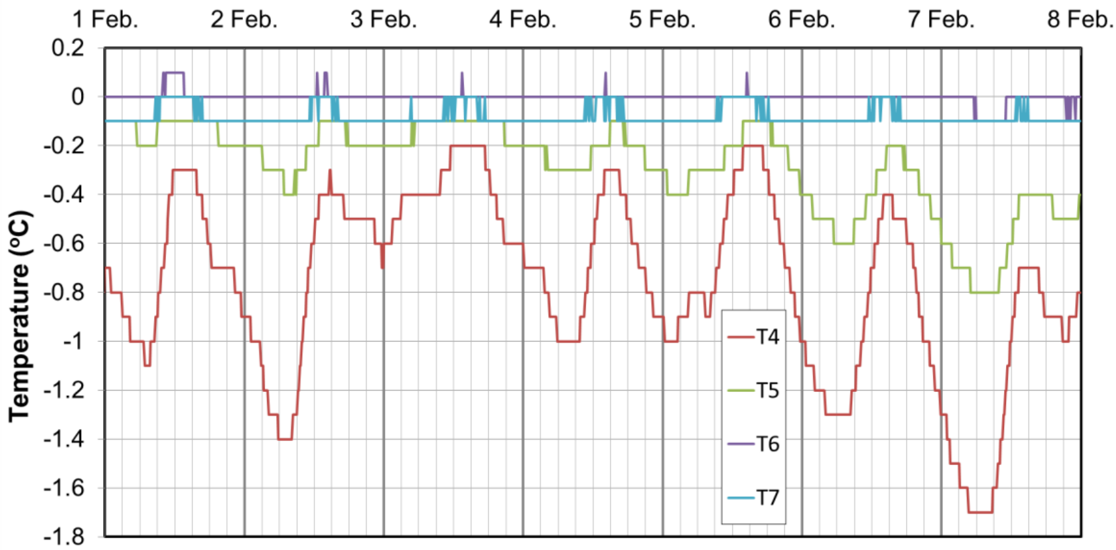

Fig. 2.15. Time series of temperatures at the positions of sensors T4, T5, T6 and T7 from 1 to 7 February 2016.

2.3.4. Possibility of frazil ice formation

As shown in sub-section 2.3.1, columnar ice was found beneath the granular ice in the crystal alignments of the lake ice collected at the downstream sites 5 and 6 in 2012/13. Here the origin of this columnar ice is discussed. According to Gow (1986) based on field observation and laboratory experiments, at quietly frozen lakes, where lake ice is formed under windless calm weather conditions, columnar structure can only be produced via a transition layer developed from granular ice which is formed by frazil ice aggregation, and in the formation of frazil ice the atmospheric seeding (e.g. snow particles and fog droplets) plays a crucial role in early stages. Thus it was suggested that under quiet conditions, granular ice and subsequent columnar ice formation cannot occur without atmospheric seeding. On the other hand, under turbulent lake-water conditions, it might be possible that frazil ice is produced in the water column without atmospheric seeding as in the case of sea ice or river ice. This frazil ice may develop into granular ice and subsequent columnar ice. (Hereafter we use “frazil ice” to refer to small discs of ice 1-4 mm in diameter and 1-100μm thick that forms in turbulent, slightly supercooled water (Kivisild, 1970; Martin, 1981).) To our knowledge, however, no clear evidence of this process has yet been reported in the case of lake water. Here the possibility that turbulent conditions work essentially to produce frazil ice and then develop the columnar ice layer found in the samples is examined.

For this purpose, more detailed vertical profiles of $\delta^{18}O$ were obtained around the boundary layer between snow ice and columnar ice for the ice samples collected at sites 3, 5 and 6, along with meteorological data at Abashiri and Memanbetsu observatories on the freezing date (11 December). This is because $\delta^{18}O$ is useful for distinguishing the origin of ice between lake water and atmospheric seeding. To do so, the ice samples were sectioned at 2 cm intervals and $\delta^{18}O$ was measured for each section. The ice at the center of the lake (site 3) was analyzed for comparison. The $\delta^{18}O$ results are shown in Figure 2.16. Whereas a sharp change in $\delta^{18}O$ is detected at the boundary between snow ice and congelation ice at site 3 (Fig. 2.16a), the change is more gradual and the granular ice just beneath the snow-ice layer takes a significantly higher value (-9.8 and -11.6‰) than snow ice (-12.4～-14.9‰) and even lake water (-11.9‰) at site 6 (Fig. 2.16c). At site 5, one section of granular ice just beneath the snow-ice layer takes a higher value (-9.9‰) than snow ice (-12.0～-14.4‰) and even lake water (-11.9‰), though the other section of the granular ice takes a low value (-13.1‰) (Fig. 2.16b). Considering the effect of fractionation during freezing, this suggests the possibility that this granular ice originated mainly from frazil ice produced in the lake water under turbulent conditions rather than solely by atmospheric seeding under calm conditions.

Next the meteorological conditions at the time of freezing (11 December) were examined. Air temperatures decreased from -0.5°C to -8.8°C at Memanbetsu (near site 1) and from -0.7°C to -3.5°C at Abashiri (near site 6) on this day (Fig. 2.17). Wind velocity varied between 1.4 and 5.5 m s^{-1} (average 3.2 m s^{-1}) at Memanbetsu, and between 3.1 and 7.7 m s^{-1} (average 5.4 m s^{-1}) at Abashiri. Snow accumulation was larger at Abashiri (10 cm d^{-1}) than at Memanbetsu (4 cm d^{-1}). Comparison of meteorological conditions between the two observatories suggests that although air temperature was more favorable to freezing at site 1 than at site 6, stronger wind and more snowfall near Abashiri may have generated more turbulent conditions, leading to higher production of frazil ice at sites 5 and 6. However, it should also be noted that snowy conditions at site 6 may have contributed to the supply of atmospheric seeding, and this effect may have been more important for the production of frazil ice than wind-induced turbulence. Even so, the fact that this granular ice takes a higher value of $\delta^{18}O$ than lake water shows that at least the freezing of lake water is essential to the formation of frazil ice even if the fallen snow particles worked as atmospheric seeding. It is plausible that wind-induced turbulence may have worked effectively to produce the granular ice with various directions of the *c*-axis near the surface.

There is another possible reason for the formation of columnar ice only at sites 5 and 6. Lake Abashiri is connected to the Sea of Okhotsk through downstream of Abashiri River. It is known that at high tide the sea water runs back to the lake through the river, which may generate turbulent conditions in the north eastern part of Abashiri Lake. However, unfortunately, due to lack of observational data, this effect cannot be examined quantitatively. At the observations in the 2014/15 and 2015/16 ice seasons, the thick/thin analysis of ice samples did not show the columnar structure, and water sampling at the freeze-up did not show frazil ice. To support the possibility that columnar ice may be produced through the formation of frazil ice without atmospheric seeding in turbulent lake water conditions, more detailed evidence will be needed in the future.

(a)

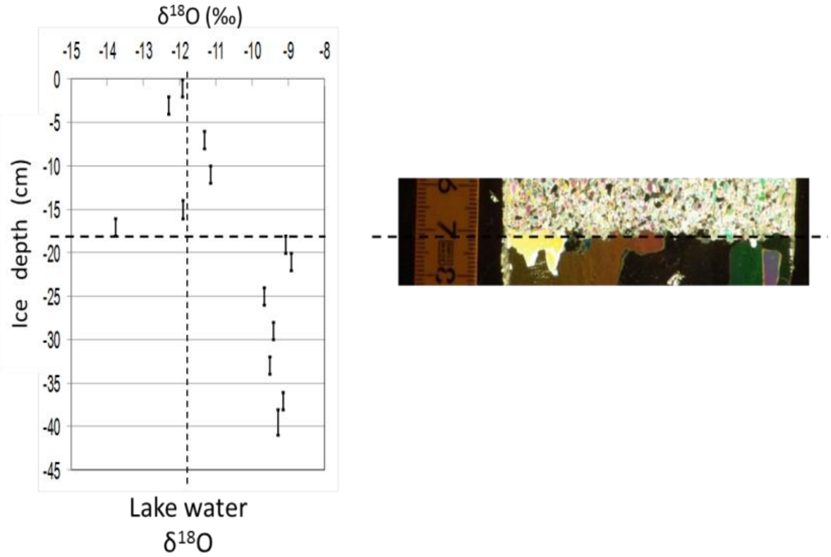
δ18O (‰)
-15 -14 -13 -12 -11 -10 -9 -8
0
-5
-10
-15
-20
-25
-30
-35
-40
-45
Ice depth (cm)
Lake water
δ18O

(b)

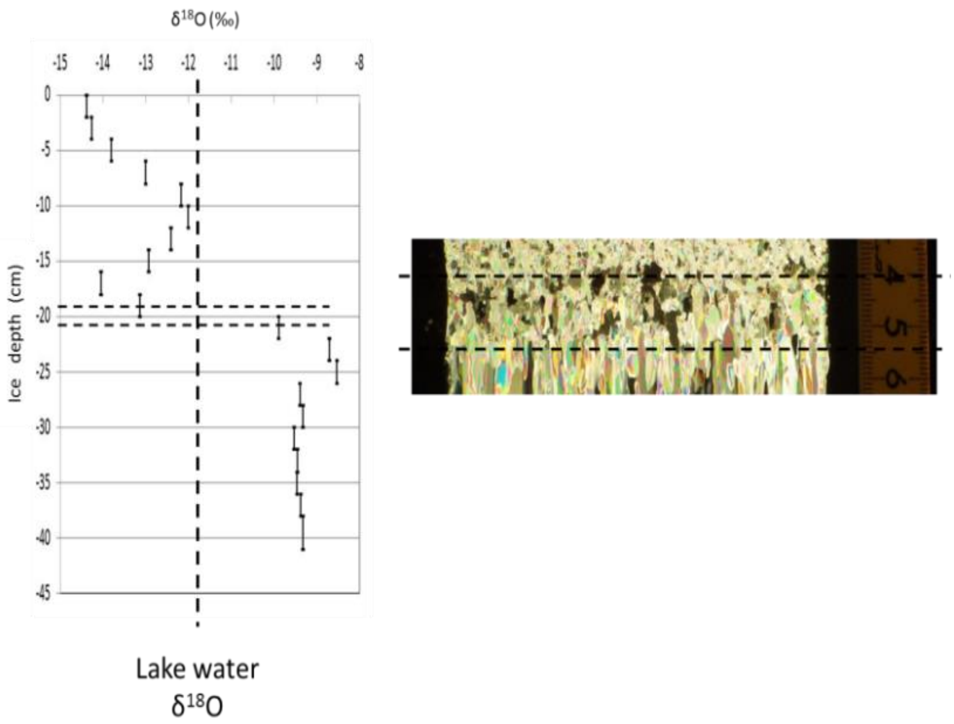
δ18O (‰)
-15 -14 -13 -12 -11 -10 -9 -8
0
-5
-10
-15
-20
-25
-30
-35
-40
-45
Ice depth (cm)
Lake water
δ18O

(c)

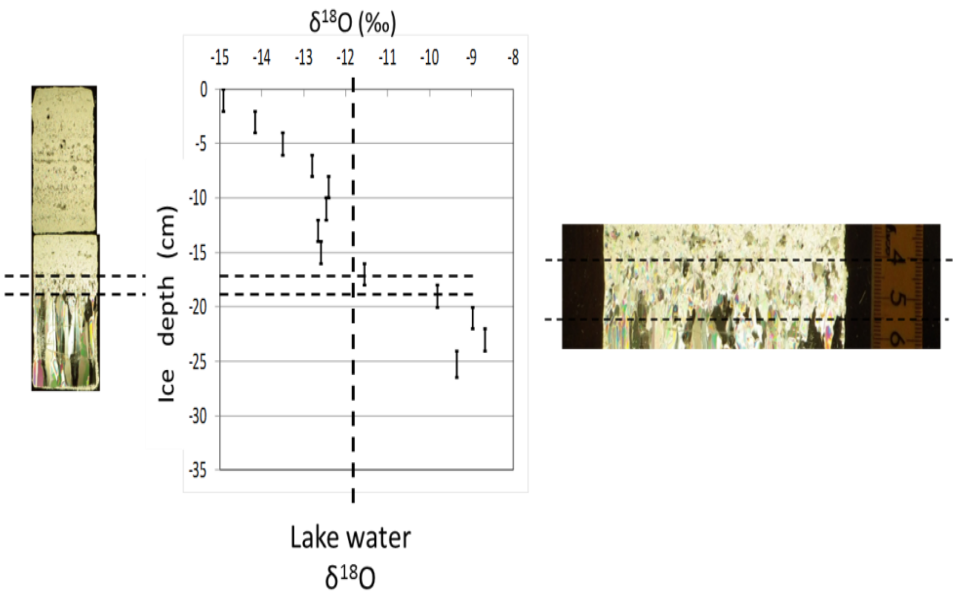

Fig. 2.16. Vertical $\delta^{18}O$ profiles of 2 cm intervals and magnified photographs near the boundaries. (a) site 3 on 18 February 2013; (b) site 5 on 19 February 2013; (c) site 6 on 18 January 2013. The full vertical thin section is shown on the left side for site 6 only (Fig. 2.16c), and the full sections for sites 3 and 5 on 18-19 February are shown in Figure 2.6. The boundaries between snow ice and congelation ice are shown by the horizontal dashed lines. The ambiguous boundaries for sites 5 and 6 are shown by two horizontal dashed lines. The vertical dashed lines show the $\delta^{18}O$ values of lake water.

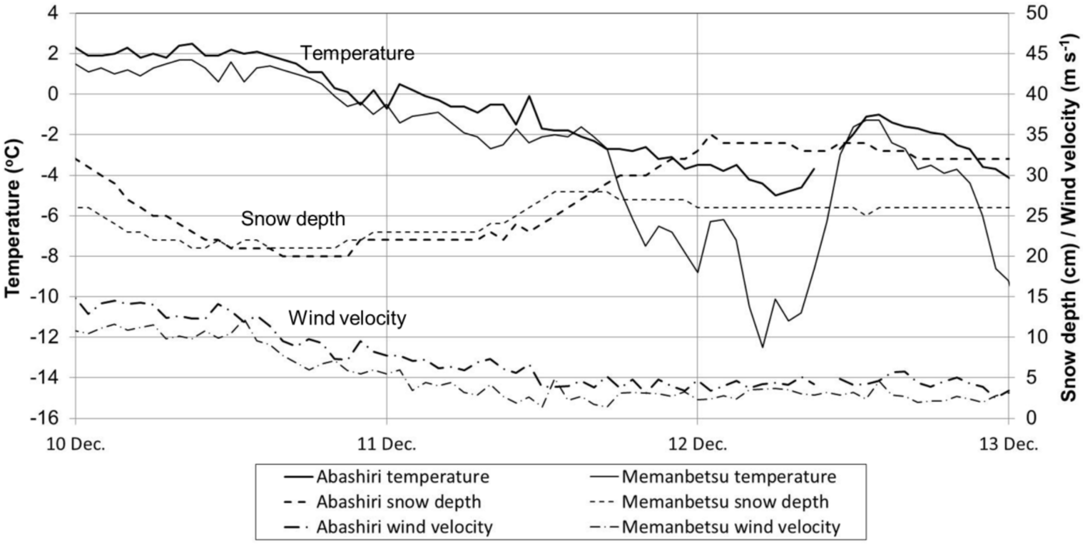

Fig. 2.17. Time series of air temperature, snow depth and wind velocity at the time of freeze-up from 10 December to 12 December 2012 at the Abashiri Meteorological Observatory and Memanbetsu Airport.

2.4. Summary of the observations

To clarify the properties of lake ice at mid-latitudes subject to moderate air temperature, heavy snow, and abundant solar radiation even in winter, field observations were conducted at Lake Abashiri in Japan for three winters.

(1) Meteorological conditions were quite different between these three ice seasons. Air temperature and snow depth were higher and deeper in the 2014/15 winter than in the two other winters. The freeze-up was relatively late in December 2015/16. On the other hand, snow depth on land around the lake was relatively deep on the freeze-up date in the 2012/13 winter, while quite small in the 2014/15 and 2015/16 winter.

(2) Commonly, lake ice was composed of whitish snow ice (SI) and translucent congelation ice (CI), and the contribution of SI to total ice thickness was significant:

29-73% for 2012/13, 40-60% for 2014/15 and 28-65 % for 2015/16.

(3) The heat flux (Q_w) from lake water to ice was estimated at 2 W m^{-2} from direct measurement of the temperature gradient within the CI layer and the thickness evolution of the CI layer at site 3 in 2012/13.

(4) Direct measurement was done on the freezing process of slush layer for lake ice by monitoring the temperatures in slush, dry snow and ice layers in 2015/16. It is found that the growth rate of SI in the slush layer is estimated to almost constantly 1.0 cm/d. Since the accumulation rate of snow is 20 cm/5d (4 cm/d) at most in 2015/16, these mean that in most cases the slush layer become frozen within a few days.

(5) The important physical parameters for SI growth; the water fraction of the slush layer ν and the thermal conductivity of snow ice k_{si} were estimated. However, to clarify the values of the parameters along with spatial and temporal variances, more observations or experiments are needed.

(6) The possibility of frazil ice formation was shown from the observation in 2012/13. However, to support the possibility that columnar ice may be produced through the formation of frazil ice without atmospheric seeding in turbulent lake water conditions, more detailed evidence will be needed in the future.

3. Thermodynamic ice growth model

3.1. Model concept

To understand ice growth processes at Lake Abashiri, a 1-D thermodynamic model was developed to calculate ice thickness evolution in the center of the lake (site 3). In the model, the estimated value of the heat flux from water and the meteorological data at the nearby observatories are used, along with the observational results for the density of snow and ice. Then, the snow compression rate during the transformation from snow to SI is parameterized to fit the model outputs to the observational results for SI thickness.

In the model, lake ice is assumed, based on observations, to be a horizontal uniform slab, composed of SI and CI with a snow cover. To calculate the growth of CI, the method of Maykut (1982) was followed, which is designed for relatively young Arctic sea ice, using the meteorological dataset obtained at nearby meteorological observatories. To calculate SI growth, it is ideal from the physical viewpoint to solve the heat conduction equation, as Saloranta (2000) did for ice growth in the Baltic Sea. Saloranta (2000) included the SI formation process in the model by applying the heat conduction equation to CI, SI and snow, and the heat budget equation to the slush refreezing as well as to the CI growth, assuming values for the density of the slush layer. Although overall model results showed good consistency with observations, a significant difference was found, depending on the year, which was caused by ambiguity in the SI formation process. Given that there is still uncertainty in the freezing process of the slush layer, including the slush formation speed, slush density and water fraction in the slush, here the following three assumptions, following Leppäranta and Kosloff (2000), are introduced.

(1) The slush layer freezes to form SI on time scales of a few days and then the freeboard recovers from negative to zero.

(2) Snow is compressed in the transformation into SI by a compression rate β, which is defined as the flooded snow layer thickness divided by the produced SI thickness.

(3) β is kept constant throughout the season.

In our model, β is a tuning parameter and is determined by fitting the model result to the observed SI thickness. Since, in the model, snow depth is given not by the in situ data but by the data obtained at the nearby meteorological observatories, the parameter β may include the effect of snow loss due to blowing snow and snow compaction (Sturm and Liston, 2003; Jeffries and others, 2005). The justification for a constant value of β is tested by examining the sensitivity of model outputs to β. Further details of the input data and the calculation method are described in the following subsections.

3.2. Input data

For the model input parameters, the meteorological datasets observed at the Abashiri Meteorological Observatory and Memanbetsu Airport are used, which are located about 10 km northeast and 9 km south respectively, from the central site of Lake Abashiri. Among the observation sites, site 1 is closer to Memanbetsu Airport and site 6 to Abashiri Meteorological Observatory. The central site 3 is approximately midway between these observatories (Fig. 2.1). While the datasets of T_a (air temperature), V_a (wind velocity) and H_s (snow depth on land) are available at both stations on a daily basis, Q_s (incoming solar radiation at the surface), C (cloudiness in tenths), r (relative humidity), and p (surface air pressure) were observed only at the Abashiri Meteorological Observatory. Therefore, to calculate ice thickness growth at site 3, T_a, H_s and V_a were inputted by taking the averages of two meteorological stations, and Q_s, C, r and p were given by the data observed at the Abashiri observatory. For H_s, the running means for 5 d were used to consider a time scale of a few days of SI formation, based on the assumptions. The sensitivity of the period of the running mean to the result will be discussed at the end of Subsection 3.4.1 The other input parameters and constants in this model are listed in Table 3.1.

The thickness, density and thermal conductivity were denoted by h, ρ and k, using subscripts i, si, ci and s for ice, snow ice, congelation ice and snow, respectively. γ (Eqn (14)) represents the critical ratio of snow depth to ice thickness that causes flooding of water due to isostasy, and was set to 0.37 from observational results of ρ_w = 1000 kg m^{-3}, ρ_i (the average of ρ_{ci} and ρ_{si}) = 890 kg m^{-3}, ρ_{ci} = 910 kg m^{-3}, ρ_{si} = 870 kg m^{-3} and ρ_s = 300 kg m^{-3}:

$$\gamma = (\rho_w - \rho_i) / \rho_s \quad (14)$$

Table 3.1. Model parameters and constants. Cited from Ohata et al. (2016a)

Parameter	Synbol	Value	Unit	Source
Congelation ice density	ρ_{ci}	910	kg m^{-3}	
Snow ice density	ρ_{si}	870	kg m^{-3}	
Snow density	ρ_s	300	kg m^{-3}	
Air density	ρ_a	1.3	kg m^{-3}	
Thermal conductivity of congelation ice	k_{ci}	2.07	W $m^{-1}K^{-1}$	Yen (1981)
Thermal conductivity of snow ice	ksi	2.07	W $m^{-1}K^{-1}$	Yen (1981)
Thermal conductivity of snow	ks	0.23	W $m^{-1}K^{-1}$	Yen (1981)
Specific heat of air	C_a	1004	J kg^{-1} K^{-1}	
Latent heat of freezing	L_f	3.34×10^5	J kg^{-1}	Yen (1981)
Latent heat of sublimation	L_v	2.84×10^6	J kg^{-1}	Yen (1981)
Surface emmisivity	ε	0.97		Omstedt (1990)
Transfer coefficient for latent heat	C_E	1.37×10^{-3}		Andreas and Makshtas (1985)
Transfer coefficient for sensible heat	C_H	1.37×10^{-3}		Andreas and Makshtas (1985)
Albedo, open water	α	0.07		Toyota and Wakatsuchi (2001)
Albedo, ice	α	0.3		Perovich (1998)
Albedo, snow	α	0.75		Pirazzini et al. (2006)
Transmittance, ice	I_0	0.18		Grenfell and Maykut (1977)
Transmittance, snow	I_0	0.0		Maykut and Untersteiner (1971)

3.3. Calculation method

3.3.1. Determination of the freeze-up date and the initial ice thickness

An important factor in calculating this model is the determination of the initial freeze-up date. Since there are no recorded data on this, the freeze-up date was determined from the surface heat budget and Moderate Resolution Imaging Spectroradiometer (MODIS) satellite images. In early winter, the lake surface water is cooled along with vertical convection with the loss of net heat flux to the air. Once the surface temperature reaches 4°C, however, the convection ceases and water surface temperature rapidly decreases to the freezing point. When the heat loss continues further, freezing starts at the water surface. Therefore, a spell of heat loss from the surface at low air temperature can be considered a good indicator for determining the freeze-up date. The heat budget (Q_x) at the surface was calculated by setting surface temperature

(T_{sfc}) to the freezing point (0°C):

$$Q_x = (1-\alpha)(1 - I_0)Q_s + Q_d - Q_b(T_{sfc}) + Q_h(T_{sfc}) + Q_{le}(T_{sfc}) \qquad (15)$$

$$Q_d = 0.7855\,(1 + 0.2232\,C^{2.75})\,\sigma_s T_a^4 \qquad \text{(Maykut and Church, 1973)}$$

$$Q_b = \varepsilon\,\sigma_s\,T_{sfc}^4$$

$$Q_h = \rho_a\,C_a\,C_H\,(T_a - T_{sfc})\,V_a$$

$$Q_{le} = 0.622\rho_a\,L_V\,C_E\,V_a\,(r\,e_{sa} - e_{sssfc}) / p$$

$$e_{sa} = aT_a^4 + bT_a^3 + cT_a^2 + dT_a + e$$

$$e_{ssfc} = aT_{sfc}^4 + bT_{sfc}^3 + cT_{sfc}^2 + dT_{sfc} + e$$

$$a = 2.7798202\times10^{-6},\ b = -2.6913393\times10^{-3},\ c = 0.97920849,$$

$$d = -158.63779,\ e = 9653.1925, \qquad \text{(Maykut, 1978)}$$

where α is the surface albedo, I_0 is the portion of solar radiation penetrating below the surface layer, Q_s is the incoming solar radiation at the surface, Q_d is the incoming longwave radiation, Q_b is the outgoing longwave radiation, Q_h is the sensible heat flux, Q_{le} is the latent heat flux, e_{sa} is the saturation vapor pressure in the atmosphere, e_{sssfc} is the saturation vapor pressure at the surface, ε is the surface emissivity, ρ_a is the air density, C_a is the air specific heat, C_H is the transfer coefficient for sensible heat, L_V is the latent heat of sublimation and C_E is the transfer coefficient for the latent heat. Here we set the freezing point as 0°C due to the salinity of the surface water (~0.1 psu).

According to the MODIS optical image (Fig. 3.1a) and the photographs taken from the top of Tento-san mountain (Elevation 200 m), located near Lake Abashiri (Fig. 2.1), no sign of freezing was detected on the lake on 7 December 2012, although air temperatures fell below 0°C at both Abashiri and Memanbetsu. On the other hand, according to the MODIS image (Fig. 3.1b) on 13 December, a large part of the lake was covered with snow, indicating that on that day freeze-up had already begun in widespread areas including site 3. Thus it is assumed that the freeze-up date was between 8 and 12 December.

The surface heat budget (Q_x) during this period was calculated based on these data. The result shows that while Q_x was positive (+33 W m^{-2}) on 10 December, it was negative (-32 W m^{-2}) on 11 December, and the air temperature stayed negative until 1 February. Therefore, the freeze-up date was assumed to be 11 December.

The initial ice growth amount (Δh_{ci}) was estimated from the heat balance equation at the bottom of the ice:

$$dh_{ci}/dt = (- Q_x - Q_w) / (\rho_i L_f), \tag{16}$$

where L_f is the latent heat of freezing. At the initial stage, both SI thickness (h_{si}) and snow depth (h_s) were set to 0 cm.

(a)

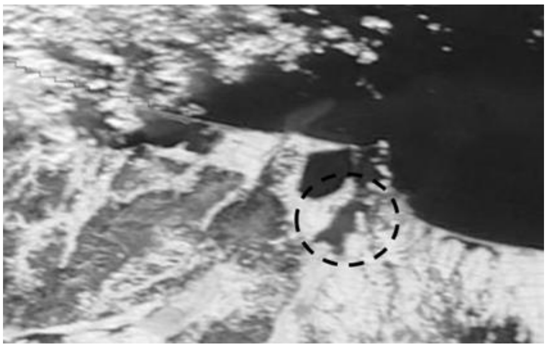

(b)

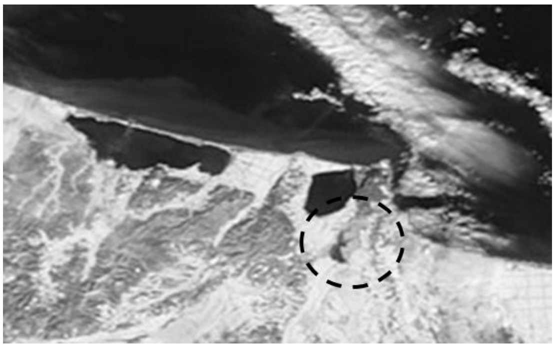

Fig. 3.1. MODIS Images (Terra/Aqua, copyrights: NASA) (a) 7 December 2012 and (b) 13 December 2012. The dashed circles show the location of Lake Abashiri. Cited from Ohata et al. (2016a)

3.3.2. Congelation ice growth and surface melting

We assume that the thermal inertia is negligible and the temperature gradient in the snow and ice is linear, since the phase delay of internal temperature variation forced by the diurnal surface temperature variation is estimated as ~13 h at most for the ice thickness of 60 cm, based on the calculation results of 1-D thermal conduction equation Eqn (12), which is sufficiently shorter than the time step (24 h) of our model. Thus the surface heat budget Q_0 is given by the following equations, assuming the upward conductive heat flux is conserved through the CI, SI and snow layers:

$$Q_0 = (1-\alpha)\,(1 - I_0)Q_s + Q_d - Q_b(T_{sfc}) + Q_h\,(T_{sfc}) + Q_{le}\,(T_{sfc}) + F_c\,(T_{sfc}) \qquad (17)$$

$$F_c = \frac{T_B\text{-}T_{sfc}}{h_s/k_s + h_{si}/k_{si} + h_{ci}/k_{ci}} \qquad (18)$$

where F_c is the conductive heat flux within ice, and T_B is the temperature of the ice bottom and is set to the freezing point. From Eqn (17), T_{sfc} is calculated at a daily step by setting Q_0 = 0, assuming that all the heat fluxes are balanced at the surface on a daily timescale.

(1) When T_{sfc} < 0°C, CI grows at the bottom.

The bottom accretion rate is given by

$$\mathrm{d}h_{ci} / \mathrm{dt} = (F_c - Q_w) / (\rho_i L_f) \qquad (19)$$

by substituting the calculated T_{sfc} into Eqn (18) and Q_w (= 2 W m^{-2}) into Eqn (19).

(2) When $T_{\mathrm{sfc}} \geq$ 0°C, melting occurs at the surface.

The snowmelt rate at the surface is calculated by substituting T_{sfc} = 0°C into Eqn (17):

$$\mathrm{d}h_s / \mathrm{dt} = -Q_0\,(0^{\circ}\mathrm{C}) / (\rho_s L_f)$$

After the snow had fully melted, the melting rate of SI and CI at the surface was calculated.

3.3.3. Snow ice growth

As shown in Section 2, SI constitutes a significant part of the total ice thickness at Lake Abashiri, and therefore the treatment of SI formation is essential to reproduce the evolution of ice thickness in the model. SI is formed through refreezing of the slush layer which is produced by the percolation of flooded lake water, rain or melting snow.

Since the air temperature stayed below 0°C at Abashiri throughout most of the winter, the major process producing the slush layer is assumed to be the flooding of the lake water in this model. For flooding to occur, the freeboard should become negative, i.e. the following inequality should be satisfied:

$$h_s / (h_{ci} + h_{si}) > (\rho_w - \rho_i) / \rho_s \equiv \gamma. \tag{20}$$

On assumption (1) in Section 3.1, the following isostatic balance equations should hold before (Eqn (21)) and after (Eqn (22)) the daily SI and CI growth:

$$\rho_i (h_{ci} + h_{si}) + \rho_s h_s = \rho_w (h_{ci} + h_{si}) \tag{21}$$

$$\rho_i (h_{ci}+h_{si}+\Delta h_{ci}+\Delta h_{si}) + \rho_s (h_s+ \Delta h_s) = \rho_w (h_{ci}+h_{si}+ \Delta h_{ci}+\Delta h_{si}) \tag{22}$$

where Δh_{ci}, Δh_{si} and Δh_s denote the increase in the thicknesses of CI, SI and snow respectively, on a daily basis. On the other hand, the relation between Δh_{si} and Δh_s is expressed by Eqn (23) from assumption (2), (3):

$$\beta = (\Delta H_s - \Delta h_s) / \Delta h_{si} \tag{23}$$

where ΔH_s denotes the increase in the snow depth at meteorological observatories on a daily basis. By solving Eqns (21), (22) and (23), Δh_{si} and Δh_s can be expressed by Eqns (24) and (25) respectively:

$$\Delta h_{si} = 1 / (\beta + \gamma)\, \Delta H_s - \gamma / (\beta + \gamma)\, \Delta h_{ci} \tag{24}$$

$$\Delta h_s = \gamma / (\beta + \gamma)\, \Delta H_s + \beta \gamma / (\beta + \gamma)\, \Delta h_{ci} \tag{25}$$

Since Δh_{ci} is calculated by Eqn (19) and ΔH_s is given by the data at the meteorological observatories, Δh_{si} and Δh_s can be obtained from these equations as a function of β. By integrating these values, SI thickness and snow depth can be estimated.

3.4. Model results and model validation

3.4.1. Optimal value of β for the 2012/13 winter

In this model, determination of a tuning parameter β is essential to reproduce the ice thickness evolution. Therefore, the optimal value of β was first sought. While h_{si} and h_s decrease with the increase in β, h_{ci} increases due to reduction of the insulating effect of snow. Judging from the fit of the calculated h_{si} to the observational data, β was determined as 2.0, larger than the β value in Finland of ~1.5 (Leppäranta and Kosloff, 2000). This may be due to an overestimation of ΔH_s. Although ΔH_s was calculated from the data obtained at nearby meteorological observatories, in reality it might be reduced on the lake due to snowdrift induced by strong wind. If this is the case, the larger value for β than that used by Leppäranta and Kosloff (2000) appears to be reasonable.

The time series of h_i (total ice thickness), h_{ci}, h_{si} and h_s calculated at site 3 are shown in Figure 3.2a and Table 3.2. Model outputs (observational results) are 17 (17.5) cm and 22 (23) cm for h_{ci}, 16 (19.5) cm and 23 (19) cm for h_{si}, and 15 (18) cm and 17 (26) cm for h_s on 17 January and 18 February respectively. Thus h_{ci} and h_{si} showed good agreement with the observations, with an RMSE of 0.8 cm and 3.8 cm respectively, although h_s was predicted to be 3-9 cm thinner than the observations, with an RMSE of 7.6 cm. The model predicted 11 April as the break-up date, which almost coincides with the dates between 12 and 14 April speculated from MODIS images and photographs. The slightly earlier model prediction compared with MODIS imagery may be attributed to the fact that the increase in ice thickness due to the refreezing of melted snow was not be taken into account, since the refreezing of melted snow might have occurred in late winter or spring.

Here, an error analysis of model simulations compared with field observations was done for the variability in β (Table 3.3). For a β value of 1.8, h_{ci}, h_{si} and h_s had an RMSE of 1.5 cm, 4.1 cm and 6.7cm compared with observations. For β of 2.2, h_{ci}, h_{is} and h_s

had an RMSE of 0.5 cm, 3.8 cm and 7.2cm. Thus the variability in β leads to no significant difference in the estimated ice thickness from the result obtained with an optimal value of 2.0. The break-up date was 13 April for β = 1.8 and 11 April for β = 2.2, almost the same as the model result (11 April) and the real break-up date (13 April). Therefore, the sensitivity of model outputs to β is considered to be small. This supports the optimal constant value (2.0) of β.

As shown in Section 2, the ice at site 6 was thinner than at the other sites in 2012/13. To find out why, the effect of different meteorological conditions at site 6 on the ice thickness evolution was examined, using the meteorological data at Abashiri Observatory instead of the average of Abashiri and Memanbetsu datasets. As a result, it was found that if Q_w of 2 W m^{-2} was used for site 6 as for site 3, the calculated h_{ci} showed a significantly larger value than observations (Fig. 3.2b). This may be because site 6 is situated near the lake output connecting to the sea via a river, which may induce the vertical mixing of lake water and more heat flux transferred from water to ice. If a higher value of Q_w (6 W m^{-2}) was used for site 6, the model output (h_{ci} = 9.0 cm) showed much better agreement with observations (8.5 cm) on 18 January.

Finally the sensitivity to the running mean period used for the input parameter of *Hs* is discussed. In this model, *Hs* was obtained from the daily meteorological snow depth data by taking a 5 d running mean (the day and 4 d ahead) to take into account the time scale required for the formation of SI, including the water filtration into snow layer and freezing of slush layer (Saloranta, 2000). However, since the time scale is expected to depend much on the situation, the validity should be checked. For this purpose, the change of outputs for the periods of 3 and 7 d was examined. As a result, it was confirmed that the calculated total thickness differed by <= 2 cm and the break-up dates were the same as those calculated with a 5 d running mean. These results indicate that running means for 5 d are valid and stable for this practical model simulation.

Table 3.2. Comparison between model outputs and observational results (2012/13). Cited from Ohata et al. (2016a)

	Model	Observation.
17 January		
Tota ice thickness (cm)	33	37
Snow ice thickness (cm)	16	19.5
Congelation ice thickness (cm)	17	17.5
Snow depth (cm)	15	18
18 February		
Total ice thickness (cm)	45	42
Snow ice thickness (cm)	23	19
Congelation ice thickness (cm)	22	23
Snow depth (cm)	17	26
Freeze up date	11 December	8-12 December
Break up date	11 April	12-14 April

Table 3.3. Errors of simulation outputs to observation (2012/13). Difference of break-up date was calculated from 13 April 2013, the middle date of the range speculated from MODIS images. Cited from Ohata et al. (2016a)

β	h_{ci} RMSE	h_{si} RMSE	h_i RMSE	h_s RMSE	Break-up date difference
	cm	cm	cm	cm	days
1.8	1.5	4.1	3.8	6.7	0
2.0	0.8	3.8	3.8	7.6	2
2.2	0.5	3.8	3.9	7.2	2

(a)

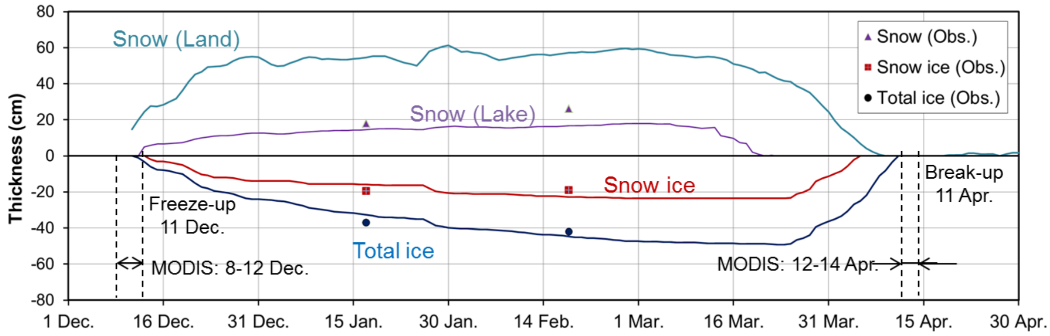

(b)

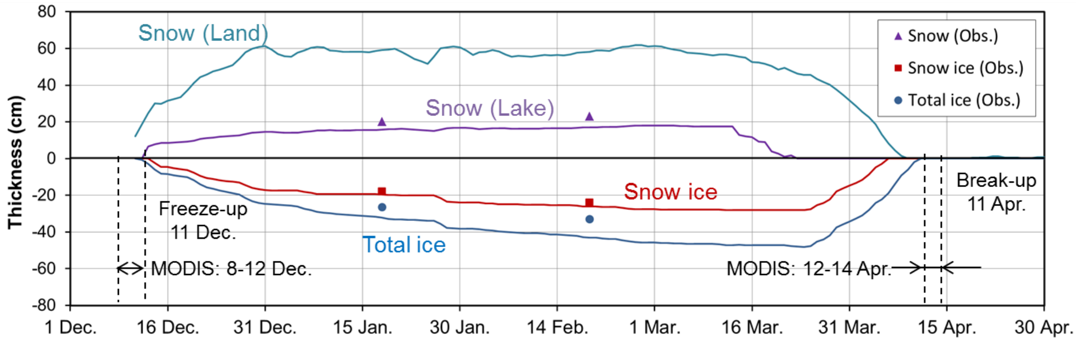

Fig. 3.2. Model results of the thickness evolution of total ice, SI and snow, with observations shown by purple triangles (snow depth), red squares (SI) and blue solid circles (total ice thickness) for (a) site 3 and (b) site 6. The light blue curve indicates the snow depth on land obtained from the daily meteorological snow depth data by taking a 5 d running mean (the day and 4 d ahead). The purple, red and blue curves show the snow depth on the lake, SI thickness and total ice thickness predicted by the model respectively. Q_w = 2 W m^{-2}, β = 2.0 and γ = 0.37 were used for calculation. Freeze-up dates used in the model and break-up dates calculated by the model are indicated in the figures, along with those estimated with MODIS images (vertical black dashed lines). Modified from Ohata et al. (2016a)

3.4.2. Model validation for the 2014/15 and 2015/16 ice seasons

To examine the validity of the model developed for the 2012/13 season, the time series of h_i, h_{si}, h_{ci} and h_s at site 3 were calculated in the same way with the same value of β for the 2014/15 and 2015/16 ice seasons. The calculated results are shown in Figure 3.3, along with the results for 2012/13. It is found that overall h_{ci}, h_{si} and break-up dates show a good agreement with the observed values except for h_{si} in January 2016 and h_i in March in both years. The discrepancies between model and observational results were 4 cm for h_i, 3 cm for h_{si}, 1 cm for h_{ci}, and 12 cm for h_s in February and 4 d for break-up date in 2015, and 0 cm, 4 cm, -4 cm, 6 cm and 1 d, respectively, in 2016. These results are almost the same as the values of -3 cm, -4 cm, 1 cm, 9 cm and 2 d in 2013 (Fig. 3.3). Thus it is suggested that this model can reproduce the observed ice thickness evolution and break-up date well to some extent under different meteorological conditions, and to examine the interannual variability of these parameters with the model is allowed.

As for the strong discrepancy (11 cm) for h_i in January 2016, in light of the fact that the slush layer in snow amounted to as thick as 22 cm, the model assumption (1) in Section 3.1 did not apply in this case, that is, the flooded snow layer was not converted to SI on a few days' time scale. On the other hand, the fact that no slush layer was observed on 19 February 2016 shows that slush layer was converted to snow ice completely during this period. Thus an opportunity to examine the formation process of SI in details was provided from the temporal evolution of temperature profile. The detail was discussed in Section 2.3.

As for the discrepancy (15 and 7 cm) for h_i in March, in light of the fact that it is attributed mainly to the underestimation of h_{si} (Fig. 3.3) and air temperature sometimes exceeded 0^{o}C in March (Fig. 2.4), the omission of the increase in h_i due to the refreezing of melted snow in the model is presumably most responsible. This also explains the reason for somewhat earlier break-up prediction in the model than the observed dates. Despite this deficiency, it is noted that the predicted break-up date almost coincides with the observation within 4 days. This result suggests that break-up date may be controlled more by meteorological conditions rather than by ice thickness.

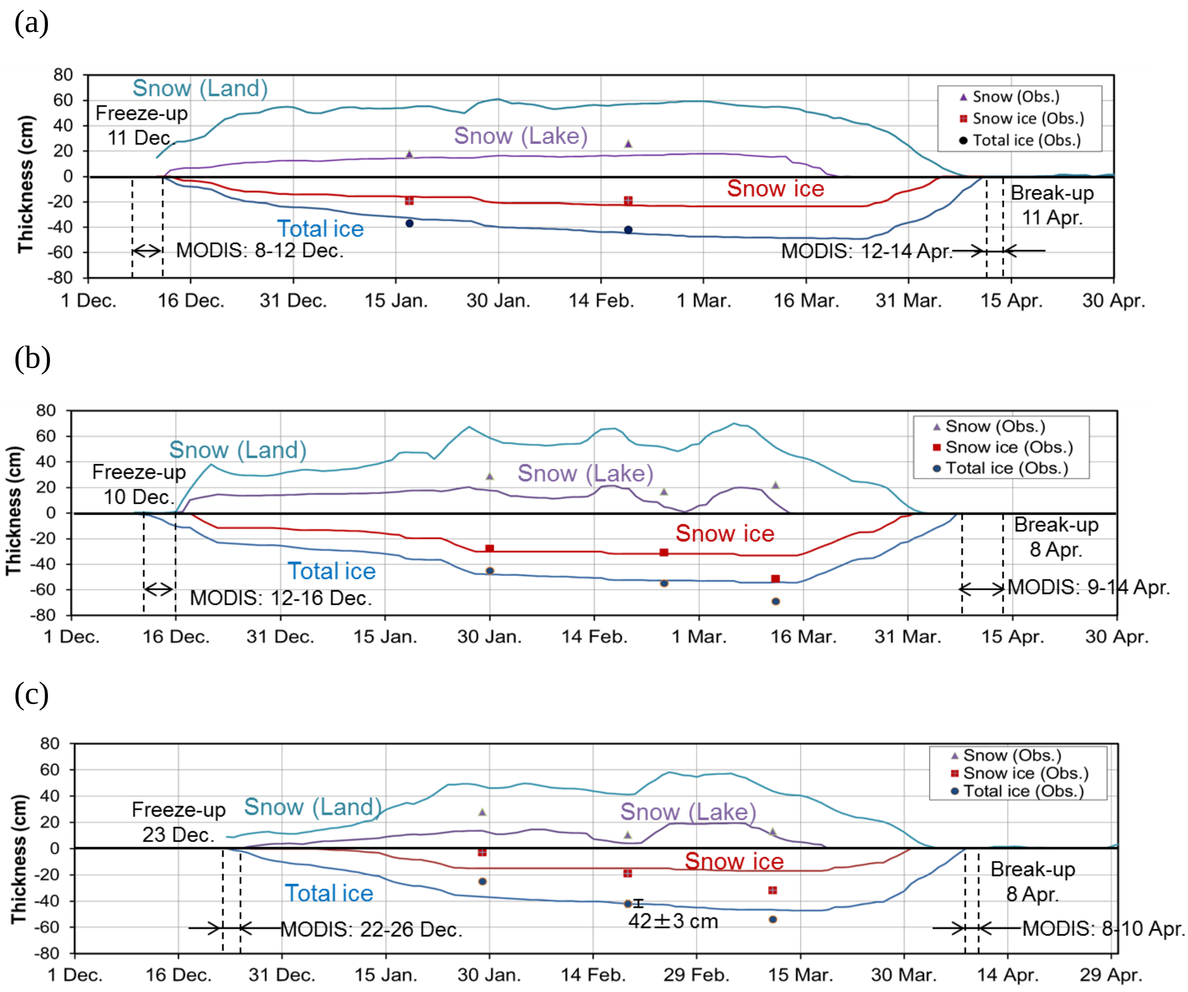

Fig. 3.3. Model results of thickness evolution of total ice, SI and snow with observations shown by triangles (snow depth), squares (SI) and solid circles (total ice thickness) in (a) 2012/13, (b) 2014/15 and (c) 2015/16. The light blue curve indicates the snow depth on land obtained from the daily meteorological snow depth data by taking a 5 d running mean (the day and 4 d ahead). The purple, red and blue curves show the snow depth on the lake, SI thickness and total ice thickness predicted by the model, respectively. Freeze-up dates used in the model and break-up dates calculated by the model are indicated, along with those estimated with MODIS images (vertical black dashed lines). The error bars and numerals in Figure 3.3(c) show the spatial variability of total ice thickness estimated by measuring thickness at 9 points within a 10 m x 10 m grid on 19 February 2016. Modified from Ohata et al. (2016a, 2016b)

4. Examination of roles of snow in ice thickening processes

4.1. Numerical experiments using the model

Since the validity of the model was confirmed to some extent, here we investigate the roles of snow in the ice-thickening processes quantitatively with this model by examining the sensitivity of the predicted ice thicknesses to snow. For this purpose, numerical experiments for calculating the thickness evolution were conducted under the meteorological conditions of these three ice seasons for the following three cases: where (1) snow accumulates accompanied with SI formation (control run), (2) snow accumulates without SI formation (i.e. CI only) and (3) no snow accumulates. Since the meteorological conditions were quite different among the three ice seasons, as described in Section 2.2, the comparison of the results is expected to serve to check the role of snow. Considering that the accuracy of the predicted ice thickness is highest in February, the results for February are focused on. The results are shown in Figure 4.1. As shown in the previous section, it is confirmed that case 1 is in good agreement with observations for all the three winters. Therefore, the roles of snow are examined by comparing the results individually for each winter.

Firstly, to investigate a case with similar snow depth but different air temperature, the results obtained for the 2012/13 and 2015/16 winters are compared. Here, the freeze-up date was 12 d later in 2015/16 than in 2012/13. For case 3 (no snow), the difference in h_{ci} is (68 – 56) 12 cm (Fig. 4.1). This is considered to be caused by higher air temperature and later freeze-up in 2015/16. Note that for case 2 (snow included, no SI growth), h_{ci} is by 10 cm thicker in 2015/16 than in 2012/13, contrasting to case 3. This contrast is attributed to the thermal insulation effect of snow because significantly less h_s at the initial ice growing period in the 2015-2016 winter (Fig. 3.3). For case 1 (control run), although the difference in h_{ci} still remains as case 2, the difference in h_i is reduced to only 3 cm (= 45-42) by the increase in h_{si} and the difference in h_i found for case 3 (no snow) was reduced by about 75% in the presence of snow. This indicates that the difference in h_i which might have been produced in the absence of snow was significantly mitigated through the thermal insulation effect of snow and the SI formation.

Next, to investigate a case of both different snow depth and air temperature, two comparisons were made; (i) between the 2012/13 and 2014/15 winters, and (ii) between the 2014/15 and 2015/16 winters. As for (i), the result for case 3 shows that the difference in *hi* on 20 February is 13 (= 68-55) cm. For case 2, h_i is significantly thinner than that for case 1 and is thicker in 2014/2015 than in 2012/13 due to the thermal insulation effect of snow. In this case, however, h_{ci} for case 1 was calculated to be somewhat thinner in 2014/15 than in 2012/13. For case 1, this slight difference was compensated by higher SI growth in 2015 (32 cm) than in 2013 (23 cm). As a result, h_i became rather thicker in 2014/2015 than in 2012/13, although the difference in h_i was reduced about by half (45-52 = -7 cm) compared with that for case 3 (13 cm).

As for (ii), the result for case 3 shows that the difference in h_i on 20 February is only 1 cm (= 56-55). This small difference in spite of the lower temperature in 2015/16 is attributed to a later freeze-up date. On the other hand, for case 2, h_{ci} is predicted to be thinner by 7 cm in 2014/15 because the thermal insulation effect of snow worked effectively due to thicker snow depth in this season. This can explain the difference in h_{ci} calculated for case 1, where h_{ci} is thinner by 7 cm in 2014/15 than in 2015/16. However, h_i for case 1 is calculated to become thicker via larger SI conversion in

2014/15. This suggests the importance of SI formation over the effects of freeze-up date or air temperature to determine h_i in February.

To examine the effect of the snow depth change on ice thickness, based on the meteorological condition in the 2012/13 ice season, additional numerical experiment was carried out by changing the input value of snow depth on land (*Hs*) artificially, under the same meteorological conditions except for *Hs*. The results are shown in Figure 4.2. From the figure, when snow depth is small enough, CI decreases rapidly with the increase in snow depth due to the thermal insulation effect of snow without SI formation. However, when snow depth exceeds a critical value which induces flooding of lake water, SI increases rapidly and the decreasing rate of CI with *Hs* becomes slower, since a part of snow on ice is consumed in the SI formation process and the thermal insulation effect is suppressed. Resultantly total ice thickness tends to increase with the increase in *Hs*.

Thus it is indicated from all these results that while snow works to mitigate the variability of *hi* caused by different air temperature, SI formation plays a more essential role in determining h_i. In addition, comparison of the results between 2012/13 and 2015/16 suggests that although the timing of snowfall events affects h_{ci} due to the thermal insulation effect at the initial stage, h_i in February depends more on the SI growth. Schematic pictures which explain how snow works to mitigate the variability of *hi* through the thermal insulation effect and the SI formation under different meteorological conditions are shown in Figure 4.3: the same snow amount and different air temperature (Fig. 4.3a) and different snow amount and the same air temperature (Fig. 4.3b).

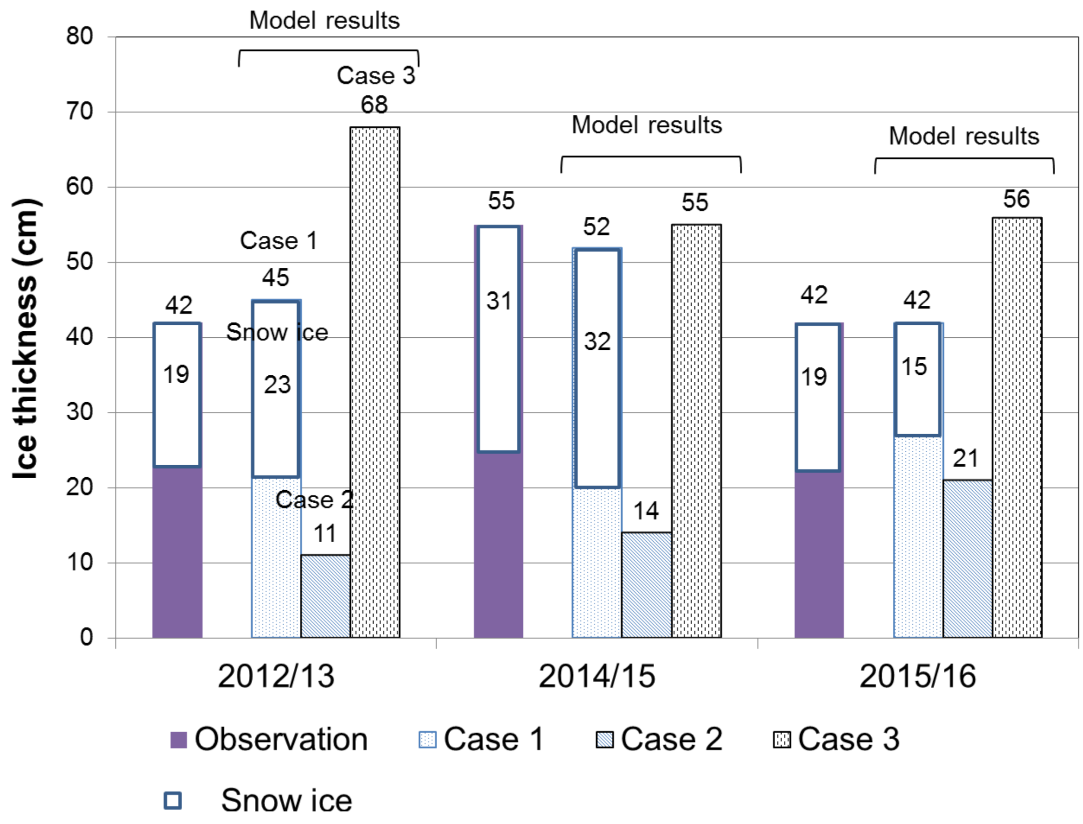

Fig. 4.1. Observations of ice thickness (at site 3 on 19 February 2013, 24 February 2015 and 19 February 2016) and the ice thicknesses on 20 February 2013, 2015 and 2016, predicted by the model for three cases; 1) snow accumulates with SI formation (control run), 2) snow accumulates without SI formation, 3) no snow accumulates.

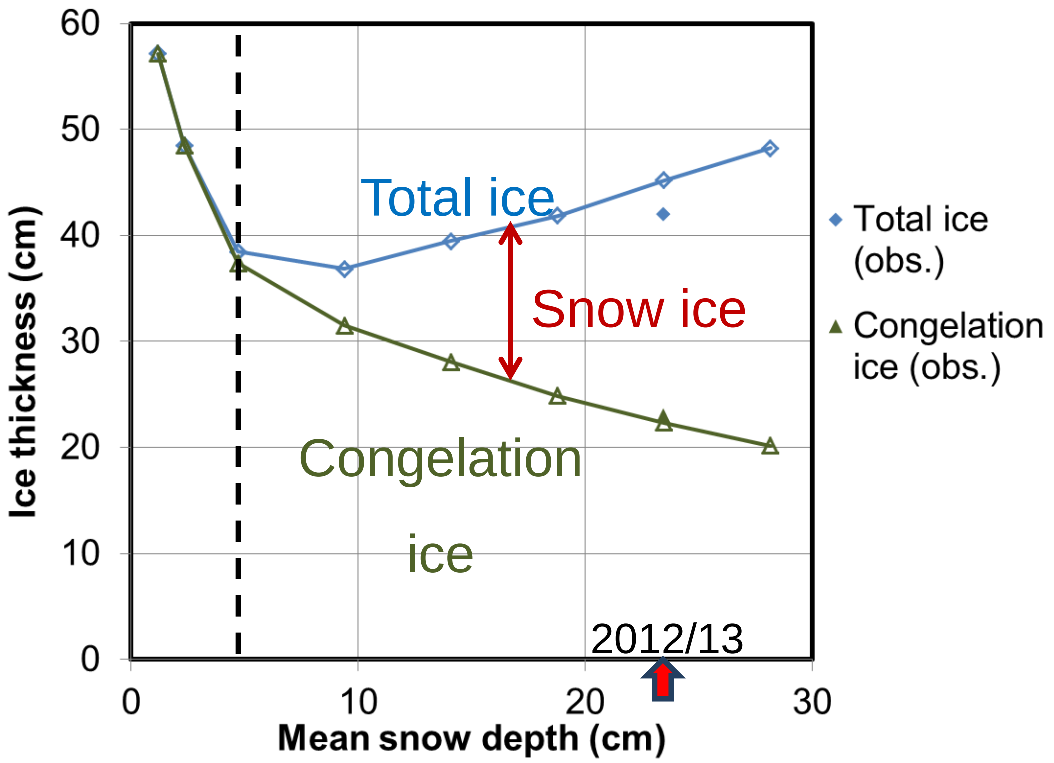

Fig. 4.2. The thickness of total ice and congelation ice on 20 February as a function of a fixed snow depth calculated with the model. Mean snow depth is given by the mean snow depth increment from freeze-up date to 20 February. The red thick arrow indicates the observed snow depth for 2012/13. Snow depths were varied from the meteorological data for 2012/13. The other meteorological conditions (the air temperature, wind velocity, incoming solar radiation, cloudiness, relative humidity and surface air temperature) correspond to the datasets at meteorological stations. Blue filled diamond and green triangle show the observations of thickness of total ice and congelation ice. Unfilled diamond and triangle show the calculated results of thicknesses of total ice and congelation ice. The difference between the thicknesses of total ice and congelation ice shows the snow ice thickness. Snow ice forms in the deeper snow depth than that indicated by vertical black dashed line.

(a)

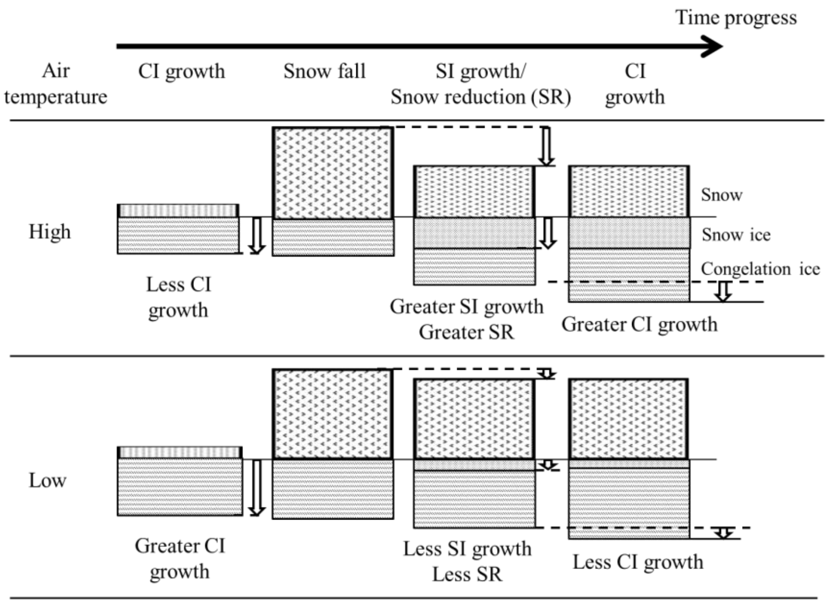

(b)

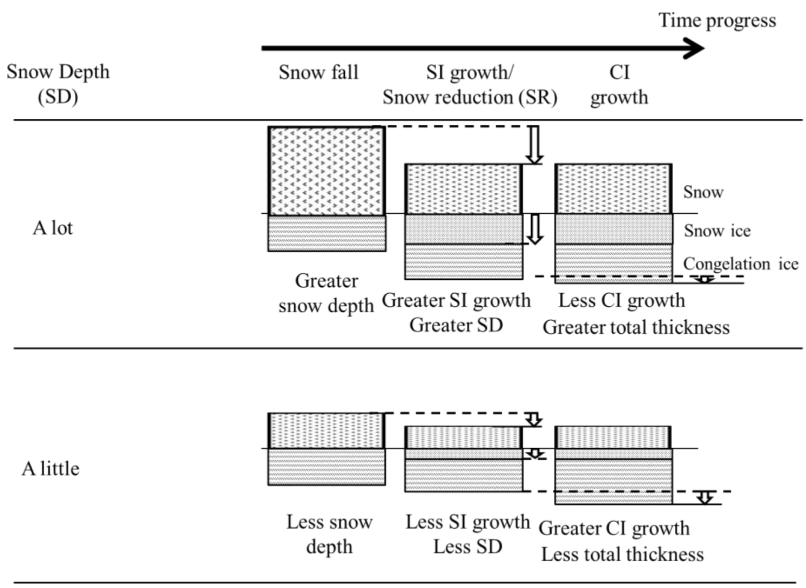

Fig. 4.3. A schematic picture showing the effect of snow and snow ice formation on the lake ice thickness for (a) the same snow amount and the different air temperature (cited from Ohata et al., 2016a), and (b) the different snow amount and the same air temperature. In Figure 4.3a, the growth of SI and CI after snow accumulation mitigates the difference of CI thickness caused by different air temperature. In Figure 4.3b, the growth difference between SI and CI yields the difference of total ice thickness, although CI growth slightly mitigates the difference caused by SI thickness.

4.2. Validation for the past 16 years with MODIS images

In Section 4.1, the roles of snow in the ice thickening processes were examined based on the field measurements conducted for recent three winters. In this section, the results obtained in the previous section will be examined further with the model under various meteorological conditions for the past 16 years (2000/01–2015/16) when MODIS satellite images are available to determine the freeze-up and break-up dates with an accuracy of a few days.

The evolutions of h_i, h_{ci}, and h_{si} were calculated with our model in the same way by inputting the meteorological data records at Abashiri. When determining the freeze-up date, although MODIS images serve to detect the freeze-up state efficiently in snow-covered conditions, they do not work well in no snow conditions due to the low albedo of lake ice. In such a case, air temperature was used to judge freeze-up date. The predicted h_i for each year was compared with the ice thickness records obtained in the nearshore region of Yobito from 2005/06 to 2015/16 for validation. The result for 15 January and 15 February is shown in Figure 4.4. The figure shows that although the absolute values of calculated h_i are smaller by 10-20 cm than the observed thicknesses, they are almost well correlated, with correlation coefficients (r) of 0.64 (p = 0.04) for 15 February and 0.52 (p = 0.10) for 15 January. When taking into account the difference in water depth between site 3 (16 m) and the nearshore region (~2 m), it is considered that this result supports the validity of the calculated h_i in the model to some extent. Therefore, the roles of snow in the thickening processes likewise for this period are examined, based on the model results.

The calculated h_i on 15 February ranged between 33 cm and 54 cm with an average of 42 cm, and showed a good (and statistically-significant) correlation with h_{si} with r =

0.78 (p < 0.01) (Fig. 4.5a). On the other hand, h_i had almost no correlation with h_{ci} (Fig. 4.5b) and h_{si} showed a significant negative correlation with h_{ci} with r = -0.65 (p < 0.01) (Fig. 4.5c). These results indicate that the SI formation certainly works to mitigate the variation of h_{ci} caused by different meteorological conditions and essentially control the total thickness (h_i). To elucidate the effect of snow on h_i more, the correlations of h_i on 15 February with mean air temperature and snow accumulation (both from the freeze-up date to February 15) were examined (Fig. 4.6). This figure shows that h_i is much better correlated with snow accumulation (r = 0.54, p = 0.03) than with mean air temperature (r = -0.37, p = 0.16). These results support those obtained in Section 4.1 and emphasize the importance of the roles of snow in determining h_i.

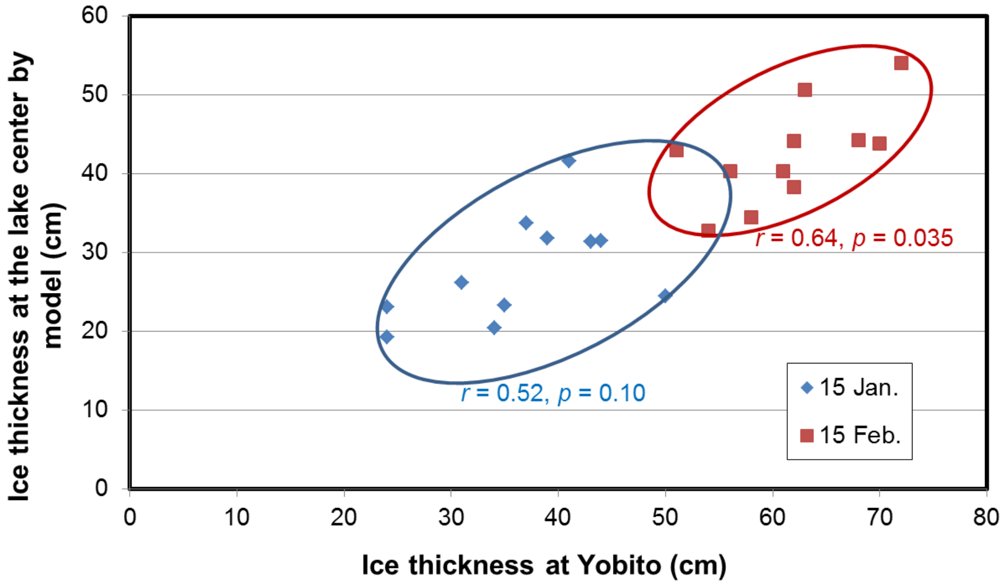

Fig. 4.4. The correlation coefficients between lake ice thickness model results and observations at Yobito on 15 January and February for 2005/06-2015/16. Diamonds and squares show ice thicknesses on 15 January and February respectively. Correlation coefficients and p-values are shown by “r” and “p” in the figure. Yobito data are from the Abashiri tourism association. Modified from Ohata et al. (2016b)

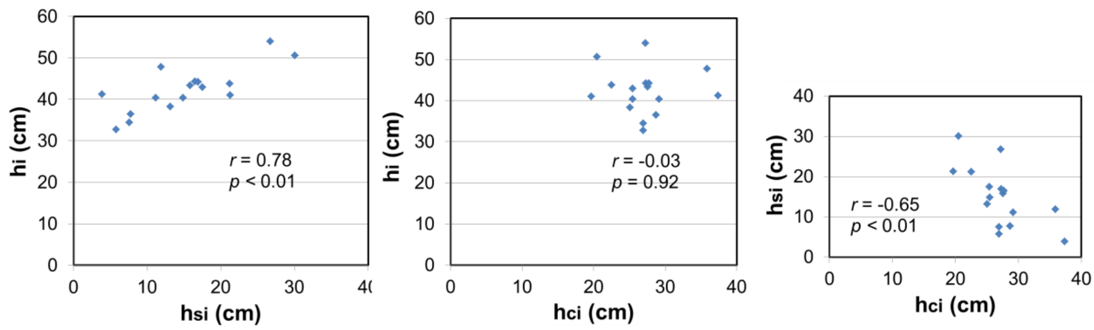

Fig. 4.5. The relationships between total ice thickness (h_i), SI thickness (h_{si}) and CI thickness (h_{ci}) on 15 February for 16 years: (a) h_i vs. h_{si}, (b) h_i vs. h_{ci} and (c) h_{si} vs. h_{ci}. Correlation coefficients and *p*-values are shown by "*r*" and "*p*" in the figure.

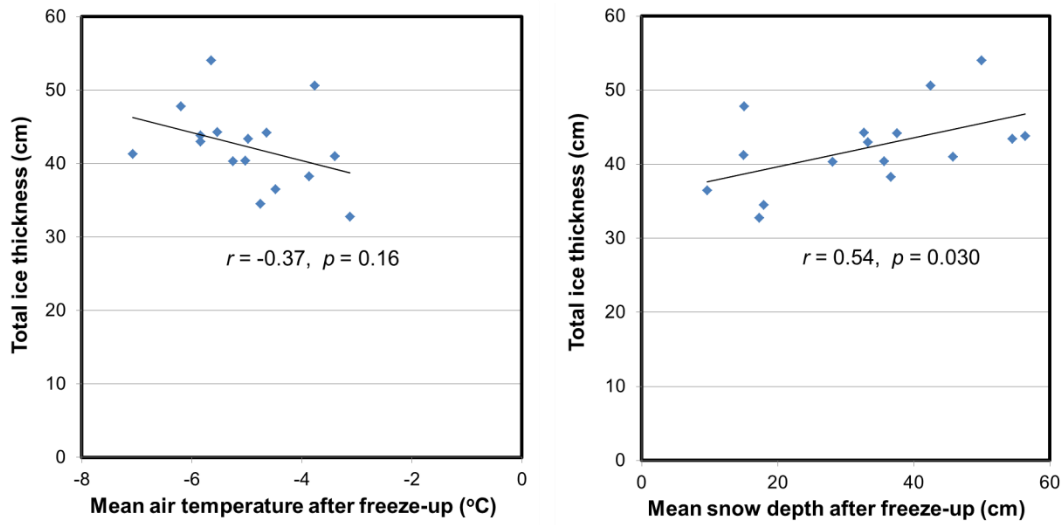

Fig. 4.6. The relationships between total ice thickness on 15 February and (a) mean air temperature or (b) mean snow depth from freeze-up date to 15 February for 2000/01-2015/16. The solid straight lines are the regression lines of best fit. Correlation coefficients and *p*-values are shown by "*r*" and "*p*" in the figure.

5. Ice phenology for Lake Abashiri

5.1. Estimation of the ice phenology parameters for the past 55 years

In this section, aspects of the ice phenology and their long-term trends at Lake Abashiri are examined with the model, and compared with other lakes in the northern hemisphere (Benson et al., 2012), in relevance to the climatological variability of air temperature and snow depth. To do so, the calculation of h_i was extended for the period 1961/62 to 1999/2000 (39 years) during which the meteorological datasets at Abashiri are available. In this calculation, air temperature was used to determine the freeze-up date for each year as proxy data. The method to calculate h_i, h_{ci}, and h_{si} is the same as that described in the previous sections.

Here the methodology to determine the freeze-up date from the air temperature data is described (Fig. 5.1). To develop the method, firstly 'the mean air temperature on freeze-up date' (T_{af}) determined with MODIS images for the 16-year period 2000 to 2015 and observations was calculated. In estimating T_{af}, to avoid the temporary fluctuation of air temperature on a daily time scale, the regression of the temperature decrease from November to December as a function of time at Abashiri was obtained and then the air temperature on the freeze-up date for individual years was calculated. By taking the average, T_{af} was estimated to be -1.44^{o}C. This method and criterion were applied to determine the freeze-up date for the extended 39 years. Yet if the surface heat budget was calculated to be positive (surplus heat at the surface), the freeze-up date was delayed until the surface heat budget became negative continuously. This method is considered to be useful, since the freeze-up dates determined in this method coincided with the results estimated from MODIS images within a difference of 4 days for 12 years (86%) among 14 (for the remaining 2 years, judged from air temperature). By combining the results for these 39 years with those of the previous section, the data set of h_i and break-up dates for the past 55 years (1961/62 to 2015/16) could be obtained.

The time series of the break-up dates calculated for the 55-year period were shown with the freeze-up dates in Figure 5.2. In the figure, the break-up dates estimated from MODIS images for the most recent 16 years are also plotted with error bars. It is found that overall the dates predicted with the model are consistent with the MODIS observation, which allows us to examine the climatology and log-term trend in break-up dates. According to Figure 5.2, the break-up date is estimated to be 17 April on average and shows a significant negative trend of -1.71 d/decade ($p < 0.01$) for 55 years, i.e. the break-up date has become earlier by 9 days for this half century. This trend is comparable with the mean trend of -1.9 d/decade for 75 lakes in the Northern Hemisphere for the 30-year period 1975/76 to 2004/05 reported by Benson et al. (2012). On the other hand, the freeze-up date is estimated to be 12 December on average and did not show a significant trend for the 55 years. The estimated slope of regression line, +0.74 d/decade (not significant), is smaller than the mean value of 1.6 d/decade reported by Benson et al. (2012). The ice-cover duration is estimated to be 127 days and shows a significant negative trend of -2.4 d/decade ($p < 0.01$). This trend is smaller than the mean value of -4.3 d/decade reported by Benson et al. (2012).

As for calculated ice thickness on 15 February, the averages of *hi*, *hsi*, and *hci* are estimated to be 43 cm, 16 cm, and 27 cm, respectively. It is notable that while mean *hi* is comparable with that observed in Finland (44 cm; Leppäranta, 2015), the fraction of *hsi* (37%) is larger than 30% in Finland. A significant decreasing trend (-1.4 cm/decade, $p = 0.01$) can be seen in *hi* for these 55 years (Fig. 5.3). The correlations of h_i with h_{si} and h_{ci} are shown to be both positive unlike the results of Section 4.2 (Fig. 5.4).

However, it is noticed that h_i is much better correlated with h_{si} than h_{ci}, and h_{si} is weakly but negatively correlated with h_{ci}. This shows that h_{si} certainly worked to mitigate the variation of h_i caused by the difference in h_{ci}. Therefore, all these results basically support the concept of the hypothesis about the role of snow that snow works to mitigate the ice thickness variation caused by meteorological conditions and that ice thickness is controlled more by snow depth than by air temperature.

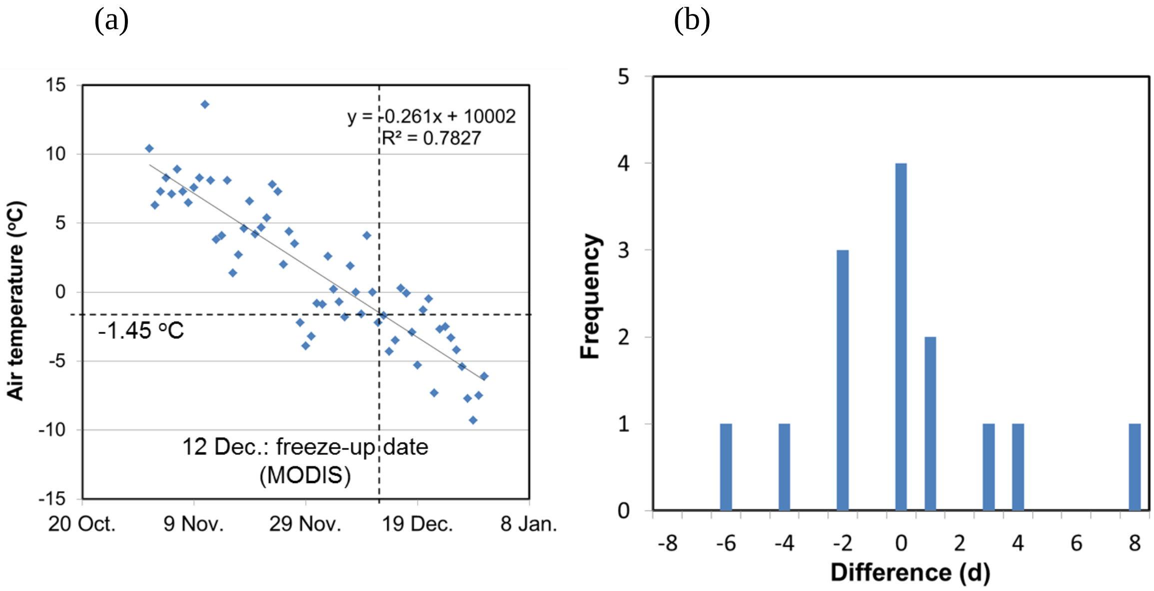

Fig. 5.1. The method to determine the freeze-up date for 1961-1999. (a) An example for 2004. The vertical and the horizontal dashed lines show the freeze-up date estimated from MODIS images and the corresponding air temperature in November/December 2004, respectively. (b) The frequency of the differences between the freeze-up dates determined from MODIS images or observations and those estimated from the mean air temperature on the freeze-up dates for 2000-2015. (to see the text).

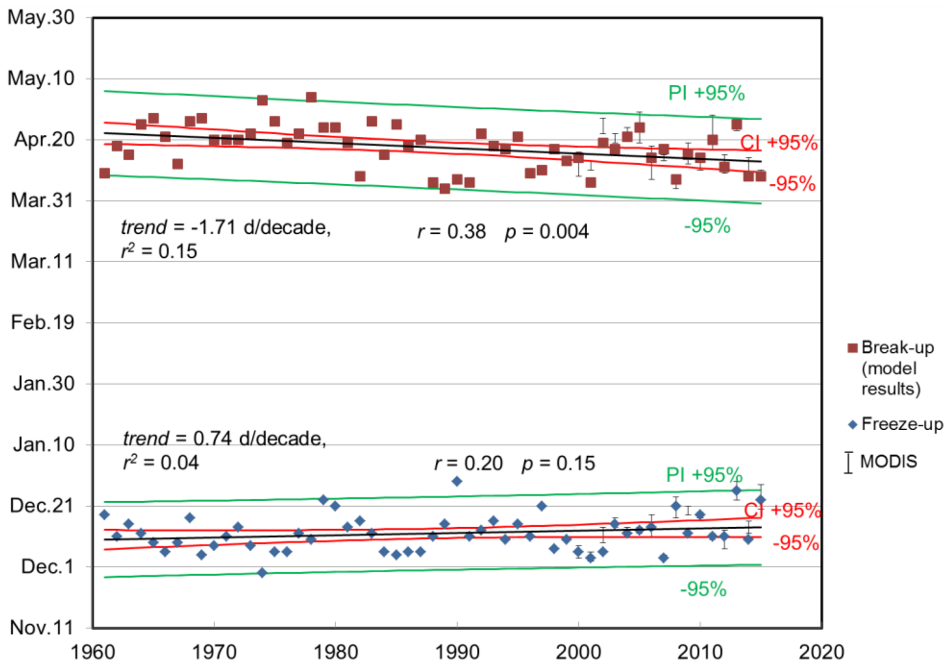

Fig. 5.2. Freeze-up and break-up dates from 1961/62-2015/16, determined by the model and MODIS images. Error bars show the time ranges estimated for freeze-up and break-up dates from MODIS images. Diamonds and squares show freeze-up dates used for the model and break-up dates calculated by the model, respectively.

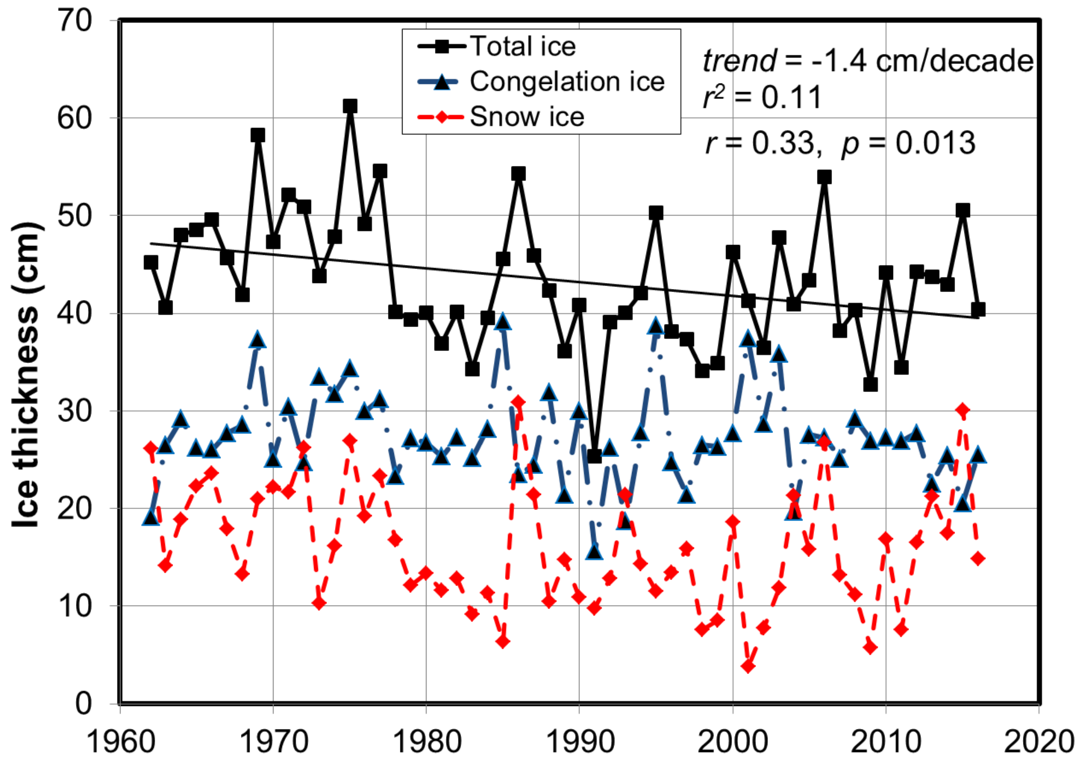

Fig. 5.3. The thicknesses of total ice, CI and SI on 15 February, determined by the model. The black solid line, blue dashed-dotted line and red dashed line show total ice thickness, CI thickness and SI thickness predicted by the model, respectively. The black solid straight line is the regression line of best fit for total ice thickness. The trend, shared variance (r^2), correlation coefficient (r) and p-value (p) are shown in the figure.

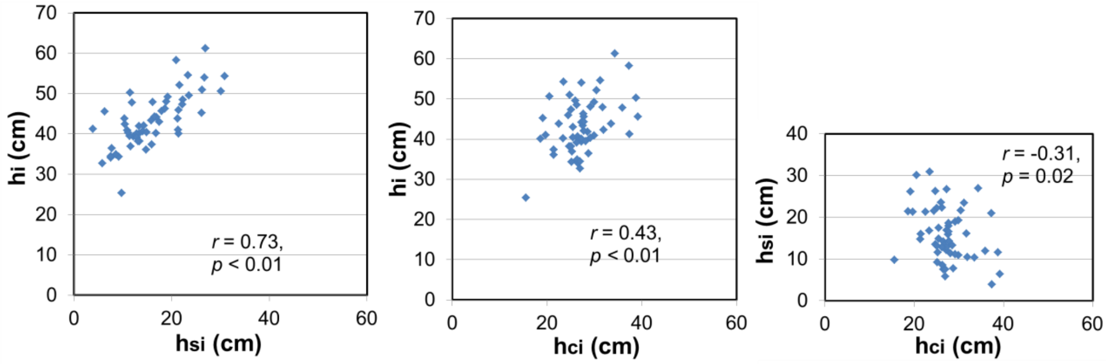

Fig. 5.4. The relationships between total ice thickness (h_i), SI thickness (h_{si}) and CI thickness (h_{ci}) on 15 February for 55 years: (a) h_i vs. h_{si}, (b) h_i vs. h_{ci} and (c) h_{si} vs. h_{ci}. Correlation coefficients and *p*-values are shown by "*r*" and "*p*" in the figure.

5.2. Relationship between ice phenology and meteorological conditions

To look at the relationship with ice phenology at Lake Abashiri, the interannual variabilities of the air temperature and snow depth averaged for the period from the freeze-up date to 15 February for the 55 years are shown in Figure 5.5. It is found that whereas the air temperature exhibited a significant increasing trend of +0.23^{o}C/decade, the snow depth did not have a significant trend for the period although a slight difference in the variability of snow depth may be found before and after the mid 1990's, i.e. 26.3±9.1 cm for 1961- 2000 in contrast to 33.0±14.3 cm for 2001- 2016. The correlations of h_i with mean air temperature and mean snow depth are shown in Figure 5.6. This figure shows that h_i is correlated negatively with air temperature (r = -0.49, p < 0.01) and positively with snow depth (r = 0.41, p < 0.01). This indicates that when the long-term trend of ice phenology is looked at, while snow still plays an important role in determining h_i in February, air temperature also affects it significantly. Keeping the interannual variations of meteorological data and the relationship with h_i in mind, we conclude that the negative trend of the break-up date (becoming earlier) and h_i

(becoming thinner) may be attributed more to the warming trend of air temperature than the change in snow depth. This is possibly because air temperature tended to affect *hi* more due to thinner snow before 2000 compared with that after 2001. Thus it is found that the phenology of break-up date of lake ice at mid-latitude shows a negative trend for the past 55 years, similar to other regions at high latitudes, associated with the warming trend.

To examine the relationship between ice phenology and air temperature, time series for normalized anomalies of ice phenology and air temperatures are shown in Figure 5.7. The shared variance between mean anomalies of freeze-up and the mean anomaly of the mean air temperature in November to December is 76%. Such a high value is not surprising because it comes mainly from our method to determine the freeze-up date with air temperature, as shown in Section 5.1. The shared variances for break-up date with the air temperature in March and ice-cover duration with the mean air temperature in November to March also take high values of 35% and 69%, respectively. These high values, particularly for ice-cover duration, explain how significantly ice phenology is affected by air temperature for the past 55 years. The high correlation between ice phenology parameters and air temperature becomes more prominent when taking 8-year running means. It is found in Figure 5.7 that the interannual variability of the 8-year running mean of air temperature is well correlated positively with freeze-up date and negatively with break-up date and ice-cover duration. In addition, the phenology parameters at Abashiri were estimated for 1975/76-2004/05 to compare with those reported for the lakes in Europe and North Amaerica. The dates of break-up and freeze-up, and ice cover duration show a significant negative trend of -3.5 d/decade (p = 0.02), a negative trend -0.5 d/decade (not significant) and a negative trend of -3.0 d/ decade (not significant) for 30 years, respectively. These results are similar to those reported for the lakes in Europe (Fig. 5.8), although the relationship seems to be stronger at lower latitudes (Weyhenmeyer et al., 2004; Livingstone et al., 2010). The reason why the similar phenology to the reported results is shown at Lake Abashiri may be attributed to its average trend in the surface temperature in Europe at high latitudes (Fig. 5.9). The reason why the trend of freeze-up date at Lake Abashiri is less prominent than that of break-up date is considered to be firstly because the increasing trend of air temperature is twice as strong in March (0.43 ^{o}C/decade) as in November to December (0.21 ^{o}C/decade) and secondly because freeze-up date is affected not only by air temperature but also by lake-specific characteristics which determine the lake heat storage; for example, lake volume, as discussed in Vavrus et al. (1996), Williams et al. (2004), Duguay et al. (2006), and Benson et al., (2012).

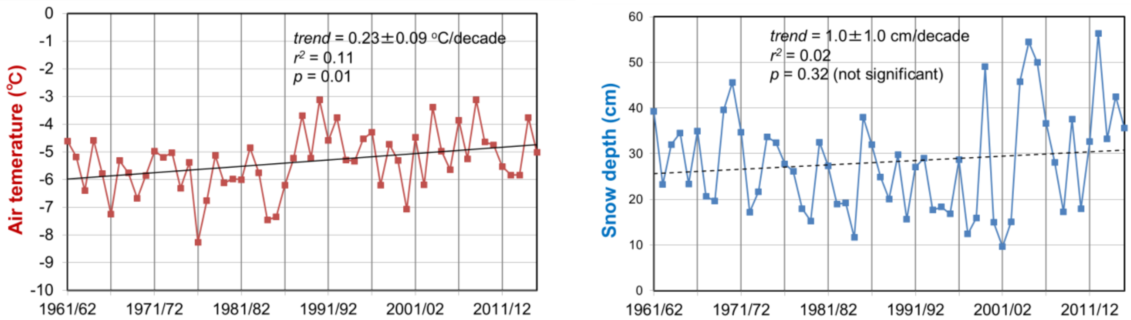

Fig. 5.5. Meteorological conditions after freeze-up date to 15 February for (a) the mean air temperature and (b) the mean snow depth. The black solid or dashed straight lines are the regression lines of best fit. The trends, shared variances (r^2) and p-values (p) are shown in the figure.

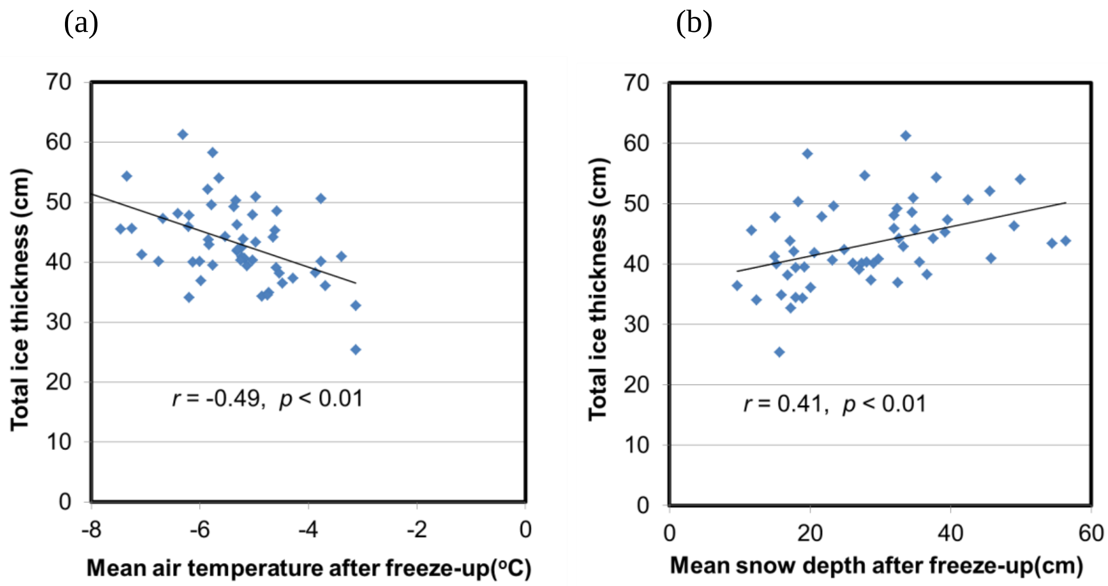

Fig. 5.6. The relationships between total ice thickness on 15 February estimated by the model and (a) the mean air temperature or (b) the mean snow depth from freeze-up date to 15 February, recorded at the Abashiri Meteorological Observatory for 1961/62-2015/16. The solid straight lines are the regression lines of best fit. Correlation coefficients and *p*-values are shown by "*r*" and "*p*" in the figure.

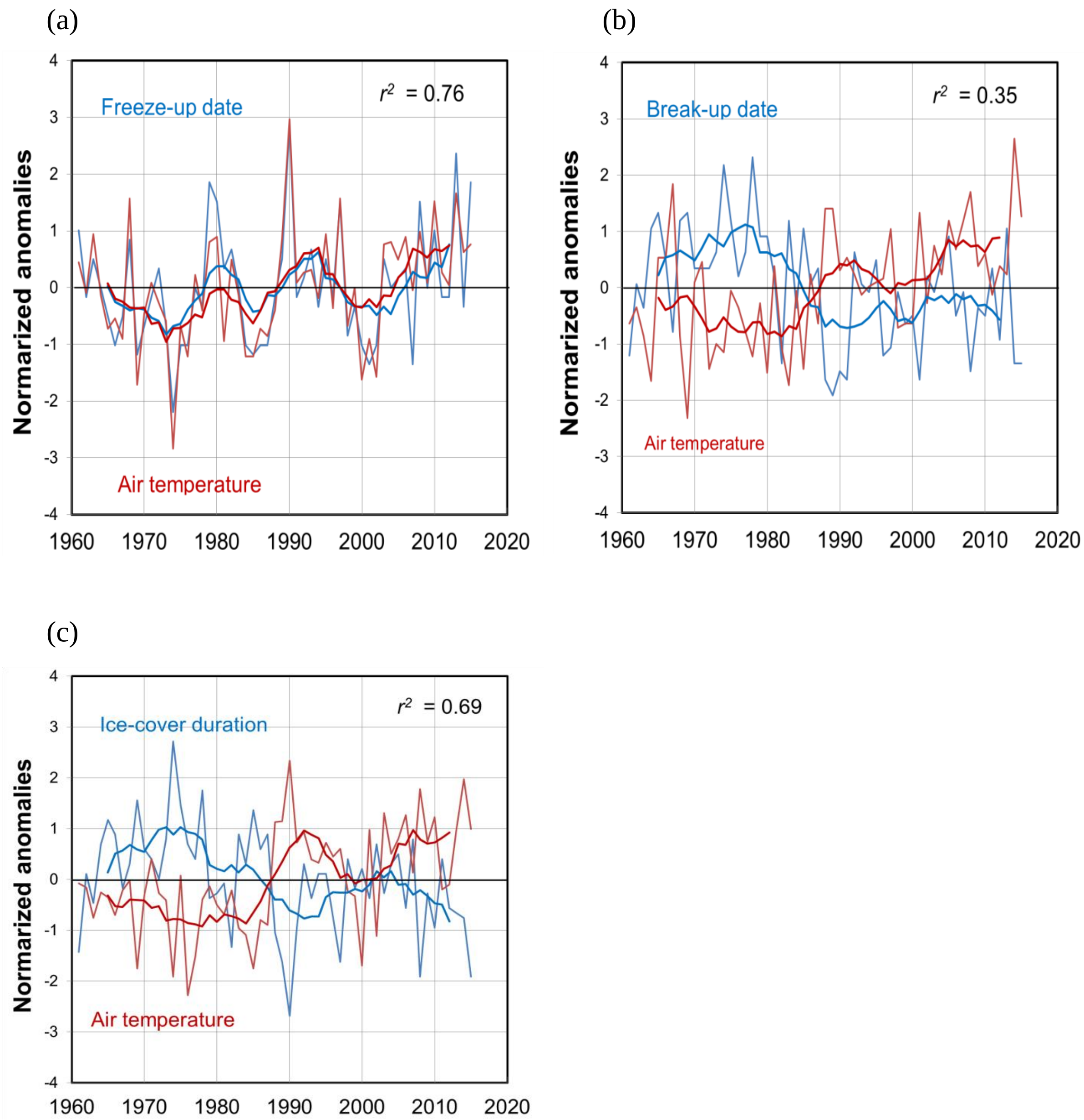

Fig. 5.7. Comparisons of anomaly time series for ice phenology parameters and air temperature from 1961/62 to 2015/16. All valuables are expressed as normalized anomalies (standard deviations of the measures being compared): (a) freeze-up date and the average of November and December temperatures, (b) break-up date and March temperatures and (c) ice-cover duration and the average of November to March temperatures. Annual values are indicated by thin lines and 8-year running means by heavy lines; ice phenology parameters are blue and air temperatures are red. r^2 is presented for the linear relationship between the ice phenology parameters and the corresponding air temperatures.

(a)

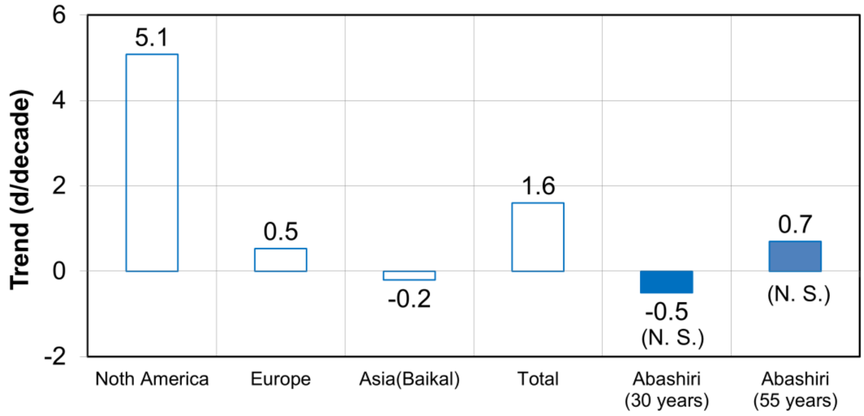

(b)

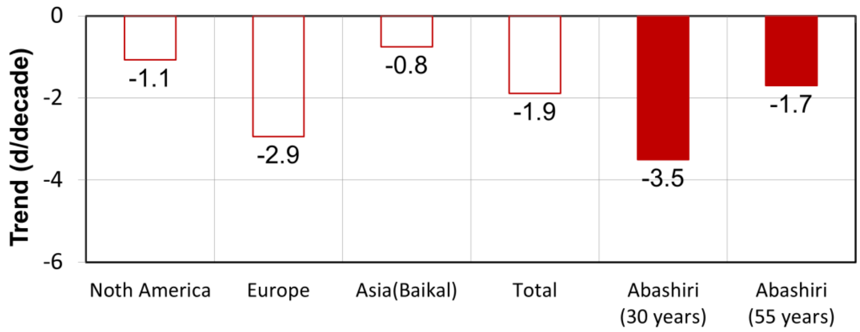

(c)

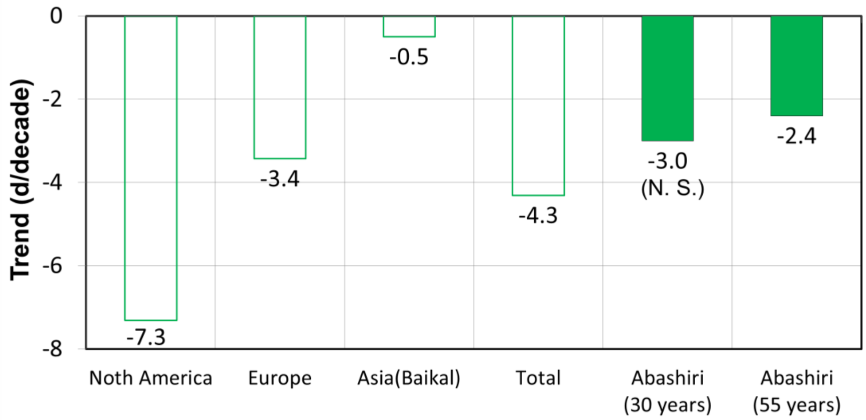

Fig. 5.8. Comparisons of trends of (a) freeze-up date, (b) break-up date and (c) ice-cover duration for 1975/76-2004/05 between the North America, Europe, Asia (Baikal), total (the Northern Hemisphere) reported by Benson et al. (2012) and those at Abashiri. Here, trends at Abashiri (30 years) and Abashiri (55 years) are for 1975/76-2004/05 and 1961/62-2015/16, respectively. "(N. S.)" in the figures shows the trend is not statistically significant.

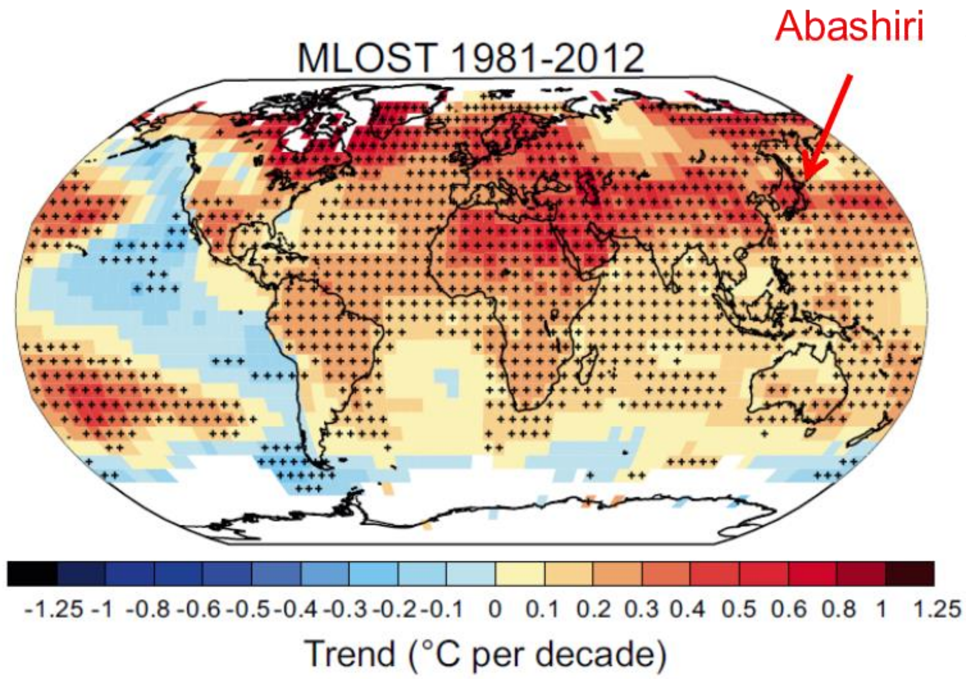

Fig. 5.9. Trends in surface temperature for the period 1881 - 2012 (Vose et al., 2012; IPCC 2013).

6. Conclusions

This study aims to clarify the properties of lake ice at mid-latitudes, subject to relatively moderate air temperature, relatively heavy snow, and abundant solar radiation even in winter, as contrasted with lakes at high latitudes. For this purpose, field observations were conducted at Lake Abashiri in Japan for three winters and a 1-D thermo-dynamical model was developed for predicting ice growth at Lake Abashiri. Using this model forced by meteorological datasets from Abashiri, the roles of snow in the ice thickening process were examined, and also ice phenology parameters were estimated and interannual trends at this lake were associated for the past 55-year period to compare with lakes at high latitudes.

Firstly, the lake ice properties were investigated at Lake Abashiri, Hokkaido, Japan, located at mid-latitudes (44.0N 144.2E) based on the observation in the 2012/13 winter. The results showed that the SI layer accounted for 29% to 73% of the total ice thickness, a much greater fraction than that for high latitude lakes (10-40%, Finland, Leppäranta, 2009). Based on the observations, a thermodynamic model that includes both formation processes of SI and CI was developed. The model successfully reproduced the thicknesses observed.

Next, to confirm the observational results and verify the model, the follow-up campaigns were conducted throughout two additional winters (2014/15 and 2015/16). Based on the results obtained, the role of snow in ice thickening process was examined from numerical experiments with this model. The results are summarized as follows:

(1) Commonly, lake ice was composed of whitish snow ice (SI) and translucent congelation ice (CI), and the contribution of SI to total ice thickness was significant: 29-73% for 2012/13, 40-60% for 2014/15 and 28-65 % for 2015/16.

(2) The model, which was developed based on the observational results in 2012/13, successfully reproduced the observed thicknesses of both h_{ci} and h_{si} for 2014/15 and 2015/16 as well, showing the validity of the model under different meteorological conditions. It was also found that the model can reproduce the break-up date well, with an accuracy of a few days.

(3) The roles of snow in lake ice growth were examined from numerical experiments with this model by comparing h_i, h_{ci}, and h_{si} calculated for three cases: (i) snow accumulates with SI formation (control run); (ii) snow accumulates without SI formation; and (iii) no snow accumulates. The results obtained for these three winters support a hypothesis that snow works to mitigate the ice thickness variation caused by meteorological conditions, and it was shown that ice thickness is controlled more by snow depth than by air temperature.

Then, to further examine the validity of the model and the role of snow in the ice growth under various meteorological conditions, the calculation of h_i, h_{ci}, and h_{si} was extended for the past 16 years (2000/01 – 2015/16), during which MODIS images are available, to determine the freeze-up dates. The results were found to be consistent with those obtained from the field observations in the three winters, as shown below:

(4) h_i, h_{ci}, and h_{si} calculated in the model are consistent with the ice thickness records measured at the near shore region of the lake.

(5) There is a significant negative correlation between h_{si} and h_{ci}, indicating that snow works to moderate the change in h_{ci} through the formation of SI. The importance of snow was also endorsed by the fact that h_i has a higher correlation with snow depth than with air temperature at Abashiri.

Furthermore, to estimate ice phenology parameters and their interannual trends at this lake for comparison with other lakes in the northern hemisphere, the calculation was extended for the past 55-year period (1961/62 – 2015/16), using our model. In the calculation, the freeze-up dates were inferred from the air temperature data at Abashiri, and the break-up dates were calculated with the model. The results are summarized as follows:

(6) The average freeze-up date, break-up date, and ice-cover duration were estimated as 12 December, 17 April, and 127 days, respectively. On average, h_{si} (16 cm) accounts for 37 % of h_i (43 cm), higher than about 30 % in Finland (Leppäranta, 2015).

(7) Statistical analysis showed that the break-up dates have experienced a significant negative trend of -1.71 d/decade for the past 55 years, i.e. the break-up date has become earlier by 9 days for the recent half century. This trend is comparable with the trend for other lakes in the Northern Hemisphere for the 30-year period 1975/76 to 2004/05 reported by Benson et al. (2012). This is presumed to be because air temperature affected h_i more strongly due to less snow before 2000 compared with that after 2001. Time series for normalized anomalies of ice phenology parameters and air temperature showed that they are highly correlated, which is consistent with the result reported for the lakes in Europe and North America. On the other hand, the freeze-up dates did not show a significant trend for the 55-year period. As for h_i on 15 February, a significant decreasing trend (-1.4 cm/decade) was found, along with a much higher correlation with h_{si} than with h_{ci}. The observed negative correlation between h_{si} and h_{ci} supports our hypothesis about the roles of snow.

In this study, the properties of lake ice at Lake Abashiri were investigated as a case study for the lakes at mid-latitudes. As a result, it was shown that the main role of snow in ice growth is to mitigate the variability of ice thickness caused by the change in meteorological conditions, and ice thickness is found to be more strongly affected by snow depth than by air temperature. Although the study is limited to a specific regional lake, the obtained results are expected to apply to other lakes where meteorological conditions are similar, irrespective of latitude. Given that air temperature is predicted to become higher along with enhanced snowfall at high latitudes in the future, the results obtained here might serve to understand the changes in lake ice properties there. In addition, in light of the fact that SI formation is regarded as one of the most important growth processes of sea ice, especially in the Antarctic, the results are also expected to contribute to broader understanding in this domain. In the case of sea ice, the SI formation processes appear to be more complex, because the freezing of water which has infiltrated through brine channels is another SI formation process, in addition to the freezing of snow flooded by sea water (Maksym and Jeffries, 2000; Toyota et al., 2011). Since the former process can be neglected in the lake ice formation, the SI formation process of lake ice may be used to study the latter process in isolation.

Although many lake ice properties at mid-latitudes were revealed through this work, some details of the processes of snow ice formation and melting still remain unresolved. Further studies including field observation are required.

Acknowledgements

I am deeply grateful to Dr. T. Toyota of ILTS, Hokkaido University, for his continued support and encouragement during the course of my study. I am also very grateful to Dr. T. Shiraiwa at ILTS, for his kind introduction to my study and my field work at Lake Abashiri. I would like to thank Dr. N. Ebuchi very much for his support and considerations for my study. I am sincerely grateful to Dr. K. Ohshima, for his insightful comments and advice on my study. I am also grateful to Dr. S. Aoki and Dr. Fukamachi of ILTS, for their invaluable comments on my study. I am very grateful to Dr. S. Matoba of ILTS for kind arrangements regarding the measurement of $\delta^{18}O$ and suggestions for my analysis. I appreciate Dr. K. Shirasawa very much for his introducing me to many relevant literatures. I would like to thank Dr. M. Leppäranta of University of Helsinki for useful and inspiring comments. I also appreciate the help of Dr. T. Sawagaki of Hosei University with field observations and Dr. J. Nishioka, Dr. K. Ono of ILTS, Dr. A. Tsushima of Research Institute for Humanity and Nature, who supported the laboratory analysis. I thank Dr. A. D. Fraser of University of Tasmania, Australia for providing MODIS images of Lake Abashiri and improving the English of my papers. I also appreciate his useful comments of Dr. T. Ozeki of Hokkaido University of Education on my doctoral dissertation. I sincerely thank Mr. T. Kawajiri of Nishi-Abashiri Fishermen’s Cooperative Association for enormous support throughout the field observations, and Mr. T. Watanabe, Mr. T. Iida and Mr. S. Sakazaki of Abashiri City for kind logistic supports. I thank Mr. E. Kudo of the Okhotsk Ryu-hyo (drift ice) Museum for providing useful pictures of ice conditions at Lake Abashiri. I also thank the Abashiri and Memanbetsu tourism associations for providing the records of ice thickness for ice fishing. I also appreciate Mr. K. Sakai of the Hokkaido Regional

Development Bureau for his offering valuable data about Lake Abashiri and Abashiri river. I appreciate the help of Mr. R. Kato and Mr. J. Ishiyama of Hokkaido University with field observations. Finally, I would like to express my thanks to my family. I am very thankful to my wife and my son for their warm encouragement and useful advices. I am also thankful to my daughters for their supportive understanding. Without the help of my family, I could not have been able to start and continue my study.

This study was carried out through a bilateral cooperative agreement between the Institute of Low Temperature Science (ILTS), Hokkaido University, and Abashiri City, and was financially supported partly by a Grant for Joint Research Program of ILTS.

References

Andreas, E. L. and Makshtas, A. P. (1985) Energy exchange over Antarctic sea ice in the spring, *Journal of Geophysical Research,* **90**(C4), 7199-7212

Barns, R. L. and Laudise R. A. (1985) Size and Perfection of Crystals in Lake Ice, *Journal of Crystal Growth,* **71**, 104-110

Bates, R. E and Bilello, M. A. (1966) Defining the cold regions of the Northern Hemisphere. Technical report 178. US Army Cold Regions Research and Engineering Laboratory, Hanover, NH

Bernhardt, J., Engelhardt, C., Kirillin, G. and Matschullat, J. (2011) Lake ice phenology in Berlin-Brandenburg from 1947-2007: observations and model hindcasts. *Clim Change* (doi: 10.1007/s10584-011-0248-9)

Benson, B. J., Magnuson, J. J., Jensen, O. P., Card, V. M., Hodgkins, G., Korhonen, J., Livingstone, D. M., Stewart, K. M., Weyhenmeyer, G. A. and Granin, N. G. (2012) Extreme events, trends, and variability in Northern Hemisphere lake-ice phenology (1855–2005). *Clim. Change*, **112**, 299–323.

Bonan, G. B. (1995) Sensitivity of a GCM simulation to inclusion of inland water surfaces. *Journal of Climate,* **8**, 2691-2704

Cheng, B., Vihma, T. and Launiainen, J. (2003) Modelling of the superimposed ice formation and subsurface melting in the Baltic Sea. *Geophysica,* **39**, 31-50

Dai, A. (2006) Recent climatology, variability, and trends in global surface humidity. *J. Clim.*, **19**, 3589–3606.

Duguay, C. R., Flato, G. M., Jeffries, M. O., Menard, P., Morris, K. and Rouse, W. R. (2003) Ice-cover variability on shallow lakes at high latitudes: model simulations and observations. *Hydrological Processes*, **17**, 3465-3483

Duguay, C. R., Prowse, T. D., Bonsal, B. R., Brown R. D., Lacroix, M. P. and Menard, P. (2006) Recent trends in Canadian lake ice cover. *Hydrological Processes*, **20**, 781-801

Efremova, T. and Palshin, N. (2011) Ice phenomena terms on the water bodies of northwestern Russia. *Meteorology and Hydrogy*, **36**(8), 559-565

Ellis, A. W. and Johnson, J. J. (2004) Hydroclimatic analysis of snowfalls trends associated with the North American Great Lakes. *Journal of Hydrometeorology,* **5,** 471-486

Flato, G. M. and Brown, R. D. (1996) Variability and climate sensitivity of landfast Arctic sea ice. *Journal of Geophysical Research*, **101**, 25767-25777

Gow, A. J. and Langston, D. (1977) Growth history of lake ice in relation to its stratigraphic, crystalline and mechanical Structure. *Cold Regions Research and Engineering Laboratory Report*, **77-1**, 1-24

Gow, A. J. (1986) Orientation textures in ice sheets of quietly frozen lakes. *Journal of Crystal Growth*, **74**, 247-258

Grenfell, T. C. and Maykut, G. A. (1977) The optical properties of ice and snow in the Arctic basin. *Journal of Glaciology*, **18**(80), 445–463

Gupta, P., Noone, D., Galewsky, J., Sweeney, C. and Vaughn, B. H. (2009) Demonstration of high-precision continuous measurements of water vapor isotopologues in laboratory and remote field deployments using wavelength-scanned cavity ring-down spectroscopy (WS-CRDS) technology. *Rapid Communications in Mass Spectrometry,* **23**(16), 2534-2542 (doi: 10.1002/rcm.4100)

Holroyd, E. W. (1971) Lake-effect cloud bands as seen from weather satellites. *Journal*

of the Atmospheric Sciences, **28,** 1165–1170.
(doi: 10.1175/1520-0469(1971)028<1165:LECBAS>2.0.CO;2)

Ikenaga, H., Mukouyama, K., Oshima, S., Uchijima, K. and Yamada, T. (1999) Study on the short term behaviors of the density interface and the formation of wind-driven current in a brackish lake. *Japan Society of Civil Engineering*, **614**, 77-96 (in Japanese)

IPCC (2001) Climate Change 2001: The scientific basis. In Houghton, J.T., Ding, Y., Griggs, D. J., Noguer, M., van der Linden, P. J., Dai, X., Maskell, K. and Johnson, C. A. eds. Contribution of working group I to the third assessment report of the Intergovernmental Panel on Climate Change (IPCC). Cambridge University Press, Cambridge, UK

IPCC (2007) Climate Change 2007: The Physical Science Basis. In Solomon, S., Qin, D., Manning, M., Chen, Z., Marquis, M., Averyt, K. B., Tignor, M. and Miller, H. L. eds. Contribution of working group I to the fourth assessment report of the Intergovernmental Panel on Climate Change (IPCC), Cambridge University Press, Cambridge, UK

IPCC (2013) Climate Change 2013. The Physical Science Basis. In Stocker, T. F., Qin, D., Plattner, G. K., Tignor, M. M. B., Allen, S. K., Boscung, J., Nauels, A., Xia, Y., Bex, V. and Midgley, P. M. eds. Contribution of working group I to the fifth assessment report of the Intergovernmental Panel on Climate Change (IPCC), Cambridge University Press, Cambridge, UK

Japan Meteorological Agency (2015) http://www.data.jma.go.jp/gmd/cpd/monitor/climatview/frame.php (in Japanese)

Jeffries, M. O., Morris, K. and Duguay, C. R. (2005) Lake ice growth and decay in central Alaska, USA: observations and computer simulations compared. *Annals of Glaciology,* **40**, 195-199

Kawamura, T. and Ono, N. (1978) A study of ice on Lake Tofutsu. Low Temperature Science Ser. A, 37, 85-91. (In Japanese with English summary)

Kerstel, E. R. T., van Trigt, R., Dam, N, Reuss, J. and Meijer, H. A. J. (1999) Simultaneous determination of the $^{2}H/^{1}H$, $^{17}O/^{16}O$, and $^{18}O/^{16}O$ isotope abundance ratios in water by means of laser spectrometry. *Analytical Chemistry*, **71**, 5297-5303 (doi: 10.1021/ac990621e)

Kirillin, G., Leppäranta, M., Terzhevik, A., Granin, N., Bernhardt, J., Engelhardt, C., Efremova, T., Golosov, S., Palshin, N., Sherstyankin, P., Zdorovennova, G. and Zdorovennov, R. (2012) Physics of seasonally ice-covered lakes: a review. *Aquatic Sciences* **74,** 659-682 (doi:10.1007/s00027-012-0279-y)

Kivisild, H. R. (1970) River and lake ice terminology. *International Association of Hydraulic Research,* 1, 10, 14

Kärkäs, E. (2000) The ice season of Lake Pääjärvi, southern Finland. *Geophysica*, 36:85–94

Launiainen, J. and Cheng, B. (1998). Modelling of ice thermodynamics in natural water bodies. *Cold Regions Science and Technology,* **27,** 153-178

Lehmann, M. and Siegenthaler, U. (1991) Equilibrium oxygen- and hydrogen-isotope fractionation between ice and water. *Journal of Glaciology*, **37**(125), 23-26

Lei, R., Leppäranta, M., Cheng, B., Heil, P. and Li, Z. (2012) Changes in ice-season characteristics of a European Arctic lake from 1964 to 2008. *Climatic Change,* **115**, 725-739 (doi: 10.1007/s10584-012-0489-2)

Leppäranta, M. (1983) A growth model for black ice, snow ice and snow thickness in subarctic basins. *Nordic Hydrology*, **14**, 59-70

Leppäranta, M. and Kosloff, P. (2000) The structure and thickness of Lake Pääjärvi ice. *Geophysica*, **36**, 233-248

Leppäranta, M. (2009) Modelling the formation and decay of lake ice, In: George, D. G. eds. *The impact of climate change on European lakes*, Springer, Germany. *Aquatic Ecology Series*, **4**, 63-83

Leppäranta, M. (2015) Freezing of lakes, In: *Freezing of lakes and the evolution of their ice cover*, Springer, Germany. 11-50 (doi: 10.1007/978-3-642-29081-7_2)

Leppäranta, M. (2015) Structure and properties of lake ice, In: *Freezing of lakes and the evolution of their ice cover*, Springer, Germany. 51-90 (doi: 10.1007/978-3-642-29081-7_3)

Leppäranta, M. (2015) Thermodynamics of seasonal lake ice, In: *Freezing of lakes and the evolution of their ice cover*, Springer, Germany. 91-136 (doi: 10.1007/978-3-642-29081-7_4)

Liston, G. E. and Hall, D. K. (1995) An energy-balance model of lake-ice evolution. *Journal of Glaciology*, **41**, 373-382

Livingstone, D. M., Adrian, R., Blenckner, T., Geoge, D. G. and Weyhenmeyer, G. A. (2010) Lake ice phenology, In George, D. G. eds. *The impact of climate change on European lakes*, Springer, Germany. *Aquatic Ecology Series*, **4,** 51-61 (doi: 10.1007/978-90-481-2945-4_4)

Magnuson, J. J, Robertson D. M., Benson, B. J., Wynne R., H., Livingstone, D. M., Arai, T., Assel, R. A., Barry, R. G., Card, V., Kuusisto, E., Granin, N. G., Prowse T. D., Stewart, K. M. and Vuglinski, V. S. (2000) Historical trends in lake and river ice cover in the Northern Hemisphere. *Science*, **289**, 1743-1746 (doi:

10.1126/science.289.5485.1743)

Maksym, T. and Jeffries, M. O. (2000) A one-dimensional percolation model of flooding and snow ice formation on Antarctic sea ice. *Journal of Geophysical Research,* **105**, 26313-26331

Martin, S. (1981) Frazil ice in rivers and oceans, *Ann. Rev. Fluid Mech.* **13**, 379-397

Marszelewski, W., Skowron, R. (2006) Ice cover as an indicator of winter air temperature changes: case study of the Polish Lowlandlakes. *Hydrol. Sciences J.,* 51:336–349

Maykut, G. A. and Untersteiner, N. (1971) Some results from a time-dependent, thermodynamic model of sea ice. *Journal of Geophysical Research,* **76**, 1550-1575

Maykut, G. A. and Church, P. E. (1973) Radiation climate of Barrow, Alaska, 1962-66. *Journal of Applied Meteorology,* **12**(4), 620-628 (doi: 10.1175/1520-0450(1973)012<0620:RCOBA>2.0.CO;2)

Maykut, G. A. (1978) Energy exchange over young sea ice in the central Arctic. *Journal of Geophysical Research*, **83**(C7), 3646-3658

Maykut, G. A. (1982) Large-scale heat exchange and ice production in the central Arctic. *Journal of Geophysical Research*, **87**(C10), 7971-7984

Maykut, G. A. (1985) The ice environment. In: Horner RA eds. *Sea Ice Biota*, 21-82, CRC Press, Boca Raton, Florida, USA

Menard, P., Duguay, C. R., Flato, G. M. and Rouse, W. R. (2002) Simulation of ice phenology on Great Slave Lake, Northwest Territories, Canada. *Hydrological Processes*, **16**, 3691-3706

Menard, P., Duguay, C. R., Pivot, F. C., Flato, G. M. and Rouse, W. R. (2003) Sensitivity of Great Slave Lake ice phenology to climate change. *Proceedng of the*

16th IAHR International Symposium on Ice, Dunedin, New Zealand. 2-6 December 2002, **3**, 57-63

Morris, K., Jeffries, M. and Duguay, C. (2005) Model simulation of the effects of climate variability and change on lake in central Alaska, USA. *Annals of Glaciology*, **40**, 113-118

Michel, B. and Ramseier, R. O. (1971) Classification of river and lake ice. *Canadian Geotechnical Journal*, **8**(36), 36-45

Muguruma, J. and Kikuchi K. (1963) Lake ice investigation at Peters Lake, Alaska. *Journal of Glaciology*, 4, 689-708.

Ohata, Y., Toyota, T. and Shiraiwa, T. (2016a) Lake ice formation processes and thickness evolution at Lake Abashiri, Hokkaido, Japan. *Journal of Glaciology*, **62**(233), 563–578. (doi: 10.1017/jog.2016.57)

Ohata, Y., Toyota, T., Fraser, A. D. and Shiraiwa, T. (2016b) The role of snow-ice in the thickening processes of lake ice at Lake Abashiri, Hokkaido, Japan. *Proceedings of the 23rd IAHR International Symposium on Ice,* Ann Arbor, Michigan USA, ISSN: 2414-6331

Omstedt, A. (1990) A coupled one-dimensional sea ice–ocean model applied to a semi-enclosed basin. *Tellus,* **42A**, 568–582

Paquette, M., Fortier, D., Mueller, D. R., Sarrazin, D., and Vincent, W. F. (2015) Rapid disappearance of perennial ice on Canada's most northern lake, *Geophysical Research Letters*, **42**, 1433-1440 (doi: 10.1002/2014GL062960)

Palosuo, E. (1965) Frozen slush on lake ice. *Geophysica* , **9**, 131-147

Perovich, D. K. (1998) The optical properties of sea ice. In: Leppäranta M eds. *Physics of ice-covered seas.* Helsinki University Press, 195–230

Pirazzini, R., Vihma, T., Granskog, M. A. and Cheng, B. (2006) Surface albedo measurements over sea ice in the Baltic Sea during the spring snowmelt period. *Annals of Glaciology,* **44**, 7-14

Pirinen, P., Simola, H., Aalto, J., Kaukoranta, J-P., Karlsson, P. and Ruuhela, R. (2012) Tilastoja Suomen ilmastosta 1981-2010 [Climatological statistics of Finland 1981-2010], *Finnish Meteorological Institute, Report 2012*:1

Rouse, W. R., Binyamin, J., Blanken, P. D., Bussieres, N., Duguay, C. R., Oswald, C.J., Schertzer, W. M. and Spence, C. (2008) The influence of lakes on the regional energy and water balance of the central Mackenzie River basin. In: Woo MK eds. *Cold Region Atmospheric and Hydrologic Studies. The Mackenzie GEWEX experience,* Springer, Germany. **1**, 309-325 (doi: 10.1007/978-3-540-73936-4_18)

Salonen, K., Leppäranta, M., Viljanen, M. and Gulati, R. D. (2009) Perspectives in winter limnology: closing the annual cycle of freezing lakes. *Aquatic Ecology*, **43**(3), 609-616 (doi: 10.1007/s10452-009-9278-z)

Saloranta T. M. (2000) Modeling the evolution of snow, snow ice and ice in the Baltic Sea. *Tellus*, **52A**, 93-108

Sellinger, C. E., Stow, C. A., Lamon, E. C. and Qian, S. S. (2008) Recent water level declines in the Lake Michigan-Huron system. *Environ. Sci. Technol.*, **42**, 367–373

Shirasawa, K., Leppäranta, M., Saloranta, T., Kawamura, T., Polomoshnov, A. and Surkov, G. (2005) The thickness of coastal fast ice in the Sea of Okhotsk. *Cold Regions Science and Technology,* **42**, 25-40 (doi: 10.1016/j.coldregions.2004.11.003)

Shirasawa, K., Leppäranta, M., Kawamura, T., Ishikawa, M. and Takatsuka, T. (2006) Measurements and modelling of the water-ice heat flux in natural waters. *Proceedings of the 18th IAHR International Symposium on Ice*, 85-91. Hokkaido

University, Sapporo, Japan.

Shuter, B. J., Finstad, A. G., Helland, I. P., Zweimuller, I. and Holker, F. (2012) The role of winter phenology in shaping the ecology of freshwater fish and their sensitivities to climate change. *Aquatic Sciences*, **74**(4), 637-657 (doi: 10.1007/s00027-012-0274-3)

Simmons, A. J., Willett, K. M., Jones, P. D., Thorne, P. W. and Dee, D. P. (2010). Low-frequency variations in surface atmospheric humidity, temperature, and precipitation: Inferences from reanalyses and monthly gridded observational data sets. *J. Geophys. Res. Atmos*., 115, D01110. (doi:10.1029/2009JD012442)

Sturm, M. and Liston, G. E. (2003) The snow cover on lakes of the Arctic Coastal Plain of Alaska, U.S.A. *Journal of Glaciology*, **49**(166), 370-380

Surdu, C. M., Duguay, C. R., Brown, L. C., and Fernández Prieto, D. (2014) Response of ice cover on shallow lakes of the North Slope of Alaska to contemporary climate conditions (1950-2011): radar remote-sensing and numerical modeling data analysis. *The Cryosphere*, **8**, 167-180 (doi: 10.5194/tc-8-167-2014)

Thiery, W., Davin, E. L., Panitz, H-J, Demuzere, M., Lhermitte, S. and Lipzig, N. V. (2015) The Impact of the African Great Lakes on the Regional Climate. *Journal of climate* **28**, 4061-4085

Toyota, T. and Wakatsuchi, M. (2001) Characteristics of the surface heat budget during the ice-growth season in the southern Sea of Okhotsk. *Annals of Glaciology*, **33**, 230-236

Toyota, T., Takatsuji, S., Tateyama, K., Naoki, K. and Ohshima, K. (2007) Properties of sea ice and overlying snow in the Southern Sea of Okhotsk. *Journal of Oceanography*, **63**, 393-411

Toyota, T. , Massom, R., Tateyama, K., Tamura, T., and Fraser, A. D. (2011) Properties of snow overlying the sea ice off East Antarctica in late winter 2007. *Deep Sea Research II,* 58(9-10), 1137-1148.

Vanderploeg, H. A., Bolsenga, S. J., Fahnenstiel, G. L., Liebig, J. R., and Gardner, W. S. (1992) Plankton ecology in an ice-covered bay of Lake Michigan: utilization of a winter phytoplankton bloom by reproducing copepods. *Hydrobiologia* **243/244**, 175-183

Vavrus, S. J., Wynne, R. H. and Foley, J. A. (1996) Measuring the sensitivity of southern Wisconsin lake ice to climate variations and lake depth using a numerical model. *Limnology and Oceanography*, **41**(5), 822-831

Vose, R. S., Arndt, D., Banzon, V. F., Easterling, D. R., Gleason, B., Huang, B., Kearns, E., Lawrimore, J. H., Menne, M. J., Peterson, T. C., Reynolds, R. W., Smith, T. M., Williams Jr., C. N., and Wuertz, D. B. (2012) NOAA'S Merged Land-Ocean Surface Temperature Analysis. *Bulletin of the American Meteorological Society*, **93**, 1677–1685 (doi:10.1175/BAMS-D-11-00241.1)

Weyhenmeyer, G. A., Meili, M. and Livingstone, D. M. (2004) Nonlinear temperature response of lake ice breakup. *Geophysical Research Letters,* **31,** L07203. (doi:10.1029/2004GL019530)

Willett, K. M., Williams Jr, C. N., Dunn, R. J. H., Thorne, P. W., Bell, S., de Podesta M., Jones, P. D., and Parker, D. E. (2012) HadlSDH: an updated land surface specific humidity product for climate monitoring. *Clim. Past D.*, **8**, 5133–5180.

Williams, G., Layman, K.L., and Stefan, H.G. (2004) Dependence of lake ice covers on climatic, geographic and bathymetric variables. *Cold Regions Science and Technology* , **40**, 145-164.

Yang, Y., Leppäranta, M., Cheng, B., and Li, Z. (2012) Numerical modelling of snow and ice thickness in Lake Vanajavesi, Finland. *Tellus* **64A**, 1-12. (doi: 10.3402/tellusa.v64i0.17202)

Yen, Y. C. (1981) Review of thermal properties of snow, ice, and sea ice. *Cold Regions Research and Engineering Laboratory Report*, 81-10, 1-27